Title
Identifying Molecular Mechanisms and Cellular Origins of Cancers of the Nervous System

Author
Nakashima, Jonathan Kikuo

Publication Date
2013

Peer reviewed|Thesis/dissertation

UNIVERSITY OF CALIFORNIA

Los Angeles

Identifying Molecular Mechanisms and Cellular Origins of Cancers of the Nervous System

A dissertation submitted in partial satisfaction of the requirements for the degree Doctor of Philosophy in Molecular and Medical Pharmacology

by

Jonathan Kikuo Nakashima

2013

ABSTRACT OF THE DISSERTATION

Identifying Molecular Mechanisms and Cellular Origins

of Cancers of the Nervous System

by

Jonathan Kikuo Nakashima

Doctor of Philosophy in Molecular and Medical Pharmacology

University of California, Los Angeles, 2013

Professor Hong Wu, Chair

Cancers of the nervous system are the most common type of solid tumors among children. They are a heterogeneous population of benign and malignant tumors that growth within the central or peripheral nervous system. The molecular mechanisms governing onset and progression, and the cellular origins of these cancers remain intense areas of research. We created mouse models that develop multiple tumors in both the central and peripheral nervous systems. We deleted *Pten* and activated *K-ras* using Cre-lox technology driven by the mouse *GFAP* promoter. Our models develop benign neurofibromas that progress to malignant peripheral nerve sheath tumors, optic nerve tumors, and malignant brain gliomas. We find that loss of the PTEN tumor suppressor is critical in the onset and progression of these tumors. In addition, we show that ^{18}F-fluorodeoxyglucose positron emission tomography can distinguish peripheral nerve sheath tumors as benign or malignant, and is an effective modality to monitor

therapeutic response to multi-kinase inhibitors. Furthermore, we establish a new cell-of-origin in malignant brain gliomas. We deleted *Pten* and activated *K-ras* in adult neural stem cells of the mouse brain and performed developmental tracing analysis to determine where in the neurogenic niche tumors initiated. We show that gliomas initiate from a region called the subcallosal zone (SCZ), the caudal extension of the subventricular zone (SVZ). We find that progenitors in the SCZ transform prior to those in the SVZ, and that the cellular compositions in each region are uniquely affected by our genetic manipulation. These results reveal a critical role of the SCZ in gliomagenesis. As such, these studies define a novel molecular mechanism in the progression of peripheral nerve sheath tumors, and propose a new cell-of-origin in brain gliomas.

The dissertation of Jonathan Kikuo Nakashima is approved.

Harvey Herschman

Caius Radu

Michael Sofroniew

Hong Wu, Committee Chair

University of California, Los Angeles

2013

To my parents, for their unrelenting support and sacrifice

so that I may pursue my dreams.

TABLE OF CONTENTS

LIST OF FIGURES AND TABLES

Chapter 1 **Page**

Chapter 2

Chapter 3

ACKNOWLEDGEMENTS

I am indebted to my advisor, Dr. Hong Wu, for providing me the opportunity to work in her lab, develop as a scientist, and grow as an individual. Her unwavering passion for the pursuit of knowledge has been an inspiration. I am thankful for her for her support and patience during my graduate career.

My committee members Drs. Harvey Herschman, Caius Radu, Michael Sofroniew, and former member Steven Bensinger have been influential throughout my graduate career and I would like to thank them for their brilliance and support.

I would not be here if it were not for Dr. Caroline Gregorian, who was my first mentor. She paved the way to graduate school for me, fueling my excitement for science with hers enthusiasm. More importantly, she has been a friend and her beautiful family has been an inspiration to start my own.

None of my graduate studies would have been possible if it were not for my collaborators. I would like to thank the formidable sarcoma team, Drs. Sarah Dry, Fritz Eilber, William Tap, and Elizabeth Shurell, and the brilliant brain tumor experts, Drs. Harley Kornblum, Whitney Pope, Jelena Zinnanti, and Tiffany Phillips, for their insight into the clinical aspect of patient care, and their wisdom and enthusiasm in my research.

To all the Wu/Liu lab members, both past and present, thank you for the tremendous scientific support and fond memories. To Dr. Antreas Hindoyan, who entered graduate school with me. He and I have battled through classes and the rigors of graduate work, become roommates, and leaned on each other to get to this point. Despite his poor taste in collegiate colors and athletics, he has been an incredible friend. Go Bruins!

I am grateful for the dedication of my undergraduate students Grace Chen, Benjamin Haugen, and Tiasha Shafiq. It has been a privilege and valuable learning experience mentoring them and I am excited to watch them pursue their dreams.

To Sharon Sampogna and my colleagues at Microscopic Techniques, thank you for helping establish my technical proficiency, and providing me with my first laboratory experience.

To all my friends, fellow graduate students and scientists, for their understanding of the trials and tribulations I have endeavored, and their support through this process.

To Jessica, my love, who never stopped believe in me. She has been, and always will be, by my side in whichever path of life purse.

Lastly, I would like to thank the California Institute of Regenerative Medicine (TG-01169) for their financial support which made my training possible.

Figures 4-6 in Chapter 2 are reprints from a previous publication, which appears in The Proceedings of National Academy of Science 106(46):19479-84. The appendix is a reprint of a previous publication, which appears in the Journal of Neuroscience 2009; 29(6):1874-86. Copyright permission to reprint is pending from the National Academy of Science and the Society of Neuroscience.

VITA

Born Daily City, California	July 12, 1982
Undergraduate Research Assistant Microscopic Techniques Core Facility, Brain Research Institute University of California, Los Angeles	2002-2005
Undergraduate Research Assistant Department of Medicine, Cardiology University of California, Los Angeles	2002-2005
Edwin E. Osgood Award American Federation for Medical Research Carmel, California	2005
B.S. Molecular, Cell, and Developmental Biology University of California, Los Angeles	2005
Laboratory Technician Department of Molecular and Medical Pharmacology University of California, Los Angeles	2005-2007
Undergraduate Student Mentor Department of Molecular and Medical Pharmacology University of California, Los Angeles	2008-2013
California Institute of Regenerative Medicine Pre-Doctoral Award University of California, Los Angeles	2010-2012
Travel Award Department of Molecular and Medical Pharmacology University of California, Los Angeles	2011

Teaching Assistant 2012-2013
Department of Life Sciences
University of California, Los Angeles

Publications

- **Nakashima J**, Shafiq TA, Sofroniew MV, Wu H. Neural stem cell heterogeneity defines transformation properties in the mouse brain (2013). (Manuscript in Preparation)
- Hsia HE, Luca R, Kumar R, Takeda M, Courchet J, **Nakashima J**, Wu S, Goebbels S, An W, Eickholt B, Polleux F, Rotin D, Wu H, Nave KA, Rossner M, Bagni C, Rhee JS, Brose N, Kawabe H (2013). The Ubiquitin E3 Ligase Nedd4-1 Acts as a Downstream Target of PI3K/PTEN-mTORC1 Signaling to Promote Neurite Growth. (Manuscript in preparation)
- Shurell E, Tran LM, **Nakashima J**, Smith KB, Tam BM, Li Y, Dry SM, Federman N, Tap WD, Wu H, Eilber FC (2013). Analysis of sex specific age of disease onset in 1029 patients with malignant peripheral nerve sheath tumors. (Manuscript in preparation).
- Gregorian C*, **Nakashima J***, Dry SM, Nghiemphu PL, Smith KB, Ao Y, Dang J, Lawson G, Mellinghoff IK, Mischel PS, Phelps M, Parada LF, Liu X, Sofroniew MV, Eilber FC, Wu H (2009). PTEN dosage is essential for neurofibroma development and malignant transformation. Proceedings of the National Academy of Sciences. *106*: 19479-84.
- Gregorian C, **Nakashima J**, Le Belle J, Ohab J, Kim R, Liu A, Smith KB, Groszer M, Garcia AD, Sofroniew MV, Carmichael ST, Kornblum HI, Liu X, Wu H (2009). *Pten* deletion in adult neural stem/progenitor cells enhances constitutive neurogenesis. Journal of Neuroscience. *29*: 1874-86

*Authors contribute equally to this work.

Chapter 1:

Overview

Introduction

Cancers of the nervous system are the most common type of solid childhood tumors, accounting for approximately 21 percent of all childhood neoplasms (American Cancer Society, 2013). These tumors represent a heterogeneous population of cancers, both benign and malignant, which grow within the central nervous system (CNS) or are associated with the peripheral nerves. There are a number of hereditary syndromes that predispose an individual to developing a nervous system tumor, the most common being Neurofibromatosis type 1 (Reed and Gutmann, 2001).

Neurofibromatosis type 1 (NF1) is one of the most common autosomal dominant disorders in the world, affecting 1 in 3000 people (Ferner, 2007). NF1 is a single gene-determined disease caused by mutations in *NF1*. This gene, residing on chromosome 17q, is one of the largest in the genome, encompassing 60 exons and producing a 320 kDa protein called neurofibromin (Chen and Gutmann, 2013). Neurofibromin negatively regulates RAS proto-oncogene activity, accelerating the conversion of GTP-bound RAS to its inactive GDP-bound form. In this respect, loss of neurofibromin leads to increased RAS activity and subsequent RAS/RAF/MAPK pathway activation, causing unregulated cell migration, differentiation, and proliferation (Zhu and Parada 2002). The somatic effects of RAS activation causes a wide spectrum of disease symptoms observed throughout multiple organ systems in NF1 patients (Ferner et al., 2006).

In particular, the nervous system is affected most by the loss of neurofibromin. A cardinal symptom of NF1 is the growth of a neurofibroma. These benign peripheral nerve sheath tumors (BPNST) are composed of a mixture of Schwann cells, fibroblasts, perineural cells, and mast cells (Le and Parada, 2007). Neurofibromas can form as cutaneous or subcutaneous masses,

or as plexiform lesions that involve multiple nerve fascicles, often invading the surround tissue or blood vessels (Ferner, 2010). Cutaneous neurofibromas occur in 99% of NF1 patients, and while they are unable to undergo malignant transformation, they are often a source of psychological distress due to disfigurement. Subcutaneous and plexiform neurofibromas develop on peripheral nerves in approximately 60% of NF1 patients. These tumors often cause pain and neurological impairment, and can undergo malignant transformation. NF1 patients have a 10% life-time chance of developing a malignant peripheral nerve sheath tumor (MPNST), which usually arises from a pre-existing neurofibroma (Patil, 2012). Individuals with NF1 are also at increased risk of developing brain tumors. The most common tumor found in the brain are low-grade pilocytic astrocytomas in the optic nerve and chiasm, occurring 20% of the time (Listernick, Louis et al. 1997). Cerebral gliomas, including the most malignant form, glioblastoma multiforme (GBM), are also observed in NF1 patients (Brems et al., 2009; Rosenfeld et al., 2010; Brokinkel et al., 2013).

Gliomas are the most common primary cancers of the central nervous system (Lim et al., 2011). They comprise a heterogeneous group of tumors that histologically resemble glial cells, including astrocytes and oligodendrocytes. Clinically, they are described as astrocytomas, oligodendrogliomas, ependyomas, and mixed gliomas. Astrocytomas are the most common of these types of tumors, and are classified by the World Health Organization (WHO) into four different grades (Louis et al., 2007). Grades I and II astrocytomas are low-grade and less aggressive tumors, whereas Grades III and IV are malignant. Malignant astrocytomas are characterized by their high proliferation rate (Grade III) and the presence of necrotic tissue and angiogenic activity (Grade IV). Grade IV astrocytoma, also referred to as glioblastoma multiforme (GBM), accounts for the majority of astrocytomas and has a median survival of less

than two years, making it one of the most lethal of all cancers (Huse et al., 2013). The propensity to develop manifestations throughout the nervous system has provided valuable insight of the role of *NF1* and the RAS/RAF/MAPK pathway in nervous system cancers, and has paved the way for the development of mouse models.

Murine homologs for *Nf1* have been knocked out via homologous recombination (Gutmann and Giovannini 2002). $Nf1^{-/-}$ mice die during embryogenesis due to cardiac development failure while $Nf1^{+/-}$ mice show no hallmark of the human NF1 phenotype (Brannan et al., 1994; Jacks et al., 1994). Chimeric mice bearing $Nf1^{-/-}$ cells develop plexiform neurofibromas, suggesting that *Nf1* loss of heterozygosity (LOH), or *Nf1* gene dosage, is essential for NF initiation. However, no dermal neurofibromas were reported (Cichowski et al., 1999). *Nf1* conditional knockout mice were since generated by multiple groups. Schwann cell- and astrocyte-specific ablation of *Nf1* leads to plexiform neurofibromas and optical nerve gliomas only in the presence of heterozygous state of tumor environment, suggesting that NF initiation may not be entirely cell intrinsic and that other cell types, such as $Nf1^{+/-}$ mast cells or fibroblasts, could be critical for disease development (Zhu et al., 2002; Bajenaru et al., 2003). In searching for pathways responsible for the malignant transformation, $Nf1^{+/-}$ mice were crossed onto *p53* null background. Mice with mutations in both genes developed soft tissue tumors resembling MPNSTs, however these tumors arose spontaneously and not from a pre-existing neurofibroma, as seen in NF1 patients (Cichowski et al., 1999; Vogel et al., 1999). While these models have provided valuable insight into NF1, the failure to recapitulate the full disease spectrum seen in humans, such as neurofibroma-to-MPNST transition and brain gliomas, suggests that additional genetic changes are required, and/or alternative initiating cell-types are involved.

In many cell types, RAS signaling leads to increased activation of downstream effector pathways, such as PI3K/AKT/mTOR (Figure 1) (Dasgupta et al., 2005). The PI3K/AKT/mTOR pathway is negatively regulated by the phosphatase PTEN (Stiles et al., 2004). PTEN's lipid phosphatase activity has been demonstrated both *in vitro* and *in vivo* to play a critical role in the receptor tyrosine kinase (RTK) growth pathway by acting as an antagonist to phosphotidylinositol-3-kinase (PI3K)/AKT signaling. When PI3K is recruited to the membrane upon RTK activation, it phosphorylates phosphotidylinositol-4,5-diphosphate (PIP_2) to form phosphotidylinositol-3,4,5-triphosphate (PIP_3). PTEN is a phosphatase specific for the 3-position of the inositol ring on PIP_3. PTEN antagonizes PI3K by dephosphorylating PIP_3 back to PIP_2 (Maehama and Dixon 1998; Sun et al., 1999). If PTEN function is lost due to mutation or deletion, PIP_3 accumulates in the cell and induces phosphorylation and activation of signaling molecules such as AKT, which are critical in controlling cell size, cell migration, proliferation, differentiation and apoptosis, all of which are important in normal development and tumorigenesis (Stambolic et al., 1998; Radimerski et al., 2002; Stiles et al., 2002; Stocker et al., 2002).

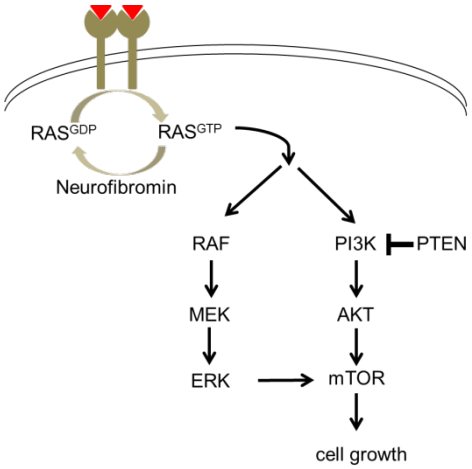

Figure 1. Regulation of neuroglial cell proliferation. Ras activation following neurofibromin loss leads to high levels of RAF/MEK/ERK and PI3K/AKT/mTOR activity. The PI3K axis is regulated by the phosphatase PTEN.

Deletion of *Pten* in mouse models revealed that PTEN is critical for animal development. *Pten* null embryos die early during embryogenesis (Di Cristofano et al., 1998; Stambolic et al., 1998; Suzuki et al., 1998; Podsypanina et al., 1999), thus precluding further studies on PTEN's function during brain development. In order to better understand the function of PTEN, our lab

as well as other groups generated *Pten*$^{loxp/loxp}$ mice (Lesche et al., 2002) and used Cre-loxP technology to conditionally delete *Pten* in different regions of the brain and at different developmental stages (Backman et al., 2001; Groszer et al., 2001; Kwon et al., 2001; Marino et al., 2002; Fraser et al., 2004; Yue et al., 2005). By conditionally deleting *Pten* in the embryonic and adult neural stem cells (NSC), we showed that PTEN negatively regulates embryonic and adult NSC/progenitor cell proliferation, survival, and self-renewal, both *in vivo* and *in vitro* (Groszer et al., 2001; Gregorian et al. 2009). PTEN regulates NSC/progenitor cell function, at least in part, by promoting G0-G1 cell cycle transition and reducing their growth factor dependency (Groszer et al., 2006). Furthermore, PTEN negatively regulates p53 (Freeman et al., 2003), a tumor suppressor responsible for NFs progression (Cichowski et al., 1999; Vogel et al., 1999; Robanus-Maandag et al., 2004).

Many studies using either primary tumor tissue or established tumor cell lines demonstrated high frequencies of *PTEN* mutation/deletion in various human cancers, including brain, bladder, breast, prostate and endometrial cancers, making *PTEN* one of the most frequently mutated human tumor suppressor gene (Stiles et al., 2004). Importantly, survey of GBM has indicated that *PTEN* and *NF1* are two of the top three gene mutations, occurring in 36% and 18%, respectively (Cancer Genome Atlas, 2008). In addition to these, 88% of GBM samples harbored mutations along the PI3K and MAPK pathways, suggesting that of coordinate activation of these two networks is critical in neurological cancers.

In addition to the genetic lesions that cause malignancy, the cellular origins of these cancers remain an intense field of study. It is generally agreed that the neurofibroma-initiating cell is derived from the Schwann cell lineage, yet the precise cell remains elusive (Carroll and Ratner, 2008). Gliomas, on the other hand, have been proposed to originate from transformed

neural stem cells (NSCs) residing in the largest germinal zone in the brain, the subventricular zone (SVZ) (Lim et al., 2007). However, many NSC subtypes reside in this vast germinal niche and are organized in a region-specific pattern (Merkle et al., 2007). Therefore, the precise cell of origin of gliomas also remains elusive.

This dissertation seeks to shed light on the molecular requirements and cellular origins of neurological tumors, as well as to evaluate the efficacy of small molecule inhibitors. We use Cre-loxP technology driven by the mouse *GFAP* promoter (line 77.6) (Figure 2) to activate, individually and simultaneously, the PI3K and MAPK pathways in the murine nervous system. This Cre line is expressed in the dorsal root ganglia in the peripheral nervous system (PNS) at E13.5, and in the subventricular zone (SVZ) at birth. We find that with RAS activation, malignant tumors form throughout the peripheral and central nervous systems in a PTEN dose-dependent manner. In Chapter 2, we find that loss of PTEN is a critical rate-limiting step in the development of neurofibromas and subsequent malignant transformation. Furthermore, we use this model to test the efficacy of small molecule inhibitors, which we later expand to patient-derived MPNST xenograft models. In Chapter 3, we develop another model that manifests the CNS hallmarks of NF1, such as optic nerve tumors and malignant cerebral gliomas. We utilize this model to examine the cellular origins of malignant gliomas, and find that tumors initiate from a particular neurogenic region in the brain called the subcallosal zone (SCZ), which has never been implicated in glioma biology. These results have direct implications regarding the coordination of pathway activation and cell-types of cancers of the nervous system.

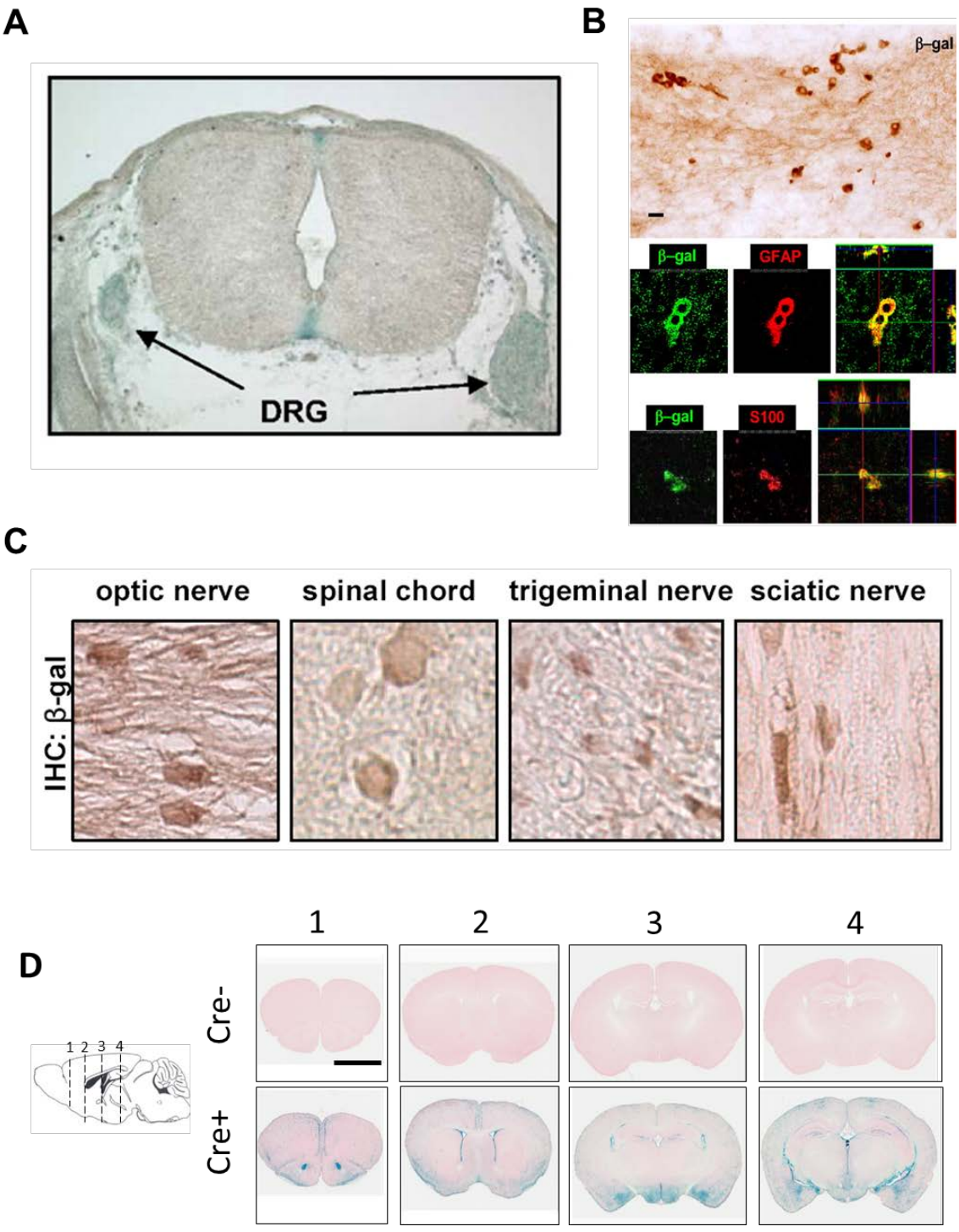

Figure 2. ***mGFAP*-Cre^{+} 77.6 expression in the murine central and peripheral nervous systems.** (A) X-gal staining of DRG of E13.5 embryo. (B) Co-localization of β-gal+ cells with endogenous GFAP and S100 expression on E13.5 embryo. (C) Survey images of β-gal reporter in the peripheral nerves of the adult mouse. (D). X-gal expression in the adult brain of coronal sections (right) corresponding to the schematic of the rostrocaudal axis of the murine brain (left).

Chapter 1 References

American Cancer Society (2013). Cancer Facts and Figures 2013. Atlanta: American Cancer Society

Backman SA, Stambolic V, Suzuki A, Haight J, Elia A, Pretorius J, Tsao MS, Shannon P, Bolon B, Ivy GO, Mak TW (2001). Deletion of Pten in mouse brain causes seizures, ataxia and defects in soma size resembling Lhermitte-Duclos disease. Nat Genet *29*: 396-403.

Bajenaru ML, Hernandez MR, Perry A, Zhu Y, Parada LF, Garbow JR, Gutmann DH (2003). Optic nerve glioma in mice requires astrocyte Nf1 gene inactivation and Nf1 brain heterozygosity. Cancer Res. *63*:8573-7.

Brannan CI, Perkins AS, Vogel KS, Ratner N, Nordlund ML, Reid SW, Buchberg AM, Jenkins NA, Parada LF, Copeland NG (1994). Targeted disruption of the neurofibromatosis type-1 gene leads to developmental abnormalities in heart and various neural crest-derived tissues. Genes Dev. *8*: 1019-29.

Brems H, Beert E, de Ravel T, Legius E (2009). Mechanisms in the pathogenesis of malignant tumours in neurofibromatosis type 1. Lancet Oncol. *10*: 508-15.

Brokinkel B, Schober O, Ewelt C, Heindel W, Hargus G, Stummer W, Holling M, Wölfer J (2013). Cerebellar Anaplastic Astrocytoma in an Adult with Neurofibromatosis Type 1: Case Report and Review of Literature. J Neurol Surg A Cent Eur Neurosurg. Advanced online publication.

Cancer Genome Atlas Research Network (2008). Comprehensive genomic characterization defines human glioblastoma genes and core pathways. Nature. *455*:1061-8.

Carroll SL, Ratner N (2008). How does the Schwann cell lineage form tumors in NF1? Glia. *56*: 1590-605.

Chen YH, Gutmann DH (2013). The molecular and cell biology of pediatric low-grade gliomas. Oncogene. Advanced online publication.

Cichowski K, Shih TS, Schmitt E, Santiago S, Reilly K, McLaughlin ME, Bronson RT, Jacks T (1999). Mouse models of tumor development in neurofibromatosis type 1. Science. *286*: 2172-6.

Dasgupta B, Yi Y, Chen DY, Weber JD, Gutmann DH (2005). Proteomic analysis reveals hyperactivation of the mammalian target of rapamycin pathway in neurofibromatosis 1-associated human and mouse brain tumors. Cancer Res. *65*: 2755-60.

Di Cristofano A, Pesce B, Cordon-Cardo C, Pandolfi PP (1998). Pten is essential for embryonic development and tumour suppression. Nat Genet *19*: 348-55.

Ferner RE (2007). Neurofibromatosis 1 and neurofibromatosis 2: a twenty first century perspective. Lancet Neurol. *6*: 340-51.

Ferner RE, Huson SM, Thomas N, Moss C, Willshaw H, Evans DG, Upadhyaya M, Towers R, Gleeson M, Steiger C, Kirby A (2007). Guidelines for the diagnosis and management of individuals with neurofibromatosis 1. J Med Genet. *44*: 81-8.

Ferner RE (2010). The neurofibromatoses. Pract Neurol. *10*: 82-93

Fraser MM, Zhu X, Kwon CH, Uhlmann EJ, Gutmann DH, Baker SJ (2004). Pten loss causes hypertrophy and increased proliferation of astrocytes in vivo. Cancer Res. *64*: 7773-9.

Freeman DJ, Li AG, Wei G, Li HH, Kertesz N, Lesche R, Whale AD, Martinez-Diaz H, Rozengurt N, Cardiff RD, Liu X, Wu H (2003). PTEN tumor suppressor regulates p53 protein levels and activity through phosphatase-dependent and -independent mechanisms. Cancer Cell. *3*:117-30.

Gregorian C, Nakashima J, Le Belle J, Ohab J, Kim R, Liu A, Smith KB, Groszer M, Garcia AD, Sofroniew MV, Carmichael ST, Kornblum HI, Liu X, Wu H (2009). Pten deletion in adult neural stem/progenitor cells enhances constitutive neurogenesis. J Neurosci. *29*:1874-86.

Groszer M, Erickson R, Scripture-Adams DD, Lesche R, Trumpp A, Zack JA, Kornblum HI, Liu X, Wu H (2001). Negative regulation of neural stem/progenitor cell proliferation by the Pten tumor suppressor gene in vivo. Science. *294*: 2186-9.

Groszer M, Erickson R, Scripture-Adams DD, Dougherty JD, Le Belle J, Zack JA, Geschwind DH, Liu X, Kornblum HI, Wu H (2006). PTEN negatively regulates neural stem cell self-renewal by modulating G0-G1 cell cycle entry. Proc Natl Acad Sci U S A. *103*: 111-6.

Gutmann, D. H. and M. Giovannini (2002). Mouse models of neurofibromatosis 1 and 2. Neoplasia *4*: 279-90.

Huse JT, Holland E, DeAngelis LM (2013). Glioblastoma: molecular analysis and clinical implications. Annu Rev Med. *64*: 59-70.

Jacks T, Shih TS, Schmitt EM, Bronson RT, Bernards A, Weinberg RA(1994). Tumour predisposition in mice heterozygous for a targeted mutation in Nf1. Nat Genet. *7*: 353-61.

Kwon CH, Zhu X, Zhang J, Knoop LL, Tharp R, Smeyne RJ, Eberhart CG, Burger PC, Baker SJ (2001). Pten regulates neuronal soma size: a mouse model of Lhermitte-Duclos disease. Nat Genet. *29*:404-11.

Le LQ, Parada LF (2007). Tumor microenvironment and neurofibromatosis type I: connecting the GAPs. Oncogene. *26*: 4609-16.

Lesche R, Groszer M, Gao J, Wang Y, Messing A, Sun H, Liu X, Wu H (2002). Cre/loxP-mediated inactivation of the murine Pten tumor suppressor gene. Genesis *32*: 148-9.

Lim SK, Llaguno SR, McKay RM, Parada LF (2011). Glioblastoma multiforme: a perspective on recent findings in human cancer and mouse models. BMB Rep. *44*: 158-64.

Listernick, R., D. N. Louis, et al. (1997). Optic pathway gliomas in children with neurofibromatosis 1: consensus statement from the NF1 Optic Pathway Glioma Task Force. Ann Neurol *41*: 143-9.

Louis DN, Ohgaki H, Wiestler OD, Cavenee WK, Burger PC, Jouvet A, Scheithauer BW, Kleihues P (2007). The 2007 WHO classification of tumours of the central nervous system. Acta Neuropathol. *114*: 97-109.

Maehama T, Dixon JE (1998). The tumor suppressor, PTEN/MMAC1, dephosphorylates the lipid second messenger, phosphatidylinositol 3,4,5-trisphosphate. J Biol Chem *273*: 13375-8.

Marino S, Krimpenfort P, Leung C, van der Korput HA, Trapman J, Camenisch I, Berns A, Brandner S (2002). PTEN is essential for cell migration but not for fate determination and tumourigenesis in the cerebellum. Development. *129*:3513-22.

Merkle FT, Mirzadeh Z, Alvarez-Buylla A (2007). Mosaic organization of neural stem cells in the adult brain. Science. *317*:381-4.

Patil S, Chamberlain RS (2012). Neoplasms associated with germline and somatic NF1 gene mutations. Oncologist. *17*:101-16.

Podsypanina K, Ellenson LH, Nemes A, Gu J, Tamura M, Yamada KM, Cordon-Cardo C, Catoretti G, Fisher PE, Parsons R (1999). Mutation of Pten/Mmac1 in mice causes neoplasia in multiple organ systems. Proc Natl Acad Sci U S A *96*: 1563-8.

Radimerski T, Montagne J, Hemmings-Mieszczak M, Thomas G (2002). Lethality of Drosophila lacking TSC tumor suppressor function rescued by reducing dS6K signaling. Genes Dev. 2002 *16*: 2627-32.

Reed N, Gutmann DH (2001). Tumorigenesis in neurofibromatosis: new insights and potential therapies. Trends Mol Med. *7*: 157-62.

Robanus-Maandag E, Giovannini M, van der Valk M, Niwa-Kawakita M, Abramowski V, Antonescu C, Thomas G, Berns A (2004). Synergy of Nf2 and p53 mutations in development of malignant tumours of neural crest origin. Oncogene. *23*: 6541-7.

Rosenfeld A, Listernick R, Charrow J, Goldman S (2010). Neurofibromatosis type 1 and high-grade tumors of the central nervous system. Childs Nerv Syst. *26*: 663-7

Stambolic V, Suzuki A, de la Pompa JL, Brothers GM, Mirtsos C, Sasaki T, Ruland J, Penninger JM, Siderovski DP, Mak TW (1998). Negative regulation of PKB/Akt-dependent cell survival by the tumor suppressor PTEN. Cell. *95*: 29-39.

Stiles B, Gilman V, Khanzenzon N, Lesche R, Li A, Qiao R, Liu X, Wu H (2002). Essential role of AKT-1/protein kinase B alpha in PTEN-controlled tumorigenesis. Mol Cell Biol. *22*: 3842-51.

Stiles B, Groszer M, Wang S, Jiao J, Wu H (2004). PTENless means more. Dev Biol *273*: 175-84.

Stocker H, Andjelkovic M, Oldham S, Laffargue M, Wymann MP, Hemmings BA, Hafen E (2002). Living with lethal PIP3 levels: viability of flies lacking PTEN restored by a PH domain mutation in Akt/PKB. Science. *295*: 2088-91.

Sun H, Lesche R, Li DM, Liliental J, Zhang H, Gao J, Gavrilova N, Mueller B, Liu X, Wu H (1999). PTEN modulates cell cycle progression and cell survival by regulating phosphatidylinositol 3,4,5,-trisphosphate and Akt/protein kinase B signaling pathway. Proc Natl Acad Sci U S A. *96*: 6199-204.

Suzuki A, de la Pompa JL, Stambolic V, Elia AJ, Sasaki T, del Barco Barrantes I, Ho A, Wakeham A, Itie A, Khoo W, Fukumoto M, Mak TW (1998). High cancer susceptibility and embryonic lethality associated with mutation of the PTEN tumor suppressor gene in mice. Curr Biol *8*: 1169-78.

Vogel KS, Klesse LJ, Velasco-Miguel S, Meyers K, Rushing EJ, Parada LF (1999). Mouse tumor model for neurofibromatosis type 1. Science. *286*: 2176-9.

Yue Q, Groszer M, Gil JS, Berk AJ, Messing A, Wu H, Liu X (2005). PTEN deletion in Bergmann glia leads to premature differentiation and affects laminar organization. Development. *132*: 3281-91.

Zhu, Y. and L. F. Parada (2002). The molecular and genetic basis of neurological tumours. Nat Rev Cancer *2*: 616-26

Zhu Y, Ghosh P, Charnay P, Burns DK, Parada LF (2002). Neurofibromas in NF1: Schwann cell origin and role of tumor environment. Science. *296*: 920-2.

Chapter 2:

PTEN Dosage is Essential for Neurofibroma Development and Malignant Progression

Introduction

Neurofibromatosis type 1 (NF1) is an autosomal dominant disorder with the propensity to develop nerve sheath tumors (Riccardi et al., 1994; Gutmann and Giovannini 2002; Theos and Korf 2006). The hallmark of neurofibromatosis type 1 (NF1) is the development of multiple benign (neurofibromas, WHO Grade I) and malignant peripheral-nerve-sheath tumors (MPNSTs, WHO Grade III-IV) which either arise from pre-existing neurofibromas or are formed *de novo* in the peripheral nervous system (PNS) (Zhu and Parada 2002). MPNSTs carry a particularly poor prognosis with a 5-year disease specific mortality of up to 75%. These malignancies respond poorly to conventional systemic chemotherapeutics often rendering surgical resection as the only viable treatment option (Grobmyer et al., 2008).

This hereditary disorder occurs in 1 in every 3000 individuals and is caused by mutations in the *NF1* tumor suppressor gene. The protein product, neurofibromin, is a RAS-GTPase-activating protein (RAS-GAP) that negatively regulates RAS activity. Murine homologs for *Nf1* have been knocked out via homologous recombination (Gutmann and Giovannini 2002). $Nf1^{-/-}$ mice die during embryogenesis due to cardiac development failure while $Nf1^{+/-}$ mice show no hallmark of the human NF1 phenotype (Brannan et al., 1994; Jacks et al., 1994). Chimeric mice bearing $Nf1^{-/-}$ cells do develop plexiform neurofibromas, suggesting that *Nf1* loss of heterozygosity (LOH) is essential for NF initiation. However, no dermal neurofibromas were reported (Cichowski et al., 1999). *Nf1* conditional knockout mice were since generated by multiple groups. Deletion of *Nf1* using Cre recombinase driven by the *Krox20* promoter, which is expressed in mature Schwann cells at E15.5, leads to Schwann cell hyperplasia without neurofibroma development (Zhu et al., 2002). In contrast, deletion via the *Desert Hedgehog* (*Dhh*)-*Cre* driver, expressed in Schwann cell precursors at E12.5, induces dermal and plexiform

neurofibromas (Wu et al., 2008). Other models develop plexiform neurofibromas and optical nerve gliomas only in the presence of heterozygous state of tumor environment, suggesting that NF initiation may not be entirely cell intrinsic and that other cell types, such as *Nf1*$^{+/-}$ mast cells or fibroblasts, could be critical for disease development (Bajenaru et al., 2003). In searching for pathways responsible for the malignant transformation, *Nf1*$^{+/-}$ mice were crossed onto *p53* null background. Although neither *p53* null nor *Nf1*$^{+/-}$ mice develop MPNSTs, mice with mutations in both genes develop soft tissue tumors resembling MPNSTs (Cichowski et al., 1999; Vogel et al., 1999).

The failure of *Nf1*$^{+/-}$ to recapitulate the disease spectrum seen in humans suggests that additional genetic changes are required for malignant phenotypes. Since RAS activity can stimulate PI3K activation, we sought to investigate the collaborative effects of RAS/RAF/MAPK pathway activation with alterations of other major intracellular pathways, such as those controlled by the PI3K/AKT/mTOR pathway.

The PI3K/AKT pathway is negatively regulated by the PTEN (phosphatase and tensin homologue deleted on chromosome 10) tumor suppressor (Stiles et al., 2004). PTEN has been identified to be frequently mutated/deleted somatically in various human cancers, including GBM (Li et al., 1997; Steck, Pershouse et al. 1997; Li, Simpson et al. 1998). Germ line mutations in the *PTEN* gene have been associated with Cowden syndrome and related diseases in which patients develop macrocephaly of the brain (Liaw et al., 1997; Nelen et al., 1997) . By conditionally deleting *Pten* in the embryonic and adult neural stem cells (NSC) driven by *Nestin* and *GFAP* promoters, respectively, we showed that PTEN negatively regulates embryonic and adult NSC/progenitor cell proliferation, survival, and self-renewal, both *in vivo* and *in vitro* (Groszer et al., 2001; Gregorian et al. 2009). PTEN regulates NSC/progenitor cell function, at

least in part, by promoting G0-G1 cell cycle transition and reducing their growth factor dependency (Groszer et al., 2006). Furthermore, PTEN negatively regulates p53 (Freeman et al., 2003), a tumor suppressor responsible for NFs progression (Cichowski et al., 1999; Vogel et al., 1999; Robanus-Maandag et al., 2004)..

To address the potential roles of PTEN/PI3K/AKT signaling pathways in NFs development, we utilized Cre-Loxp technology to perturb RAS/RAF/MAPK or PI3K/AKT/mTOR, two of the major signaling pathways known to be involved in tumorigenesis of the nervous system, individually or in combination. These efforts have yielded new mouse models with hallmark of human NF1, described herein.

Results

Pten haploinsufficiency and activation of *K-ras* leads to lethal NF1 phenotype

All *mGFAP-Cre*$^{+}$*; Pten*$^{loxp/+}$*; LSL-Kras*$^{G12D/+}$ mice (n=42) developed palpable nodules under the skin, starting at 4 months postnatal. The lesions varied in size and location, with the majority located on the backs and flanks of mice (Figure 1A). Histological analysis revealed the nodules as neurofibromas and MPNSTs (Figure 1B, C), closely resembling the hallmarks of human NF1. Neurofibromas contained delicate, elongated cells that were loosely ensheathed in a fibrous matrix (Figure 1B). MPNSTs were present in 100% of mice and were characterized as malignant based on their dedifferentiated morphology, disrupted tissue organization, and increased number of mitosis (Figure 1C). The median survival of mutant mice was 22 weeks (Figure 1D). Many MPNSTs also were characterized by an aggressively infiltrative growth pattern, with areas of residual neurofibroma, often plexiform type. These histologic features, in particular that of MPNSTs arising from pre-existing plexiform neurofibromas, are classic features of human NF1-associated MPNSTs.

When asymptomatic mutant mice were necropsied at an earlier age, multiple microscopic benign and plexiform neurofibromas were found (Figure 2). These tumors were not visible on macroscopic examination, indicating that estimates of tumor burden per animal were likely understated and that progression towards malignancy is a time-dependent event.

Since Cre expression is detected in the subventricular zone (SVZ), we examined the brains of mutant mice for the presence of abnormalities or tumors. Sagittal and coronal sectioning through the brain failed to detect alteration hydrocephaly, or any gross neoplastic lesions; in addition, no abnormalities were observed in optic, cranial, or spinal nerves (data not shown). However, significant increase of cellularity in the periventrical regions was observed in

the mutant lateral ventricles compared to control (Figure 3) or *Pten* heterozygous alone, suggesting that *Pten* haploinsufficiency and *K-Ras* activation is sufficient to cause neural stem/progenitor cells expansion in the periventrical regions. These results suggest synergy between PI3K and RAS pathways in neural stem/ progenitor cells in adult SVZ.

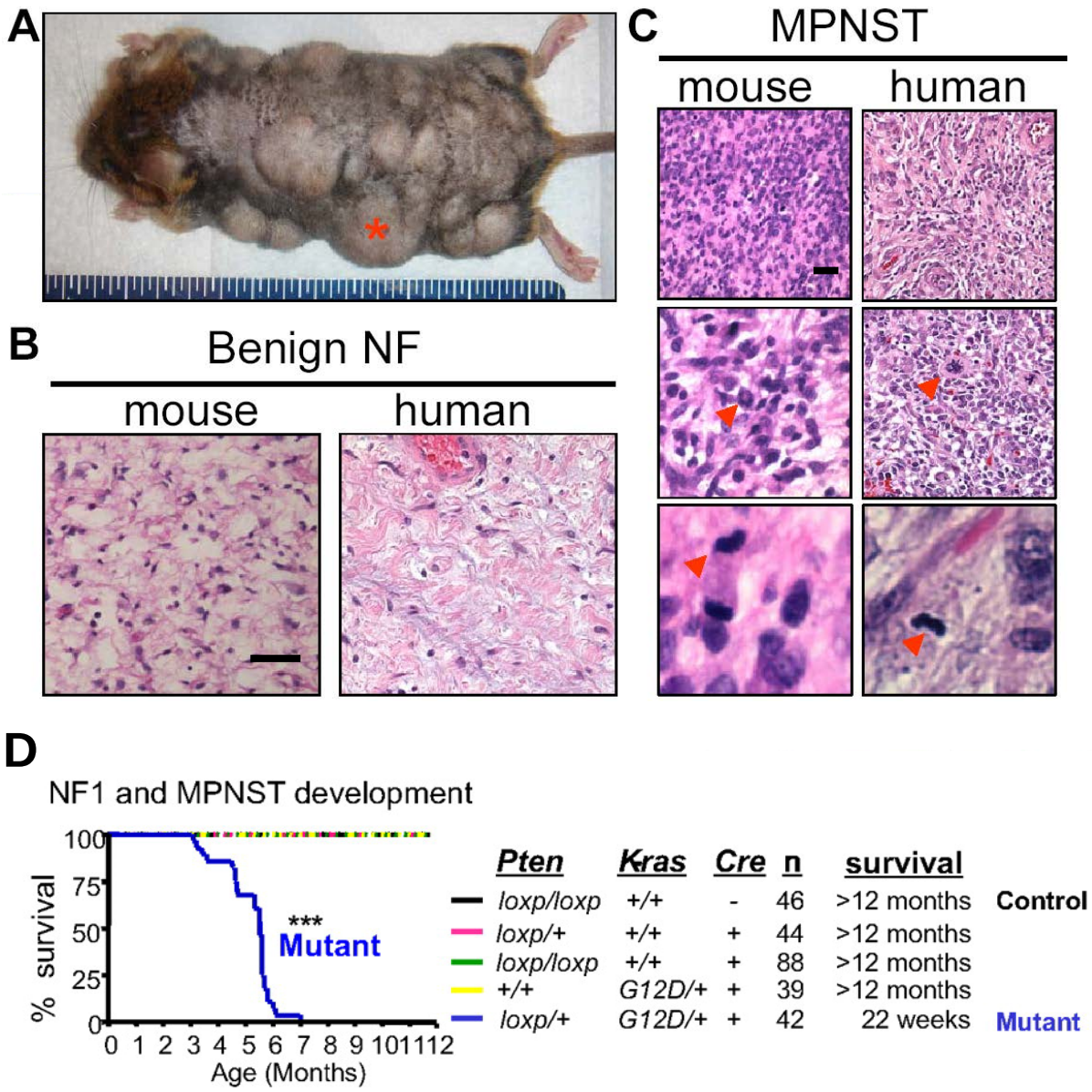

Figure 1. Manifestations of human-like NF1-associated peripheral tumors. (A) Representative picture of mutant mouse bearing multiple tumors. Tumor marked with an asterisk was the only protruding and visible mass. Other tumors were revealed upon removal of body hair. Tumors per animal ranged from 2 to 25 per animal. Ruler ticks: 1 mm. (B,C) Peripheral tumors were dissected, post-fixed, and subjected to immunohistochemical analysis which revealed presence of benign neurofibromas (NF) and malignant peripheral nerve sheath tumors (MPNSTs), common features of human NF1 (scale bar, 25 μm). Malignant tumors had increased cellularity (C, top panels), cellular anaplasia (nuclear pleomorphism, C, middle panels, arrows), and obvious mitoses (C, bottom panels, arrows), compared to benign tumors. (D) Median survival of 22 weeks.

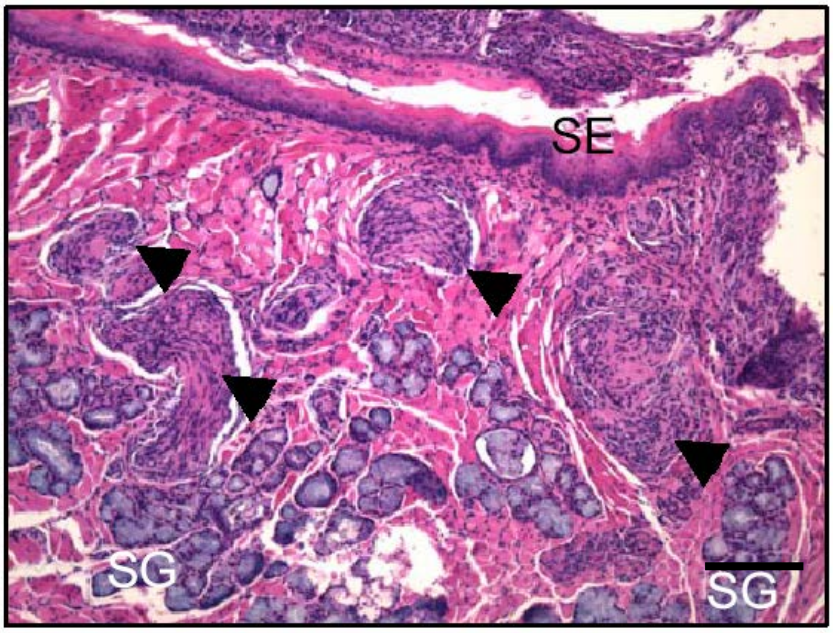

Figure 2. Representative picture of mutant mouse with plexiform neurofibromas. H&E stain of hard palate of mouse revealed multiple microscopic tumor nodules (arrows) which were classified as plexiform neurofibromas. SE, squamous epithelium; SG, salivary glands (scale bar, 155 µm).

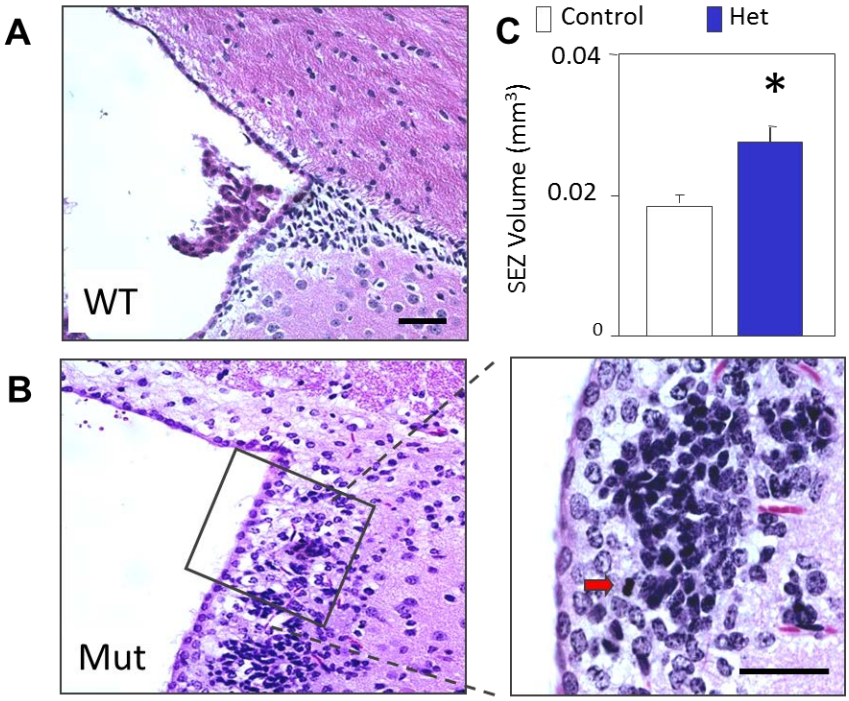

Figure 3. Adult NSC-specific activation of *K-Ras* and heterozygous deletion of *Pten* leads to increased cellularity in the SVZ. SVZ regions of control (A) and mutant mice (B). SVZ volumes were quantified (C) and mitotic figure is indicated by a red arrow in.

Pten LOH correlates with malignant transformation

MPNSTs were observed originating from a lower grade lesion resembling a plexiform neurofibroma (Figure 4A), a classic feature of NF1-associated MPNST. In addition, MPNSTs exhibited higher expression of the proliferation marker Ki-67 compared to neurofibromas (Figure 4B). We focused our attention on the transition region from neurofibroma to MPNST to determine the basis of malignant transformation. Staining for PTEN showed marked reduction in PTEN expression in all MPNSTs. P-AKT and P-S6, surrogate markers for PTEN-controlled PI3K activation, also showed enhanced reactivity in MPNSTs. In contrast, the NFs from which MPNST developed showed relatively normal PTEN expression, and low levels of P-AKT and P-S6. P-ERK, a downstream effector of K-Ras, was detected in both lesions, although MPNSTs showed significantly higher staining (Figure 4A). Additionally, quantitation of Ki-67 showed a higher proliferative index in MPNSTs than NFs, suggesting that PTEN controls malignant transformation, at least in part, by negatively regulating cell cycle.

Loss of PTEN expression of MPNST could result from destabilizing mutations in the PTEN protein, epigenetic silencing of *Pten* mRNA expression, or genetic loss of the second *Pten* allele. To determine the cause of PTEN loss, we first analyzed the WT *Pten* allele by PCR analysis. We found complete loss of the WT allele in three independent MPNSTs. In contrast, we did not detect any defects in *p53*, or *Nf1* (Figure 4C). This study clearly demonstrates that *Pten* LOH is essential for malignant transformation.

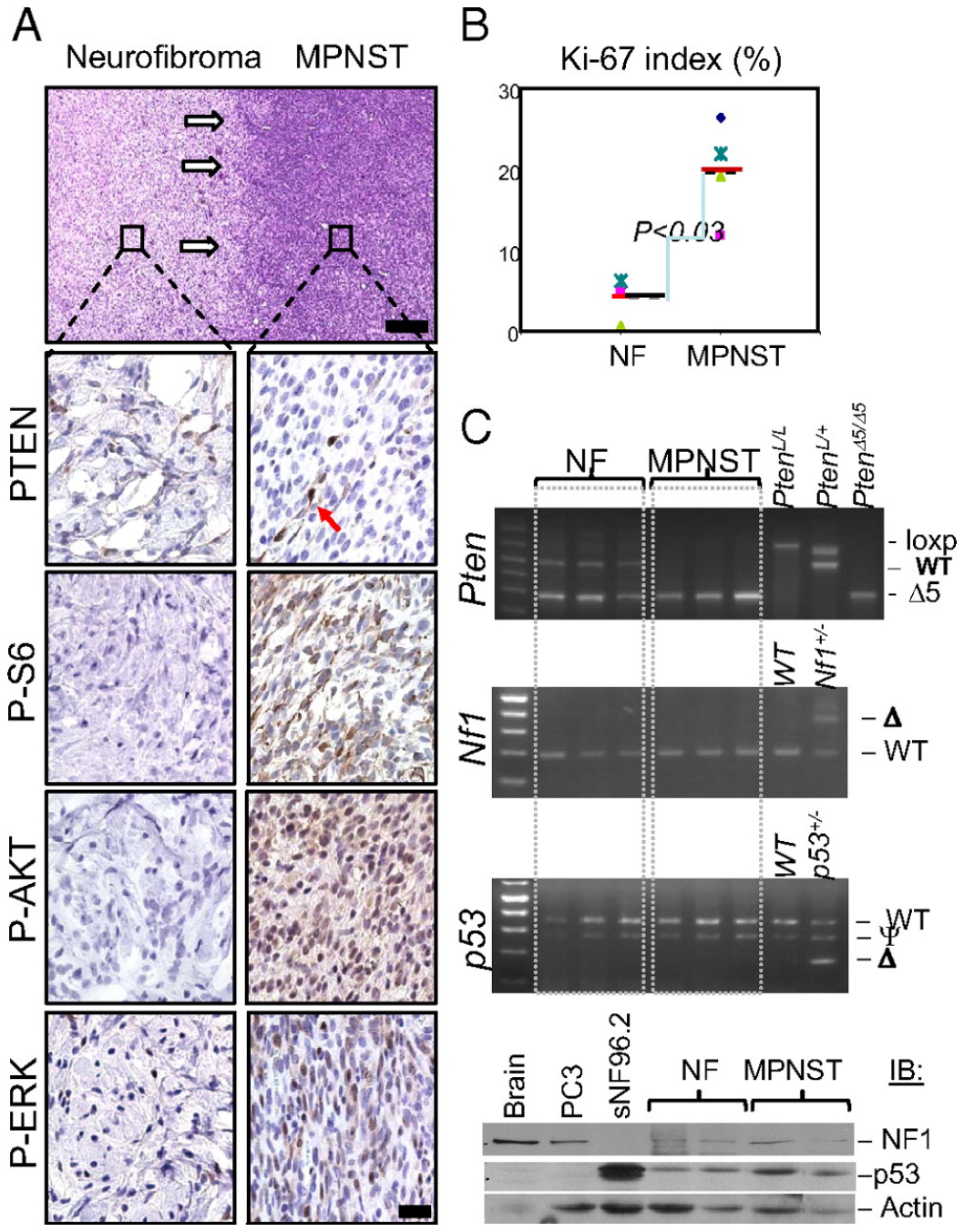

Figure 4. PTEN loss is critical for malignant transformation from benign neurofibroma in mice. (A) NF and MPNST are clearly demarcated (white arrows indicate "transition zone"). MPNSTs showed marked reduction in immunoreactivity for PTEN in tumor cells, with PTEN+ stained endothelial cells as an internal positive control (arrow). MPNSTs also show intensive staining with antibodies specific for surrogate markers of activated PI3K/AKT (P-AKT, P-S6) and RAS/MAPK (P-ERK) pathways. Scale bars, 150 µm (H&E) and 25 µm (IHC). (B) MPNSTs have higher Ki-67 labeling index than NF tumors ($P < 0.3$). (C) Upper three panels: PCR analysis of NF and MPNST tumor DNA from mutant mice, indicating loss of *Pten* WT allele and retaining of both *p53* and *Nf1* genes in MPNST lesions; lower panel, Western blot analysis showing NF1 and p53 proteins in NF and MPNST samples. PC3 and sNF96.2 are human cell lines used here as controls that are null for p53 and NF1, respectively.

Reduction of PTEN in human MPNST

The correlation of *Pten* loss and malignant progression in our NF murine model prompted us to examine if PTEN expression was reduced in human NF1-assosicated MPNSTs. We surveyed human MPNSTs (n=14) and, if possible, the NF from which they arose. Similar to our murine model, we found marked reduction in PTEN expression in all of the human MPNST samples (Figure 5A). Quantitative analysis revealed that 11 of the 14 samples had less than 20% PTEN positive tumor cells, with PTEN positive endothelial cells serving as an internal positive control (Figure 5B). Corresponding to PTEN loss, all MPNST samples had increased P-AKT and P-S6 expression, as well as P-ERK. Conversely, all NF samples (n=5) had increased PTEN staining, and low and sporadic levels of P-AKT, P-S6, and P-ERK staining patterns (Figure 5A). Similar to our murine model, quantification of proliferation by Ki-67 staining revealed increased proliferation in the MPNSTs compared to the NFs (Figure 5C). These results suggest that, similar to our murine model, loss of PTEN expression is important for malignant transformation of NF to MPNST.

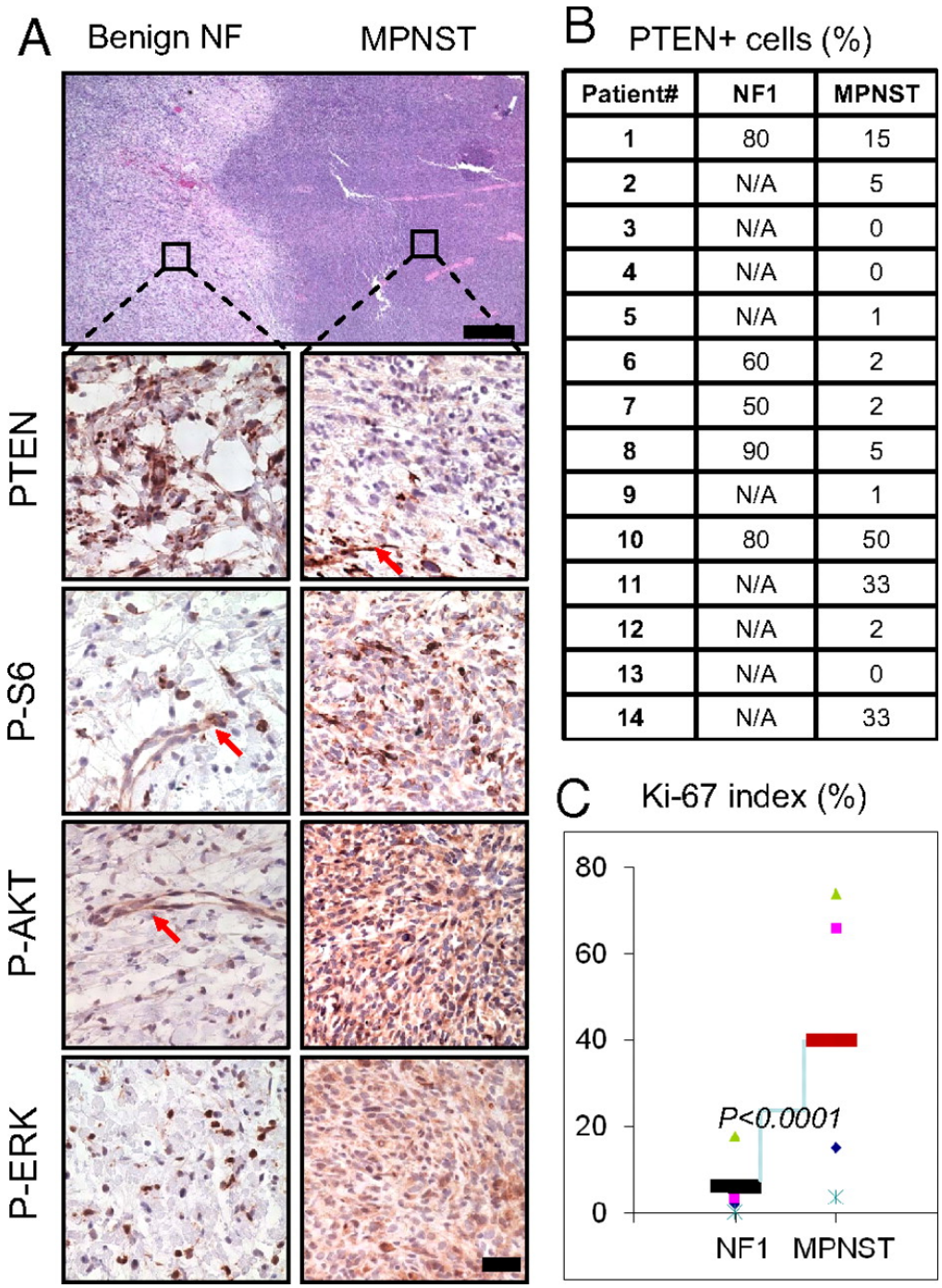

Patient#	NF1	MPNST
1	80	15
2	N/A	5
3	N/A	0
4	N/A	0
5	N/A	1
6	60	2
7	50	2
8	90	5
9	N/A	1
10	80	50
11	N/A	33
12	N/A	2
13	N/A	0
14	N/A	33

Figure 5. Decreased PTEN expression in human NF1-associated MPNSTs. (*A*) Histological and immunohistological analyses of transition zone of human NF-MPNST lesions demonstrate reduced PTEN expression (second right panel; arrows indicates PTEN+ vascular endothelial cells) and activated PI3K and RAS/MAPK pathways. Scale bars, 150 μm (H&E) and 25 μm (IHC). (*B*) Summary of PTEN IHC staining results, presented as percentages of PTEN+ tumor cells, of 14 NF1 patients with MPNST lesions. N/A, only MPNST samples are available. (*C*) Human MPNST tumors have higher Ki-67 labeling index than NF tumors (P _ 0.0001).

Distinguishing NF from MPNST using noninvasive PET/CT imaging

MPNSTs are diagnosed pathologically, often through needle core biopsies. Unfortunately, this procedure can yield inaccurate results due to the heterogeneous nature of these tumors. In addition, the location of the tumor can make obtaining a biopsy unfeasible. A noninvasive modality that can distinguish NF from MPNST would greatly contribute to the management of NF1 patients. Recent studies from UCLA and other investigators have shown that FDG-PET is a promising non-invasive imaging technique with the potential to distinguish benign from malignant tumors (Benz et al., 2010). We show here, in an NF1 patient with a left gluteal tumor, that the MPNST component has a 4.85-fold increase of FDG uptake relative to the benign region (SUVmax of MPNST = 6.3 g/mL vs. SUVmax of NF = 1.3 g/mL) (Figure 6A). Similar to human studies, we used noninvasive *in vivo* PET/CT imaging on our murine model to determine if we could monitor malignant transformation. Murine MPNSTs could be detected with FDG (n=10), whereas benign NFs were low or negative for FDG (n=29). As seen in Figure 6B, a mouse with three independent lesions had low FDG uptake in the two benign NFs (T1 and T2), and increased FDG uptake in the MPNST (T3) (Figure 6B, C). Importantly, malignant transformation was confirmed via histology, with the FDG-high MPNST showing increased cellularity, loss of PTEN expression, and massive angiogenesis (Figure 6D). Similar to our histopathological analysis, the percentage of animals with detectable FDG^{low} and FDG^{high} uptake was age-dependent (Figure 6E). Our results suggest that noninvasive FDG-PET can be used to monitor malignant transformation in NF1 patients and animal models, as well as provide a valuable noninvasive diagnostic strategy to assess potential therapeutic responses.

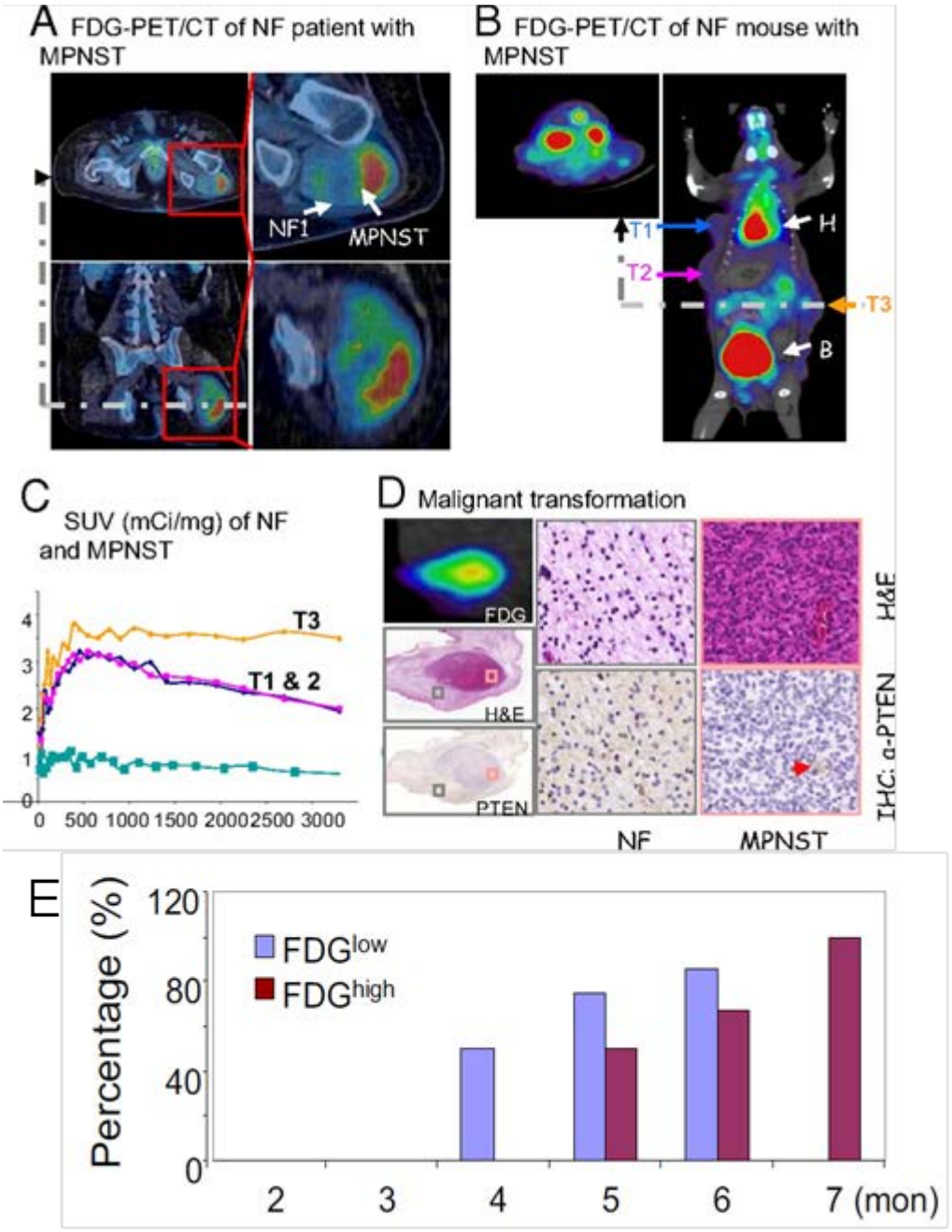

Figure 6. Noninvasive *in vivo* imaging of MPNST transformation within NF lesions. (*A*) FDG-PET/CT image of a NF1 patient with MPNST. (*B*) FDG-PET/CT image of a mutant mouse with three independent tumors: T1 and T2 are NF with low FDG intake, while T3 is MPNST with increased FDG intake. (*C*) The FDG-PET SUVs, measured from the ROI for each tumor, compared to baseline uptake (blue) measured from limb muscle without tumor. (*D*) Correlation of FDG uptake, H&E staining, and PTEN expression (left panels) in a NF lesion (gray boxed sample area, middle panels) with MPNST transformation (red boxed sample area, right panels). Red arrow points to PTEN+ vessel. T, tumor; H, heart; B, bladder. (E) Percentage of animals with detectable FDG^{low} and FDG^{high} uptake.

Evaluation of small molecule inhibitors on NF1 murine model using PET/CT

Diagnosis of MPNST (NF1 associated or spontaneous) carries a poor prognosis with a 5-year disease specific mortality of up to 75% (Eilber et al., 2004; Grobmyer et al., 2008). Unfortunately, MPSNTs respond poorly to conventional chemotherapeutic drugs (Eilber et al., 2006). Recent analyses demonstrated over expression of receptor tyrosine kinases in certain MPNSTs (Holtkamp, 2006) prompting preclinical and clinical evaluation of targeted therapies. Sorafenib is a multi-kinase inhibitor that has shown promising results in several UCLA patients with MPNST, resulting in a significant and durable reduction in tumor FDG uptake and improved outcome (data not shown). Since our mouse model provides a unique modality to evaluate therapeutic response to small molecule inhibitors, we initiated treatment with sorafenib alone and in combination with rapamycin to evaluate the efficacy of small molecule inhibitors on NF and MPNST.

Treatment with either drug alone was unable to block NF to MPNST transformation. Since our model is dependent upon activation of the PI3K/AKT/mTOR and RAS/RAF/MAPK pathways, we combined sorafenib with the mTOR inhibitor rapamycin. Daily treatment with both drugs was able to effectively block malignant transformation, based on FDG-PET/CT imaging and diagnostic pathology (Figure 7). Importantly, when applied to tumors that have undergone malignant transformation, sorafenib and rapamycin combination treatment lead to significant tumor necrosis and loss of FDG signal, a clear indication for tumor regression (Figure 7).

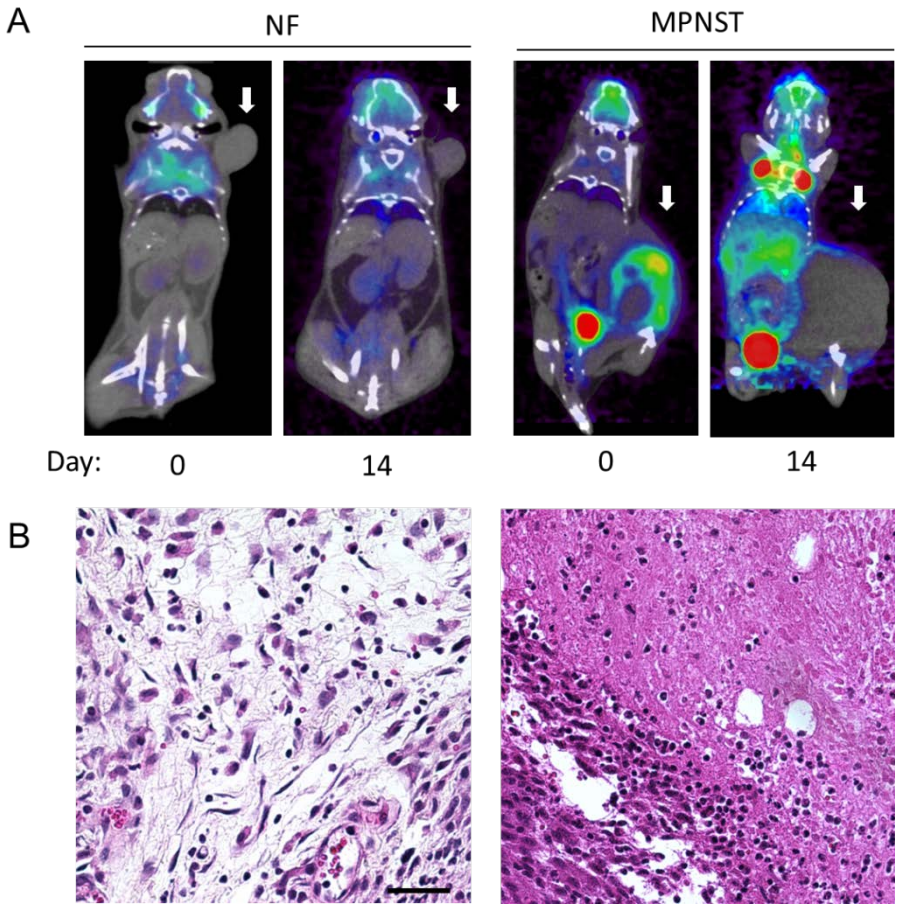

Figure 7. Sorafenib plus rapamycin treatment delays NF to MPNST progression and causes regression of MPNST. (A) FDG-PET/CT of NF mouse (left) shows delay of malignant progression of neurofibroma (arrow). MPNST mouse (right) shows reduction of FDG uptake in tumor (arrow). (B) Histology of treated tumors shows neurofibroma without malignant progression (left), and massive necrosis in MPNST (right). Scale bar, 25 μm.

Xenograft model

Genetically engineered models provide valuable insight into the biology of disease, however they cannot fully recapitulate the entire disease spectrum. Since UCLA is one of the busiest sarcoma centers in the United States, we sought to develop clinically relevant xenograft models from surgically resected tumors. Tissue obtained from 17 peripheral nerve sheath tumors (Schawnnoma, n=2; neurofibroma, n=4; NF-associated MPNST, n=4; spontaneous MPNST, n=7) was engrafted subcutaneously into the rear flanks of NOD-SCID/IL2rγ null mice. 9 of the 11 MPNSTs (4 NF-associated, 5 spontaneous) were able to engraft and be serially passaged at least twice. In contrast, none of the benign tumors were able to engraft, suggesting that xenograftability is dependent upon malignant transformation. Histological analysis revealed that pathological features from primary tumors were maintained in xenografts (Figure 8). These xenografts provide an additional novel platform for the evaluation of targeted therapies against MPNSTs.

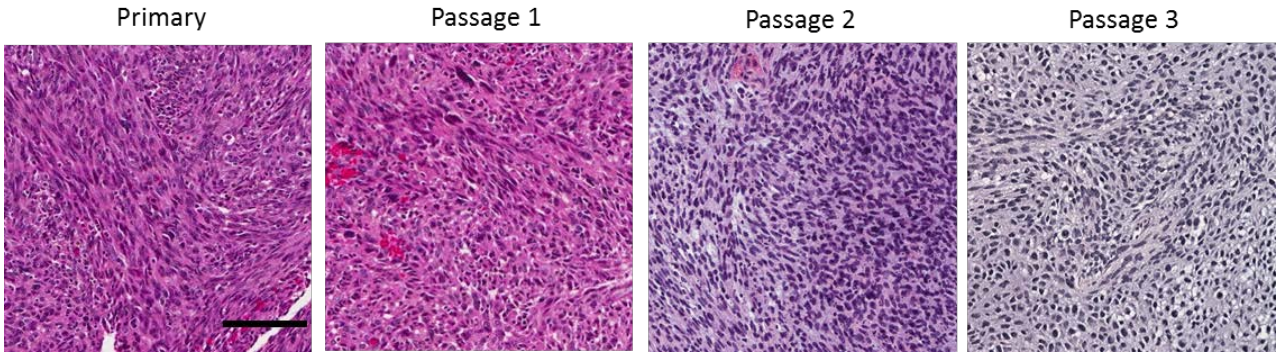

Figure 8. Histopathological features of human MPNSTs are maintained in xenografts over serial passages. Representative H&E sections from an NF1-associated MPNST. Scale bar, 100 μm.

Evaluation of small molecule inhibitors on a patient-derived MPNST xenograft model using FDG-PET/CT

Based on our treatment results from our genetically engineered murine model, we expanded our sorafenib and rapamycin treatment regime to our patient-derived MPNST model. We treated one xenograft line from an NF1-associated MPNST with rapamycin and sorafenib, individually and in combination, for a period of eleven days. Treatment with either drug resulted in significant decrease in tumor volume compared to control ($n=5$; $p<0.001$) (Figure 9A). Tumor response was monitored via FDG-PET/CT and showed different metabolic responses to each drug. Rapamycin, but not sorafenib, significantly reduced FDG-uptake in our human MPNST model (Figure 9B). Tumors were removed after eleven days of treatment and stained for proliferation markers and downstream effectors of the PI3K and MAPK pathways. Interestingly, we observed little to no change in P-S6 or P-ERK in tumors treated individually with rapamycin or sorafenib. Only the tumors treated with both drugs in combination showed reduced staining (Figure 9C). In contrast, staining and quantification of Ki-67 revealed that proliferation was significantly reduced with sorafenib and rapamycin individually, and even more so in combination ($p=0.006$, $p<0.001$, $p<0.0001$ respectively) (Figure 9C).

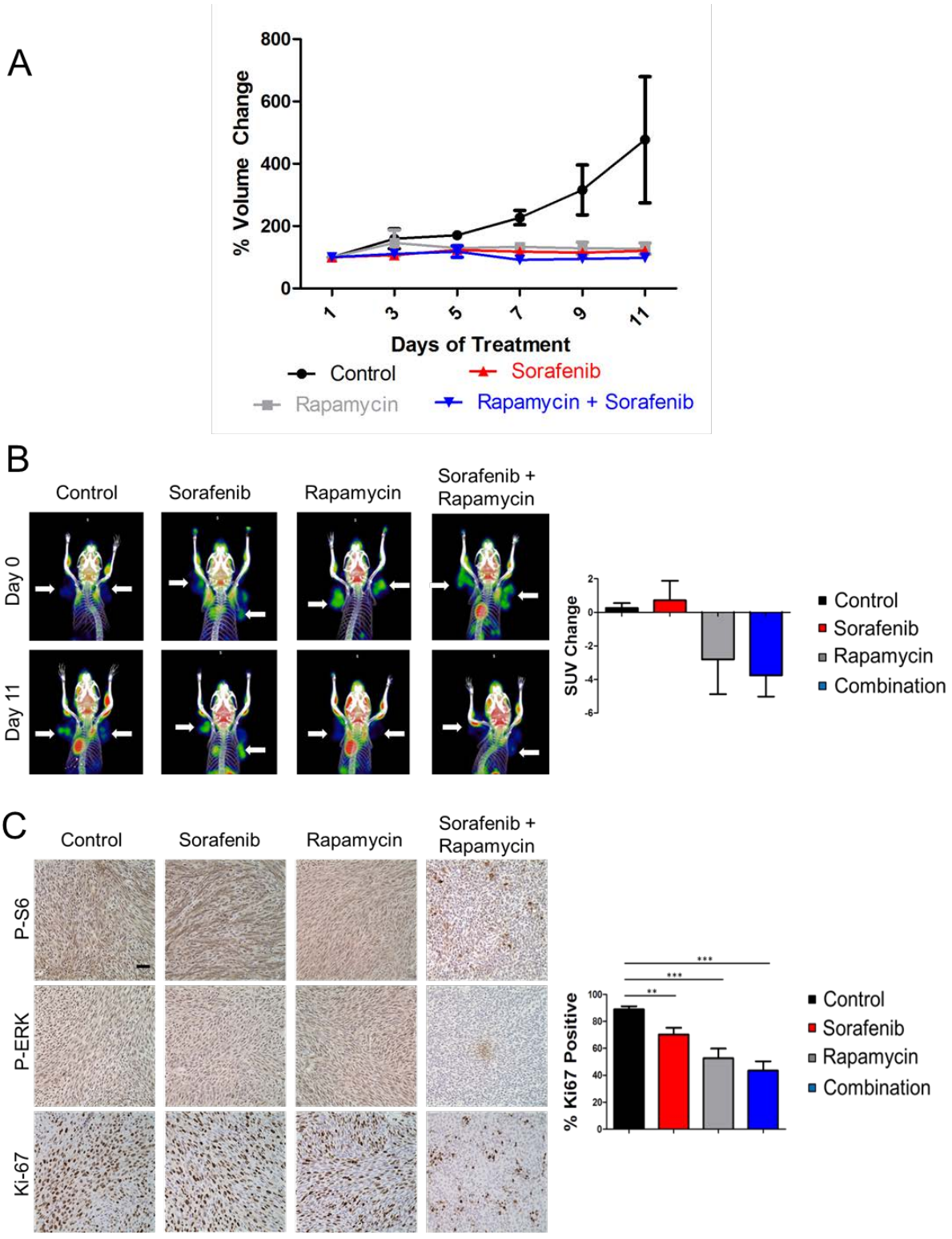

Figure 9. Sorafenib and rapamycin treatment on human NF1-associated MPNST xenograft induces metabolic, signaling pathway, and proliferative response. (A) Tumor volume change in response to treatment. (B) Decreased FDG uptake in rapamycin and combination treated tumors (arrows). (C) Reduction of P-S6, P-ERK, and Ki-67 in combination treated tumors. Scale bar, 50 µm.

Discussion

Generation of mouse mutants at suspected tumor suppressor and oncogene loci have provided important information about the underlying mechanisms of tumor formation. However, the original knockout of the *Nf1* gene as well as conditional knockout models that have been generated since did not reproduce the full disease spectrum observed in human. Here we describe a novel mouse model for NF1, which encompasses key features not observed in previously generated models for NFs. In addition, our data is the first demonstration of PI3K/AKT pathway activation and cooperation with RAS/MAPK pathway in PNS tumors associated with NFs.

Although RAS or PTEN mutations per se have not been identified in human NFs, several reports support the alteration of RAS or PTEN and the activation of their respective pathways in multiple cancers, including NFs. Several groups have identified constitutive Ras activation as a result of NF1 deletion (Basu et al., 1992; DeClue et al., 1992; Bollag et al., 1996). Previous studies have shown that Ras activity and its downstream effectors are elevated in the cortex and hippocampus of $NF1^{+/-}$ mice, leading to impairments in long-term potentiation, which is a key cellular apparatus of learning and memory (Costa et al., 2001; Li et al., 2005) and that the learning deficits in $Nf1^{+/-}$ mice can be rescued by decreasing Ras function either by genetic (crossing with the $K\text{-}Ras^{+/-}$ heterozygote) or pharmacologic manipulations (treated with farnesyl-transferase inhibitors of Ras) (Costa, Federov et al. 2002; Li et al., 2005). Although mice with oncogenic N-Ras expression in nerve and neural crest-derived cells mimic two previously unreported main features of human NF1, pigmentary abnormalities and dermal neurofibromas, additional characteristic tumors such plexiform neurofibromas, and astrocytomas were not detected (Saito et al., 2007). Since the three forms of Ras, (H, K, N) are expressed in different

cells, this could explain the absence of some of these tumor types in our model and the presence of various other tumors.

The *NF1* tumor suppressor gene is inherited as an autosomal-dominant trait, suggesting a possible gene dosage effect. In fact, haploinsufficiency is apparently enough to bring about many of the clinical manifestations seen in NF1 patients. However, consistent with the Knudson 'two-hit' model of tumorigenesis, loss of heterozygosity (LOH) in *NF1* is responsible for the formation of neurofibromas (Cichowski et al., 1999). On the other hand, the development of malignant cancers in NF1 individuals requires further acquisition of additional genetic aberrations, whether it is inactivation of *PTEN*, *TP53*, *CDKN2A* or amplification of platelet-derived growth factor receptor or epidermal growth factor receptor (Zhu et al., 2002; Castle et al., 2003; Levy et al., 2004; Stemmer-Rachamimov et al., 2004). Reminiscent of the malignancies seen in NF1 patients, compound heterozygous mice for both *Nf1* and *p53* develop malignant peripheral nerve sheath tumors with full penetrance, however these tumors develop *de novo,* and show no signs of a pre-existing neurofibroma. (Cichowski et al., 1999; Vogel et al., 1999). In addition, as NF1 has a spectrum of specific tumors, modifying genes and epigenetic phenomena have been shown to play a role in modulating NF1-associated tumor susceptibility (Easton et al., 1993; Reilly et al., 2004).

Consistent with this hypothesis, the conditional knockout mice for PTEN (Gregorian et al., 2009) or constitutive activation of K-Ras did not produce tumors. However, neurofibromas and MPNSTs were found in mice with both perturbations. Interestingly, neurofibromas had PTEN expression, while MPNSTs found in the same mice were inactivated for the wild-type *Pten* allele. When human samples were tested for PTEN expression, the results matched those found in mice. This demonstrates that PI3K/AKT activation is the rate limiting step in murine

and human MPNST. Since PTEN negatively regulates p53 (Freeman et al., 2003), it is not surprising that our model encompasses the MPNST formation found in mice compound heterozygous for both *p53* and *NF1* (Cichowski et al., 1999; Vogel et al., 1999).

Activation of multiple receptor tyrosine kinases have been found in MPNST, calling for the use of molecular targeted therapy (Holtcamp, 2006). Sorafenib is a multi-kinase inhibitor that has been approved for the treatment of renal cell and hepatocellular carcinomas (Hasskarl, 2010), and in phase 2 trial of advanced soft-tissue sarcomas (von Mehren et al., 2012). Sorafenib inhibits multiple receptor tyrosine kinases, such as VEGFR and PDGFR, as well as the intracellular RAF kinases. *In vitro*, sorafenib has been shown to inhibit proliferation and RAF-dependent MAPK activation in MPNST cells, resulting in a G(1) cell cycle arrest (Ambrosini et al., 2008). The loss PTEN observed in our murine model and in human samples provides a novel molecular axis to specifically target in the treatment of MPNST. Rapamycin is a small molecule inhibitor of the mTOR kinase (Ballou and Lin, 2008). However, inhibition of mTOR may cause feedback-dependent activation of upstream AKT and receptor tyrosine kinases, leading to therapeutic resistance (Sun et al., 2005; Rodrik-Outmezguine et al., 2011). Therefore, we reasoned that inhibiting both mTOR and RAF kinases would lead to increased therapeutic benefit. We observed that combination treatment with rapamycin and sorafenib was able to impede neurofibroma-to-MNPST transition in our murine model. Furthermore, combination treatment in established MPNSTs caused massive necrosis in the tumor, causing a reduction in FDG-uptake. Unfortunately, the 12.5% procurement rate of obtaining the correct genotype, coupled with the 5 month latency, makes high-throughput treatment studies difficult with this model. Therefore we turned to our patient-derived xenograft models. Although there was no difference in tumor size between single-treated and combination-treated cohorts, we found that

combination treatment was more effective in reducing FDG-uptake, proliferation, and downstream kinases of the PI3K and MAPK pathways. Glucose uptake and expression of the glucose transporter GLUT1 has been shown to be regulated by mTOR (Buller et al., 2008), which explains the decreased FGD uptake in rapamycin (single and combination) treated tumors. The decrease in proliferation is also consistent with previous reports showing that inhibition of mTOR prevents cell-cycle entry (Zou et al., 2009; Bhola et al., 2010). While the reasons for the additive effects of sorafenib remain elusive, the combination therapy has proven useful in other systems (Newell et al., 2009; Ramakrishnan et al., 2012; Pawaskar et al., 2013), most likely due to crosstalk between the MAPK and PI3K pathways (Sunayama et al., 2010).

In summary, we developed a novel mouse model of NF1 that exhibits the key feature of neurofibroma-to-MPNST transition. We found that loss of PTEN is the critical rate limiting step in malignant progression, and established FDG-PET as a promising non-invasive modality in monitoring malignant transition and therapeutic response. The loss of PTEN in mouse and human samples provides a novel pathway to target in the treatment of peripheral nerve sheath tumors. Furthermore, we show that combining molecular inhibitors is more effective than single agent therapy, highlighting the benefits of synergistic multi-kinase inhibition (Gahr et al., 2012; Singh et al., 2013).

Experimental Procedures

Animals

Pten$^{loxp/loxp}$;*mGFAP-Cre*$^{+}$ transgenic mice line were generated previously (Gregorian et al. 2009) and crossed to *LSL-Kras*$^{G12D/+}$ (Jackson, Willis et al. 2001)on a C57, 129/Balb/c background. loxP-Stop-loxP-K-ras$^{G12D/G12D}$ (LSL-K-ras$^{G12D/G12D}$) mice are embryonically lethal. Animals were genotyped by standard genomic PCR techniques (Lesche, Groszer et al. 2002). *Pten*$^{loxp/loxp}$*;mGFAP-Cre*$^{+}$ mice were crossed to ROSA26 mice for reporter analysis as described previously (Gregorian et al., 2009). Mice were observed daily for evidence of illness or tumor formation. If palpable tumors exceeded 1.5 cm in diameter or interfered with feeding and grooming, mice were sacrificed. Moribund mice with possible internal tumors were also sacrificed. Animals were housed in a temperature-, humidity-, and light-controlled room (12-h light/dark cycle), and allowed free access to food and water. All experiments were conducted according to the research guidelines of the UCLA Chancellor's Animal Research Committee.

Polymerase Chain Reaction (PCR)

The specificity of *Pten* excision and Cre expression was evaluated by PCR using DNA from tail clip biopsy as described previously (Gregorian et al., 2009). The *K-ras* and *Lox-K-ras G12D* alleles were detected via combination of 3'universal with either 5'wt and 3'mut, The yielding a 265-bp and a 305-bp product, respectively. dt5' new (5'wt) 5'GTC GAC AAG CTC ATG CGG G 3' , Uni'new (3'universal) 5' CGC AGA CTG TAG AGC AGC G 3', and SD5'-new (5'mut) 5' CCA TGG CTT GAG TAA GTC TGC 3'. PCR was performed in 20 µl reactions using standard procedures for forty cycles; each cycle consisted of denaturing at 94˚C for 30", annealing at 60˚C

for 1:30', and extension at 72˚C for 1', followed by a single 5' extension at 72˚C. The PCR products were analyzed on 2% agarose gels.

Histology and Immunohistochemistry of Tissue Sections

All tumors were graded according to World Health Organization (WHO) histopathological criteria (Kleihues, Louis et al. 2002). IHC staining was performed on age-matched control and mutant sections. 5 μm sections that were prepared from paraffin-embedded blocks were placed on charged glass slides. The slides were deparaffinized with xylene and rehydrated in descending grades (100%–70%) of ethanol. The endogenous peroxidase activity was inactivated in 3% hydrogen peroxide (H_2O_2). After washing in deionized water, antigen retrieval was performed by incubating the slides in 0.01 M citric acid buffer (pH 6.0) at 95°C for 13.5 min. Slides were then allowed to cool for 30 min in citric acid buffer. After washing in deionized water, the slides were then transferred to either PBS (pH 7.4) or TBST for 5 min. For DAB staining, slides were first blocked with 5% normal donkey serum then incubated with primary antibody overnight at 4°C. Following three 5 min washes in either PBS or TBST, slides were incubated with biotinylated secondary antibody (1:200, Jackson Immunoresearch) for 30 min at room temperature. Amplification was performed with a horseradish peroxidase system (Vectastain ABC kit, Vector, PK-6100) using a liquid DAB peroxidase substrate (Biogenex, HK130-5K). Slides were counterstained in Gill's hematoxylin, dehydrated, cleared, and cover-slipped. Negative control slides were run without primary antibody. Primary antibodies used were PTEN (1:100, Cell Signaling), P-AKT (1:50; Cell Signaling); P-S6 (1:100 Cell Signaling); P-ERK (1:100, Cell Signaling); Ki-67 (1:500; Vector).

Ki-67 Quantification

Slides were digitally scanned at 20x magnification using an Aperio XL system (Aperio, Vista, CA), and images were quantified using the Definiens imaging software.

microPET/CT Imaging and Analysis

microPET/CT imaging was performed with a microPET FOCUS 220 PET scanner (Siemens Preclinical Solutions) and micro-CAT II CT scanner (Siemens Preclinical Solutions) with UCLA Chancellor's Animal Research Committee approval. Briefly, mice are anesthetized with isofluorane 15 min before receiving 18F-fluoro-D-glucose (200 μCi ^{18}FDG per mouse) via tail vein. The mice are then placed in the imaging chamber and imaged over 1 h in the microPET scanner, followed by a 10-min microCAT scan for anatomical localization. PET images were analyzed with the AMIDE software. Regions of interest (ROIs) were manually drawn on the area of tumor with maximal tracer uptake at 1mmin diameter. Activity concentrations were quantified as SUVs normalized to injected dose per weight of mouse (mCi/g).

Human NF1-MPNST Analysis

Following UCLA IRB approval (IRB#: 99-05-085-12) for studies on human MPNSTs, the UCLA Sarcoma and Pathology databases were used to identify patients with NF1 who underwent surgical treatment for a MPNST. Slides from the selected cases were reviewed. Whenever possible, we chose cases in which we could identify a MPNST arising from the associated NF and selected sections demonstrating a transition from NF to MPNST. Anonymously labeled sections for immunohistochemistry studies, as detailed above, were

prepared by the UCLA Department of Pathology Translational Pathology Laboratory. Additionally, an H&E slide was made from each block to confirm the diagnosis.

Collection of Tumor Samples

Patients with PNST who underwent surgery at the University of California, Los Angeles (UCLA), were enrolled on an Institutional Review Board approved tissue procurement protocol after giving written informed consent. Each surgically resected tumor was sliced into sections with a sterile razor blade and was divided as follows: one portion was immediately frozen and stored at 80ºC for genomic and gene expression analyses, another portion of the tumor was fixed in 10% formalin for histology, and the remainder was minced into small pieces for xenograft implantation and tissue culture studies. Histological review by a sarcoma pathologist confirmed diagnosis, subtype, and grade of tumors used in the present study.

Xenograft Implantation and Passage

Transplantation studies were performed using NOD-SCID/IL2rγ null mice in accordance with protocol number 2007-189-11A, approved by the Animal Research Committee within the Office for the Protection of Research Subjects at UCLA. For the initial xenograft, approximately 100 mg of the patient tumor was cut into fragments (approximately 3 mm3), using a sterile razor blade. Mice were anesthetized with isoflurane, and the fur on the hindquarters was shaved and prepared with an antiseptic agent. An incision was made, and one of the tumor fragments (approximately 3 mm3) was inserted into the subdermal space. The incision was closed with either 5-0 Prolene suture or a skin stapler; the closure was removed on postoperative day 10. Mice were maintained in barrier cages on standard chow diet with food and water available ad

libitum; 2 mg/mL sulfamethoxazole and 0.4mg/mL trimethoprim was added to drinking water to prevent infection. All studies were performed in accordance with the UCLA Animal Research Committee and Division of Laboratory Animal Medicine (protocol no. 96-126). All surgery was performed under isoflurane anesthesia, and all efforts were made to minimize suffering. Implanted samples were allowed a 6-month incubation period to form a palpable tumor. When successful engraftment occurred, tumors were collected before reaching 1.5 cm in diameter. Harvested tumors were separated into three fragments: for histopathology, gene expression analysis, and serial transplantation for establishing stable xenograft models or cell culture models.

Sorafenib and rapamycin treatment

Rapamycin powder (LC Laboratories, Woburn, MA) was reconstituted in 100% ethanol to a stock solution of 10 mg/mL and was stored at -20ºC. Working solution was made each time by diluting the stock solution to 1 mg/mL with vehicle (5.68% Tween-80, 5.68% polyethylene glycol 400 in water). Rapamycin (4 mg/kg) in vehicle or an equal volume of vehicle alone was administered via intraperitoneal injection daily. Sorafenib pills were weighed, then crushed into powder and stored at -20ºC. Powder was dissolved into freshly made vehicle (12.5% ethanol, 12.5% cremophor in water) to 20 mg/mL. Sorafenib (70 mg/kg) in vehicle or an equal volume of vehicle alone was administered via oral gavage daily. Body weight and tumor measurements were collected every other day. Tumors were collected, and the mouse was sacrificed if the tumor reached 1.5 cm in diameter.

Chapter 2 References

Ambrosini G, Cheema HS, Seelman S, Teed A, Sambol EB, Singer S, Schwartz GK (2008). Sorafenib inhibits growth and mitogen-activated protein kinase signaling in malignant peripheral nerve sheath cells. Mol Cancer Ther. 7: 890-6.

Ballou LM, Lin RZ (2008). Rapamycin and mTOR kinase inhibitors. J Chem Biol.*1*: 27-36.

Basu TN, Gutmann DH, Fletcher JA, Glover TW, Collins FS, Downward J (1992). Aberrant regulation of ras proteins in malignant tumour cells from type 1 neurofibromatosis patients. Nature. *356*: 713-5.

Benz MR, Czernin J, Dry SM, Tap WD, Allen-Auerbach MS, Elashoff D, Phelps ME, Weber WA, Eilber FC (2010). Quantitative F18-fluorodeoxyglucose positron emission tomography accurately characterizes peripheral nerve sheath tumors as malignant or benign. Cancer. *116*: 451-8.

Bollag G, Clapp DW, Shih S, Adler F, Zhang YY, Thompson P, Lange BJ, Freedman MH, McCormick F, Jacks T, Shannon K (1996). Loss of NF1 results in activation of the Ras signaling pathway and leads to aberrant growth in haematopoietic cells. Nat Genet. *12*:144-8.

Bhola P, Banerjee S, Mukherjee J, Balasubramanium A, Arun V, Karim Z, Burrell K, Croul S, Gutmann DH, Guha A (2010). Preclinical in vivo evaluation of rapamycin in human malignant peripheral nerve sheath explant xenograft. Int J Cancer. *126*: 563-71.

Buller CL, Loberg RD, Fan MH, Zhu Q, Park JL, Vesely E, Inoki K, Guan KL, Brosius FC 3rd (2008). A GSK-3/TSC2/mTOR pathway regulates glucose uptake and GLUT1 glucose transporter expression. Am J Physiol Cell Physiol *295*: C836-43.

Castle B, Baser ME, Huson SM, Cooper DN, Upadhyaya M (2003). Evaluation of genotype-phenotype correlations in neurofibromatosis type 1. J Med Genet. *40*: e109.

Costa RM, Yang T, Huynh DP, Pulst SM, Viskochil DH, Silva AJ, Brannan CI (2001). Learning deficits, but normal development and tumor predisposition, in mice lacking exon 23a of Nf1. Nat Genet. *27*: 399-405.

Costa RM, Federov NB, Kogan JH, Murphy GG, Stern J, Ohno M, Kucherlapati R, Jacks T, Silva AJ (2002). Mechanism for the learning deficits in a mouse model of neurofibromatosis type 1. Nature. *415*: 526-30.

DeClue JE, Papageorge AG, Fletcher JA, Diehl SR, Ratner N, Vass WC, Lowy DR (1992). Abnormal regulation of mammalian p21ras contributes to malignant tumor growth in von Recklinghausen (type 1) neurofibromatosis. Cell. *69*: 265-73.

Easton DF, Ponder MA, Huson SM, Ponder BA (1993). An analysis of variation in expression of neurofibromatosis (NF) type 1 (NF1): evidence for modifying genes. Am J Hum Genet. *53*: 305-13.

Eilber FC, Brennan MF, Eilber FR, Dry SM, Singer S, Kattan MW (2004). Validation of the postoperative nomogram for 12-year sarcoma-specific mortality. Cancer. *101*: 2270-5.

Eilber FC, Tap WD, Nelson SD, Eckardt JJ, Eilber FR (2006). Advances in chemotherapy for patients with extremity soft tissue sarcoma. Orthop Clin North Am. *37*: 15-22.

Gahr S, Wissniowski T, Zopf S, Strobel D, Pustowka A, Ocker M (2012). Combination of the deacetylase inhibitor panobinostat and the multi-kinase inhibitor sorafenib for the treatment of metastatic hepatocellular carcinoma - review of the underlying molecular mechanisms and first case report. J Cancer. *3*:158-65.

Gregorian C, Nakashima J, Le Belle J, Ohab J, Kim R, Liu A, Smith KB, Groszer M, Garcia AD, Sofroniew MV, Carmichael ST, Kornblum HI, Liu X, Wu H (2009). Pten deletion in adult neural stem/progenitor cells enhances constitutive neurogenesis. J Neurosci. *29*:1874-86.

Grobmyer SR, Reith JD, Shahlaee A, Bush CH, Hochwald SN (2008). Malignant Peripheral Nerve Sheath Tumor: molecular pathogenesis and current management considerations. J Surg Oncol. *97*:340-9.

Groszer M, Erickson R, Scripture-Adams DD, Lesche R, Trumpp A, Zack JA, Kornblum HI, Liu X, Wu H (2001). Negative regulation of neural stem/progenitor cell proliferation by the Pten tumor suppressor gene in vivo. Science. *294*: 2186-9.

Groszer M, Erickson R, Scripture-Adams DD, Dougherty JD, Le Belle J, Zack JA, Geschwind DH, Liu X, Kornblum HI, Wu H (2006). PTEN negatively regulates neural stem cell self-renewal by modulating G0-G1 cell cycle entry. Proc Natl Acad Sci U S A. *103*: 111-6.

Gutmann, D. H. and M. Giovannini (2002). Mouse models of neurofibromatosis 1 and 2. Neoplasia *4*: 279-90.

Hasskarl J (2010). Sorafenib. Recent Results Cancer Res. *184*: 61-70.

Herrmann K, Benz MR, Czernin J, Allen-Auerbach MS, Tap WD, Dry SM, Schuster T, Eckardt JJ, Phelps ME, Weber WA, Eilber FC (2012). 18F-FDG-PET/CT Imaging as an early survival predictor in patients with primary high-grade soft tissue sarcomas undergoing neoadjuvant therapy. Clin Cancer Res. *18*: 2024-31.

Holtkamp N, Okuducu AF, Mucha J, Afanasieva A, Hartmann C, Atallah I, Estevez-Schwarz L, Mawrin C, Friedrich RE, Mautner VF, von Deimling A (2006). Mutation and expression of

PDGFRA and KIT in malignant peripheral nerve sheath tumors, and its implications for imatinib sensitivity. Carcinogenesis. *27*: 664-71.

Lévy P, Vidaud D, Leroy K, Laurendeau I, Wechsler J, Bolasco G, Parfait B, Wolkenstein P, Vidaud M, Bièche I (2004). Molecular profiling of malignant peripheral nerve sheath tumors associated with neurofibromatosis type 1, based on large-scale real-time RT-PCR. Mol Cancer. *3*: 20.

Li W, Cui Y, Kushner SA, Brown RA, Jentsch JD, Frankland PW, Cannon TD, Silva AJ (2005). The HMG-CoA reductase inhibitor lovastatin reverses the learning and attention deficits in a mouse model of neurofibromatosis type 1. Curr Biol. *15*: 1961-7.

Liaw D, Marsh DJ, Li J, Dahia PL, Wang SI, Zheng Z, Bose S, Call KM, Tsou HC, Peacocke M, Eng C, Parsons R (1997). Germline mutations of the PTEN gene in Cowden disease, an inherited breast and thyroid cancer syndrome. Nat Genet. *16*: 64-7.

Nelen MR, van Staveren WC, Peeters EA, Hassel MB, Gorlin RJ, Hamm H, Lindboe CF, Fryns JP, Sijmons RH, Woods DG, Mariman EC, Padberg GW, Kremer H (1997). Germline mutations in the PTEN/MMAC1 gene in patients with Cowden disease. Hum Mol Genet. *6*: 1383-7.

Newell P, Toffanin S, Villanueva A, Chiang DY, Minguez B, Cabellos L, Savic R, Hoshida Y, Lim KH, Melgar-Lesmes P, Yea S, Peix J, Deniz K, Fiel MI, Thung S, Alsinet C, Tovar V, Mazzaferro V, Bruix J, Roayaie S, Schwartz M, Friedman SL, Llovet JM (2009). Ras pathway activation in hepatocellular carcinoma and anti-tumoral effect of combined sorafenib and rapamycin in vivo. J Hepatol. *51*: 725-33.

Pawaskar DK, Straubinger RM, Fetterly GJ, Hylander BH, Repasky EA, Ma WW, Jusko WJ (2013). Synergistic interactions between sorafenib and everolimus in pancreatic cancer xenografts in mice. Cancer Chemother Pharmacol.*71*: 1231-40.

Ramakrishnan V, Timm M, Haug JL, Kimlinger TK, Halling T, Wellik LE, Witzig TE, Rajkumar SV, Adjei AA, Kumar S (2012). Sorafenib, a multikinase inhibitor, is effective in vitro against non-Hodgkin lymphoma and synergizes with the mTOR inhibitor rapamycin. Am J Hematol. *87*: 277-83.

Reilly KM, Tuskan RG, Christy E, Loisel DA, Ledger J, Bronson RT, Smith CD, Tsang S, Munroe DJ, Jacks T (2004). Susceptibility to astrocytoma in mice mutant for Nf1 and Trp53 is linked to chromosome 11 and subject to epigenetic effects. Proc Natl Acad Sci U S A. *101*: 13008-13.

Riccardi VM, Womack JE, Jacks T (1994). Neurofibromatosis and related tumors. Natural occurrence and animal models. Am J Pathol. *145*: 994-1000.

Rodrik-Outmezguine VS, Chandarlapaty S, Pagano NC, Poulikakos PI, Scaltriti M, Moskatel E, Baselga J, Guichard S, Rosen N (2011). mTOR kinase inhibition causes feedback-dependent biphasic regulation of AKT signaling. Cancer Discov. *1*: 248-59.

Saito H, Yoshida T, Yamazaki H, Suzuki N (2007). Conditional N-rasG12V expression promotes manifestations of neurofibromatosis in a mouse model. Oncogene. *26*: 4714-9.

Singh I, Amin H, Rah B, Goswami A (2013). Targeting EGFR and IGF 1R: a promising combination therapy for metastatic cancer. Front Biosci (Schol Ed).*5*: 231-46.

Stemmer-Rachamimov AO, Louis DN, Nielsen GP, Antonescu CR, Borowsky AD, Bronson RT, Burns DK, Cervera P, McLaughlin ME, Reifenberger G, Schmale MC, MacCollin M, Chao RC, Cichowski K, Kalamarides M, Messerli SM, McClatchey AI, Niwa-Kawakita M, Ratner N, Reilly KM, Zhu Y, Giovannini M (2004). Comparative pathology of nerve sheath tumors in mouse models and humans. Cancer Res *64*: 3718-24.

Sun SY, Rosenberg LM, Wang X, Zhou Z, Yue P, Fu H, Khuri FR (2005). Activation of Akt and eIF4E survival pathways by rapamycin-mediated mammalian target of rapamycin inhibition. Cancer Res. *65*: 7052-8.

Sunayama J, Matsuda K, Sato A, Tachibana K, Suzuki K, Narita Y, Shibui S, Sakurada K, Kayama T, Tomiyama A, Kitanaka C (2010). Crosstalk between the PI3K/mTOR and MEK/ERK pathways involved in the maintenance of self-renewal and tumorigenicity of glioblastoma stem-like cells. Stem Cells. *28*: 1930-9.

Theos A, Korf BR; American College of Physicians; American Physiological Society (2006). Pathophysiology of neurofibromatosis type 1. Ann Intern Med. *144*: 842-9..

von Mehren M, Rankin C, Goldblum JR, Demetri GD, Bramwell V, Ryan CW, Borden E (2012). Phase 2 Southwest Oncology Group-directed intergroup trial (S0505) of sorafenib in advanced soft tissue sarcomas. Cancer. *118*: 770-6.

Wu J, Williams JP, Rizvi TA, Kordich JJ, Witte D, Meijer D, Stemmer-Rachamimov AO, Cancelas JA, Ratner N (2008). Plexiform and dermal neurofibromas and pigmentation are caused by Nf1 loss in desert hedgehog-expressing cells. Cancer Cell. *13*:105-16.

Zhu, Y. and L. F. Parada (2002). The molecular and genetic basis of neurological tumours. Nat Rev Cancer *2*: 616-26

Zou CY, Smith KD, Zhu QS, Liu J, McCutcheon IE, Slopis JM, Meric-Bernstam F, Peng Z, Bornmann WG, Mills GB, Lazar AJ, Pollock RE, Lev D (2009). Dual targeting of AKT and

mammalian target of rapamycin: a potential therapeutic approach for malignant peripheral nerve sheath tumor. Mol Cancer Ther. *8*: 1157-68.

Chapter 3:

Heterogeneous Transformation of Neural Stem Cells

INTRODUCTION

Gliomas are the most common primary cancers of the central nervous system (Lim et al., 2011). Clinically, they are described as astrocytomas, oligodendrogliomas, ependyomas, and mixed gliomas, based on the cell types they histologically resemble. Astrocytomas are the most common of these types of tumors, and are classified by the World Health Organization (WHO) into four different grades (Louis et al., 2007). Grades I and II astrocytomas are low-grade and less aggressive tumors, whereas Grades III and IV are malignant. Malignant astrocytomas are characterized by their high proliferation rate (Grade III) and the presence of necrotic tissue and angiogenic activity (Grade IV). Grade IV astrocytoma, also referred to as glioblastoma multiforme (GBM), accounts for the majority of astrocytomas and has a median survival of less than two years, making it one of the most lethal of all cancers (Huse et al., 2013). Approximately 90% of GBMs are characterized as primary GBM, developing rapidly *de novo* in elderly patients without evidence of a less malignant precursor. Secondary GBMs arise from a lower grade glioma, have a lesser degree of necrosis, are preferentially located in the frontal lobe, and carry a significantly better prognosis (Ohgaki and Kleihues, 2013). Primary and secondary GBMs are indistinguishable histologically, yet they differ in their genetic signatures, namely the mutational status of *IDH1*. Secondary GBMs often have *IDH1* mutations which occur as early events in precursor gliomas. These tumors are believed to be derived from neural precursor cells that differ from those of primary GBM (Lai et al., 2011).

Recent analysis by The Cancer Genome Atlas (TCGA) Research Network provided a detailed view of the genomic changes in a large primary GBM cohort containing 206 patient samples. This study described the mutational spectrum of GBM, confirming previously reported *TP53, RB1* and *PTEN* mutations, and identifying new associated mutations in such genes as *NF1*,

PIK3R1, and *ERBB2* (TCGA, 2008). Furthermore, gene expression analysis on GBM has identified clinically relevant subtypes based on aberrations in *EGFR, NF1,* and *PDGFRA*/*IDH1*, classifying each as Classical, Mesenchymal, and Proneural, respectively. Another subtype, classified as Neural due to expression of neuronal genes, had mutations in many of the same genes as the other groups; however, it did not stand out from the others as having significantly higher or lower rates of mutations (Verhaak et al., 2010). The four subtypes also varied in clinical characteristics, such as survival length, average patient age, and treatment response. The Classical group, characterized by high expression of *EGFR*, survived the longest of the subgroups in response to aggressive treatment with temozolomide and radiation. The Mesenchymal group, containing the most frequent number of mutations in *NF1*, *PTEN,* and *TP53*, also had increased survival with aggressive treatment. Patients in the Neural group were the oldest, on average, and showed some improvement in survival after aggressive treatment, but not as much as the Classical and Mesenchymal groups. In contrast to the other groups, patients from the Proneural subgroup were significantly younger and tended to survive longer. These patients exhibited the most mutations in *IDH1*, *PDGFRA*, and *TP53*, and unlike the other groups, showed no survival benefit with aggressive treatment. Importantly, there was a strong relationship between gene signatures of the subtypes and different neural lineages, highlighting the impact that cellular origin has on glioma biology.

The identification of adult neural stem cells (NSCs) that divide throughout the lifetime of an individual presents attractive targets for acquisition of oncogenic mutations. Self-renewing NSCs are capable of producing new neurons, oligodendrocytes, and astrocytes, a process that is evolutionarily conserved in mammals (Doestch et al., 2003). In the brain, the subventricular zone (SVZ) is the largest adult germinal niche and is located along the walls of the lateral

ventricles (LV). Glial fibrillary acidic protein (GFAP) expressing cells residing in this layer act as slow-dividing NSCs capable of multi-lineage differentiation (Imura et al., 2003; Garcia, 2004). Neurons born throughout the SVZ form chains of neuroblasts that migrate tangentially through a complex network and merge into the rostral migratory stream (RMS), a major pathway that leads into the olfactory bulb (OB) (Doetsch and Alvarez-Buylla, 1996). In the OB, these young neurons mature and differentiate into various olfactory interneurons, including granule and periglomerular neurons (Petreanu and Alvarez-Buylla 2002). In addition to neurons, the SVZ produces mature glial cells (Gonzalez-Perez and Alvarez-Buylla, 2011). Glial progenitors expressing the transcription factor Olig2 migrate radially from the SVZ into the corpus callosum, striatum, and fimbria fornix to differentiate into oligodendrocytes and astrocytes (Marshall et al., 2005; Menn et al., 2006). The SVZ was previously thought to be restricted to the anterior lateral wall of the lateral ventricle, but recent work shows that the adult neurogenic niche is significantly more extensive. In the developing mouse brain, the posterior sections of the lateral ventricles collapse due to the emerging hippocampus. The hippocampus presses against the corpus callosum, compressing the opposing walls of the ventricle together. This region still contains multi-potent NSCs that produce oligodendrocytes and astrocytes in the corpus callosum, but since it is no longer associated to an open ventricular cavity, this portion of the SVZ is referred to as the subcallosal zone (SCZ) (Seri et al., 2006). An important characteristic of this niche is that NSCs in different regions produce different types of cells, and even when they are heterotopically grafted into another region, they retain their innate differentiation programming, suggesting that NSCs are a restricted and diverse population of progenitors (Merkle et al., 2007).

Previous studies have shown that SVZ NSCs have the potential to induce malignant gliomas upon deletion of key tumor suppressor genes (Alcantara Llaguno et al., 2009; Jacques et

al., 2010; Chow et al., 2011). However, the precise location of tumor initiation within this extensive niche remains to be determined. This is of particular importance because anatomical positioning of gliomas has been implicated as a prognostic factor (Simpson et al., 1993; Fontaine and Paquis, 2010). It has also been suggested that tumor location reflects the contributions of region-specific precursor cells and the stage in the development cycle they are in when they transform (Zlatescue et al., 2001; Lai et al., 2011).

We created a malignant glioma mouse model in which we targeted adult NSCs using a mouse *GFAP* promoter to drive Cre recombinase. We simultaneously perturbed the PI3K and MAPK pathways by deleting the *Pten* tumor suppressor gene and activating the *K-ras* oncogene, resulting in 100% penetrant malignant gliomas. Importantly, the rate of progression allows us to assess the natural history of tumor development and determine the location of initiation within the extensive niche. We consistently observed increased proliferation in the SCZ prior to the rostral SVZ, resulting in tumorigenesis at the caudal-most regions of the corpus callosum. Furthermore, we show that treatment with the small molecule inhibitors rapamycin and lovastatin is able impede the observed directional tumor progression and reduce proliferation. Finally, we observed that our mutations affected the cellular composition of the SVZ and SCZ uniquely by expanding the glial population in the SCZ, and re-directing the neural precursors in the SVZ towards a glial fate. Our results indicate that transformative potential between NSCs in the SVZ and SCZ is not uniform, and that intrinsic heterogeneity is an underlying determinant of gliomagenesis.

RESULTS

Homozygous deletion of *Pten* and activation of *K-ras* in SVZ stem cells induces malignant gliomas

We employed the *mGFAP-Cre* mouse (line 77.6) (Gregorian et al., 2009) to mediate recombination of the *Pten* and *K-ras* alleles in SVZ stem cells. Neither homozygous deletion of *Pten* alone (Gregorian et al., 2009), activation of *K-ras* alone, or heterozygous deletion of *Pten* with activation of *K-ras*, were able to produce malignant brain gliomas (Supplemental Figure 1). Only homozygous deletion of *Pten* with activation of *K-ras* induced a malignant CNS phenotype (henceforth *Pten/K-ras*).

The median survival of *Pten/K-ras* mice was 14 weeks (n=20) (Figure 1A). Mutant mice started showing symptoms as early as 6 weeks postnatal, such as doming of the head, vestibular imbalance, and cachexia (Figure 1B). Mice showed a decrease in body mass and increase of brain size (Figure 1C and D). Histological analysis revealed various tumors including optic nerve gliomas, anaplastic oligodendroglioma, grade III astrocytoma and GBM (Table 1, Figures 1 and 2). Tumors showed multiple mitotic bodies and enhanced Ki-67 staining, and were immunoreactive for glioma makers such as GFAP, Olig2, and Nestin (Figure 1E and 2D). Staining for the PI3K and MAPK pathways showed marked reduction in immunoreactivity for PTEN in tumors cells, with PTEN positive endothelial cells as an internal positive control (Figure 1E and 2D). Elevated levels of P-AKT and P-S6, two surrogate markers for PTEN-controlled PI3K pathway activation, and P-ERK, a downstream marker of K-Ras, were also observed. GBM was also observed, showing massive bilateral necrosis in the brain.

Histological analysis revealed additional hallmarks, such as pseudopalisades and microvascular proliferation (Figure 1F).

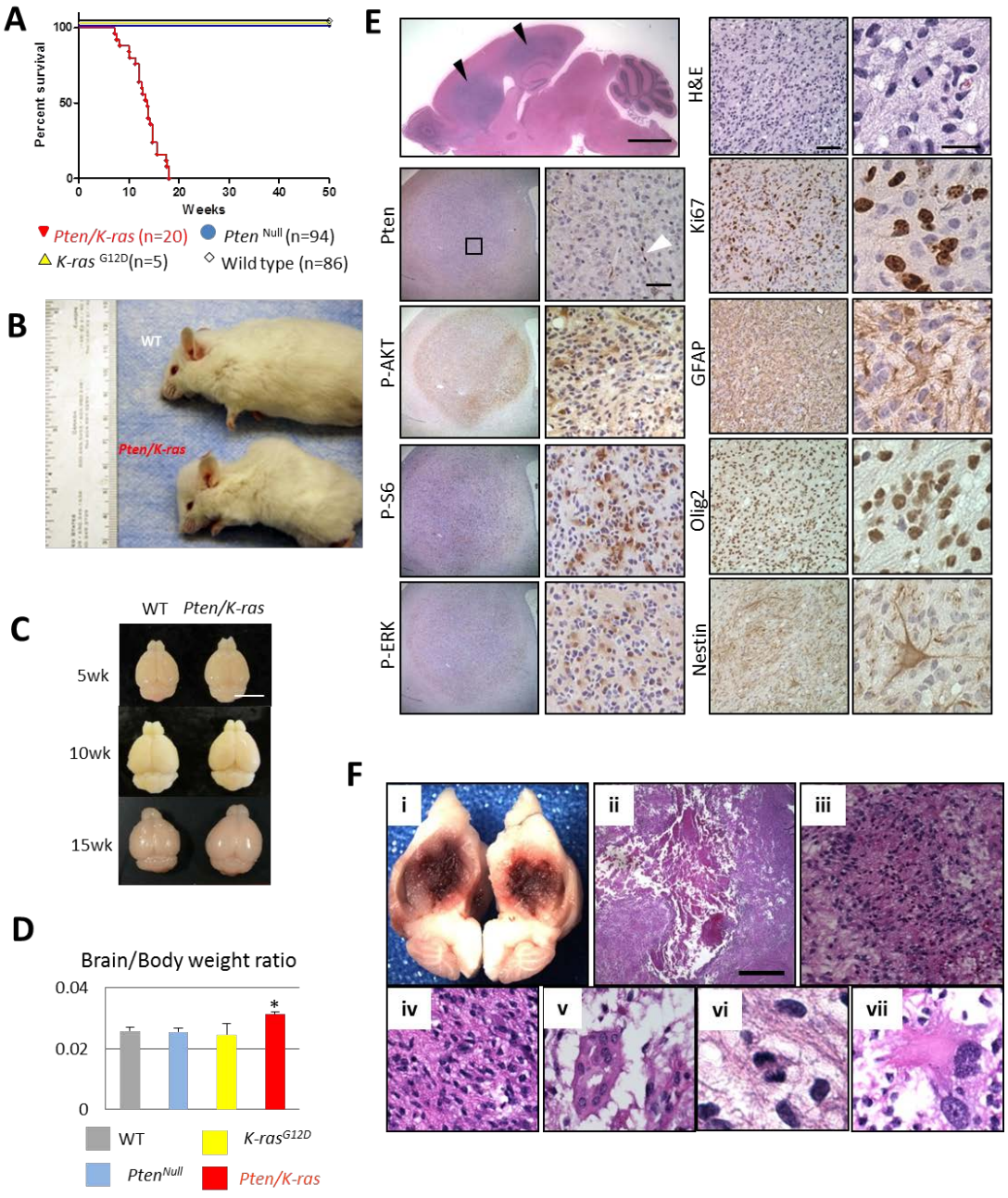

Figure 1. Deletion of *Pten* and activation of *K-ras* in SVZ stem cells induces malignant glioma. (A) *Pten/K-ras* mice have a median survival of 14 weeks and (B) are visibly distinguishable from WT. (C) Images of mutant brains at various ages. Scale bar, 0.5cm. (D) Brain-to-body weight ratio shows a significant increase in mutant mice. (E) Representative sagittal section of a *Pten/K-ras* brain harboring multiple grade III astrocytomas (black arrows) in the cerebral cortex. Scale bar: 250 µm. Tumors contained multiple mitotic figures (right), robust Ki-67 staining, and classic astrocytoma immunoreactivity for GFAP, Olig2, and Nestin. Scale bar: 75 µm and 25 µm.

Astrocytomas showed marked reduction in immunoreactivity for PTEN in tumor cells, with PTEN+ stained endothelial cells as an internal positive control (white arrow). Tumors also show intensive staining with antibodies specific for surrogate markers of activated PI3K/AKT (P-AKT, P-S6) and RAS/MAPK (P-ERK) pathways. Scale bar: 75 µm. (F)(i) Bilateral tumor showing classic GBM histological hallmarks such as (ii) extensive necrosis, (iii) pseudopalisading necrosis, (iv) astrocytic morphology, (v) microvascular proliferation, (vi) mitosis, (vii) and nuclear atypia.

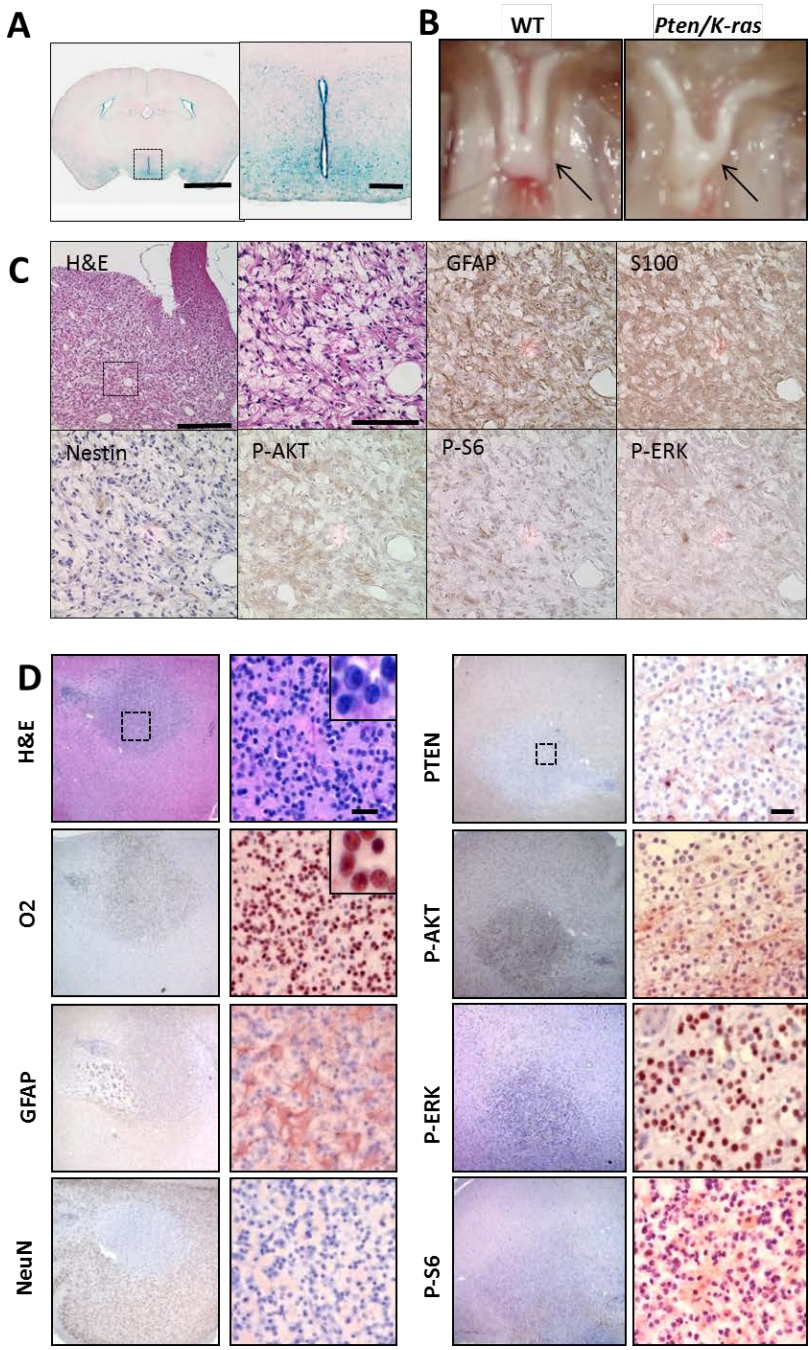

Figure 2. Optic nerve tumor and anaplastic oligodendroglioma in *Pten/K-ras* mice. (A) Cre expression in the third ventricle of the brain. Scale bar: 2mm, 500µm. (B) Representative of wild-type (left) and mutant (right) optic nerves and chiasm (arrowheads) from 8 week old mice. (C) H&E and immunostaining of optic nerve and chiasm showing positivity for glial markers and activation of PI3K and MAPK pathways. (D) Histology of anaplastic

oligodendroglioma showing classic “fried egg” appearance, immunoreactivity for glial markers and activation of PI3K and MAPK pathways.

Age (weeks)	Cerebral Glioma	Optic Nerve Glioma
4	No Tumor	No
4	No Tumor	No
5	Grade II Astrocytoma	Yes
5	Grade II - III Astrocytoma	No
5	Grade II - III Oligoastrocytoma	Yes
5	Grade II - III Oligoastrocytoma	No
5	Grade III Astrocyotma	Yes
5	Grade III Astrocytoma	No
6	Grade III Astrocytoma	Yes
7	Anaplastic Oligodendroglioma	Yes
7	Grade III Astrocyotma	Yes
7	Grade III Astrocyotma	Yes
7	Grade II Astrocytoma	No
9	Grade III Astrocyotma	Yes
9	Grade III Astrocytoma	No
9	Grade III Astrocyotma	No
9	Grade III Astrocyotma	Yes
9	Grade III Astrocyotma	Yes
10	Grade III Astrocyotma	Yes
10	Grade IV Astrocytoma	No
11	Grade III Astrocyotma	Yes
12	Grade III Astrocyotma	Yes
12	Grade III Astrocyotma	Yes
12	Grade III Astrocyotma	No
14	Grade III Astrocytoma	No
14	Grade III Astrocytoma	No
15	Grade III Astrocytoma	Yes
15	Grade III Astrocytoma	No
15	Grade III Astrocytoma	No

Table 1. Pathological diagnosis of tumors in *Pten*/*K-ras* mice.

Early stage tumors originate in the posterior white matter and follow a caudorostral progression

The stem cell niche lining the lateral ventricles is the largest germinal zone in the brain and includes the thin layer of diving cells that extends caudally between the hippocampus and corpus callosum (Seri et al., 2006). Our model allows us to investigate the age and location of tumor initiation in the brain. To assess this, we crossed our mice to the *Rosa26-LacZ* reporter strain so that all stem/progenitor cells and their progeny would be marked by β-galactosidase and visualized by X-gal staining (Soriano, 1999). The earliest observation of tumors was at 5 weeks of age (Table 1). Sagittal sections revealed grade II or III astrocytomas located in the posterior corpus callosum, dorsal of the hippocampus (Figure 3A). Tumors were reactive to X-gal staining, confirming that they were from SVZ origin. Analysis of older mice showed additional tumor cells in the rostral corpus callosum, suggesting an age-dependent caudorostral tumor progression.

To further analyze the development of tumors and to obtain a complete three dimensional understanding, coronal brain sections were obtained from another set of mice. X-gal reactivity was observed throughout the lateral ventricles. Mice at 5 weeks of age showed increased reactivity in the SCZ, dorsal to the hippocampus, with little staining in the rostral SVZ. Consistent with our previous results, we first observed tumors in the caudal extension of the corpus callosum (Figure 3B). Tumors were only observed in the rostral corpus callosum in older mice. Our results indicate a specific region of tumor initiation and subsequent caudorostral progression.

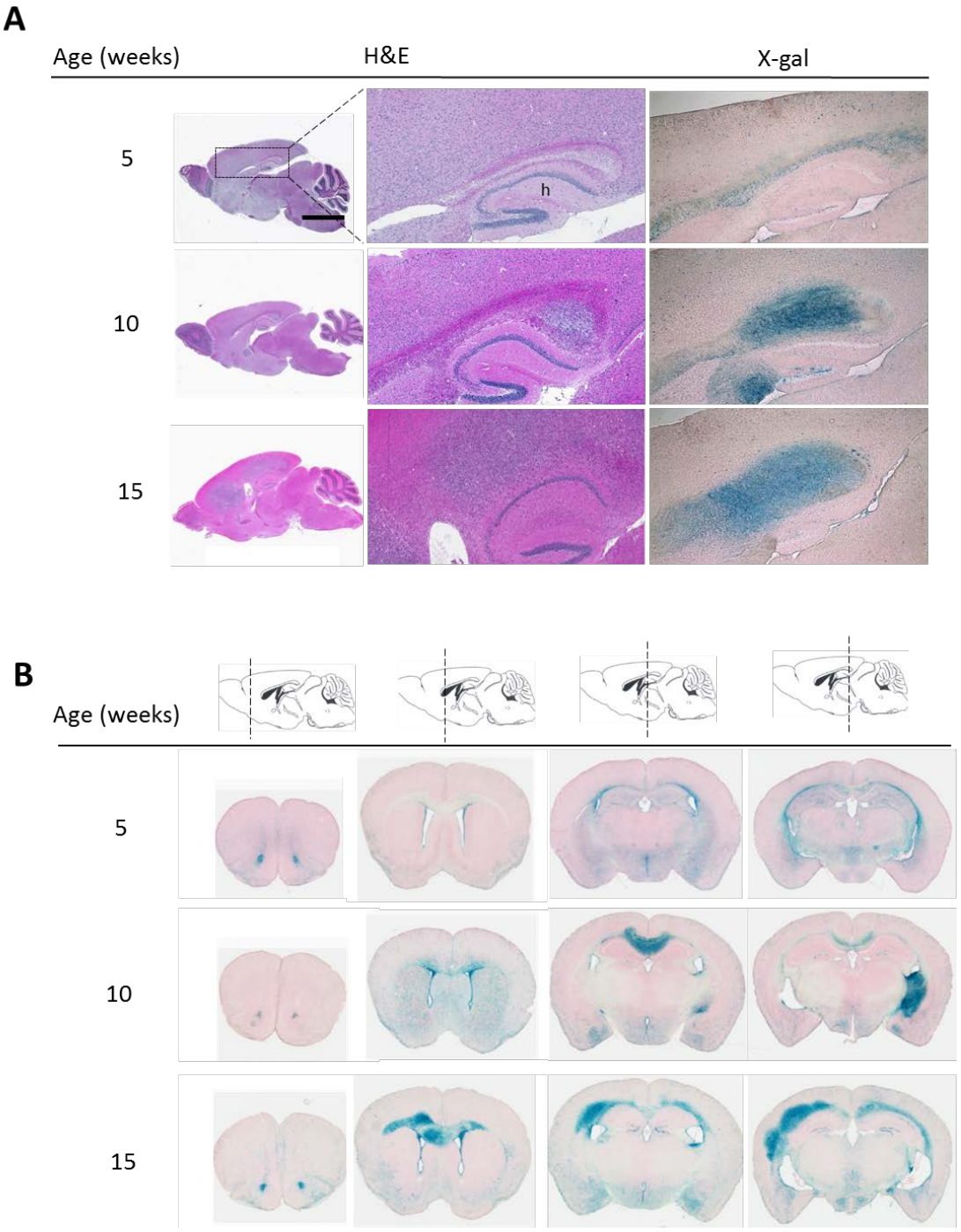

Figure 3. Glioma initiation in the posterior white matter and subsequent caudorostral progression. (A) H&E and X-gal staining of representative sagittal sections of mice at various ages show tumor origins in the posterior white matter, dorsal of the hippocampus (h). (B) X-gal staining of coronal sections show increased reporter staining in the posterior sections prior to anterior sections in 5 week old mice. 10 and 15 week old mice show increased staining along the caudorostral axis.

Treatment of brain gliomas with rapamycin and lovastatin delays caudorostral glioma progression and malignant transformation

Our model provides a unique platform to test targeted therapies against gliomas. We reasoned that treatment would also allow us to further interrogate the progression patterns in our model. The HMG-CoA reductase inhibitor lovastatin has been shown to reverse learning and attention deficits in a mouse mode of NF1 by reducing MAPK activity (Li et al., 2005). Therefore, we treated two cohorts of our mice, starting at 5 or 10 weeks of age, with lovastatin alone or in combination with the mTOR inhibitor rapamycin (Figure 4A).

Treatment with rapamycin or lovastatin individually did not have an effect on tumor progression in either cohort (data not shown). Only a combination of both drugs showed a therapeutic response. In our first cohort, we treated 5-week-old mice (n=5) with daily injections for a period of three weeks to determine drug efficacy on tumor initiation. Upon histological examination, vehicle treated mice showed grade III astrocytomas throughout the rostrocaudal axis of the corpus callosum. In contrast, two out of five treated mice showed no presence of tumor, whereas the remaining three contained small, confined tumors in the caudal corpus callosum (Figure 4B and C). Importantly, all treated tumors were diagnosed as grade II astrocytomas, showing reduced Ki-67 and P-S6 staining (Figure 4D).

Mice were also treated with lovastatin and rapamycin to determine the efficacy on established gliomas. 10-week-old mice (n=5) were treated daily until they exhibited symptoms of morbidity, such as excessive weight loss, or the development of additional peripheral tumors. Dual treated mice showed a significant increase of survival compared to vehicle treated, or single drug treated mice (Supplemental Figure 2A). Examination of the brains of dual treated mice revealed grade II astrocytomas based of Ki-67 staining and cellular morphology, and showed

reduction in P-S6 and P-ERK staining. Interestingly, three out of five treated mice developed MPNST. Interrogation of MPNSTs showed high expression in Ki-67, and moderate P-S6 and P-ERK staining (Supplemental Figure 2B).

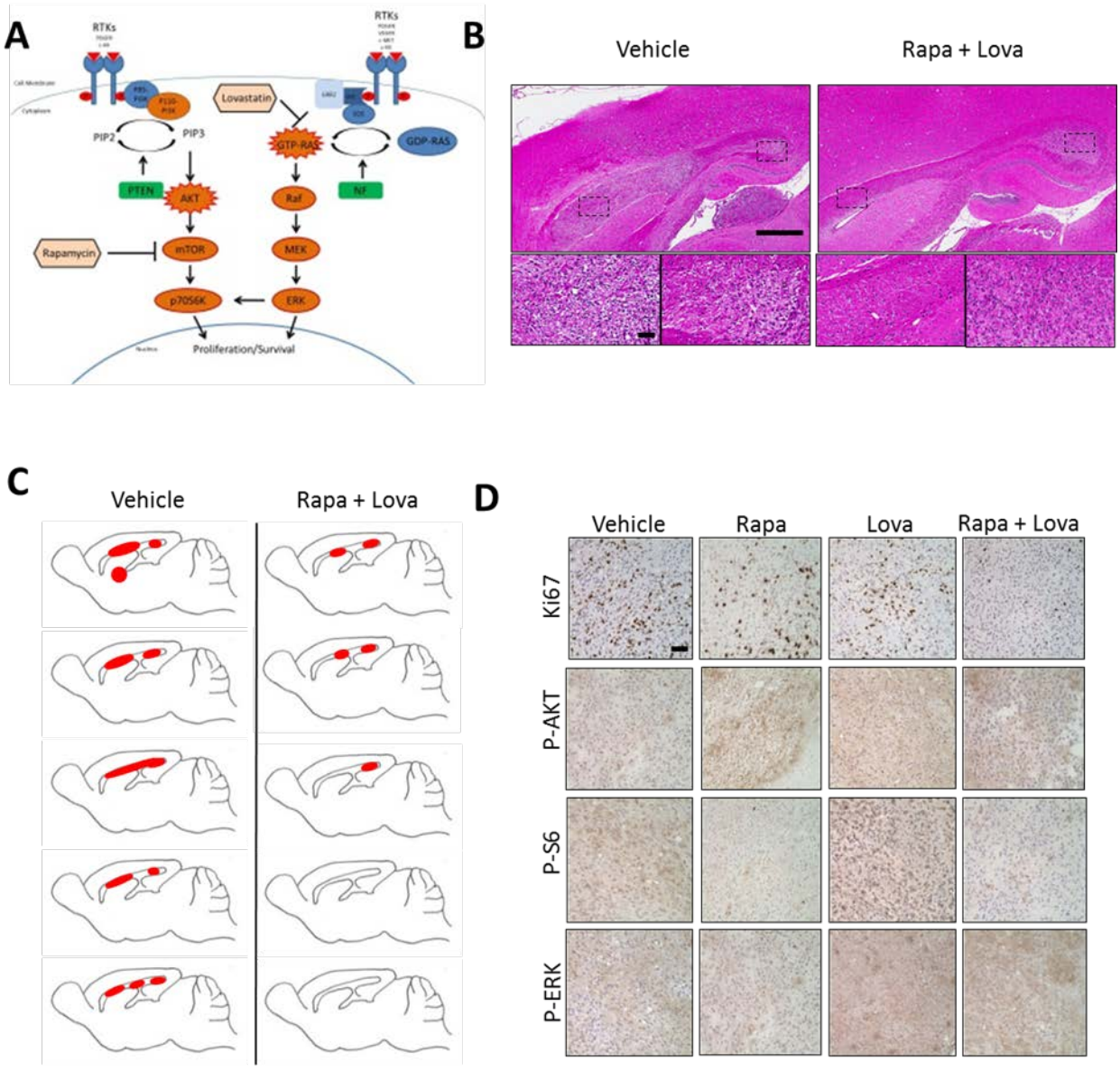

Figure 4. Treatment of 5-week-old mice with rapamycin and lovastatin delays caudorostral tumor progression. (A) Schematic of treatment strategy. (B) Representative H&E sagittal sections of control and treated mice. Scale bars: 200 µm, 50 µm. (C) Illustration of treatment results showing tumor location (red) in sagittal sections. (D) Immuostaining for Ki-67 and downstream effectors of the PI3K and MAPK pathways. Scale bar: 50 µm

Increased reporter staining and proliferation in the caudal brain regions prior to rostral regions

The presence of tumors in the caudal corpus callosum prompted us to interrogate the proliferation along the rostrocaudal axis of the brain. Since we first observed tumors as early as 5 weeks of age, we interrogated mice at this time point for our studies. 30 μm frozen coronal brain sections were obtained from mutant mice (n=5) and stained for X-gal reactivity. Mutant brains showed intense staining along the thin lamina of cells separating the hippocampus from corpus callosum, a germinal niche referred to as the SCZ (Seri, 2006) (Figure 5A), as well as the white matter extension of the hippocampus known as the fimbria fornix (FF). In contrast, rostral regions did not show marked differences between WT and mutant. In addition to reporter staining, we performed Ki-67 immunostaining on 5 μm paraffin coronal sections along the rostrocaudal axis of the lateral ventricles and adjacent white matter (n=5). The only areas of altered proliferation were the SCZ and the FF (Figure 5B). *Pten/K-ras* mice showed an increase total number of Ki-67 positive cells in the SCZ compared to WT controls (1186.4 ± 83.6 vs. 457 ± 63.4). The fimbria fornix, another destination of glial progenitors of the SCZ, also showed increased proliferation (552 ± 70.9 vs. 219.8 ± 26.8). Surprisingly, the posterior SVZ (PSVZ), adjacent to the SCZ and FF, did not exhibit altered proliferation despite showing darker X-gal staining (Figure 5A and C). Contrary to our caudal findings, there were no significant changes in proliferation in the rostral features such as the anterior corpus callosum, anterior commissure, or along the anterior ventricular surface (Figure 5D). Our results suggest that our mutations affect each region uniquely, and that transformation along the rostrocaudal axis is not uniform.

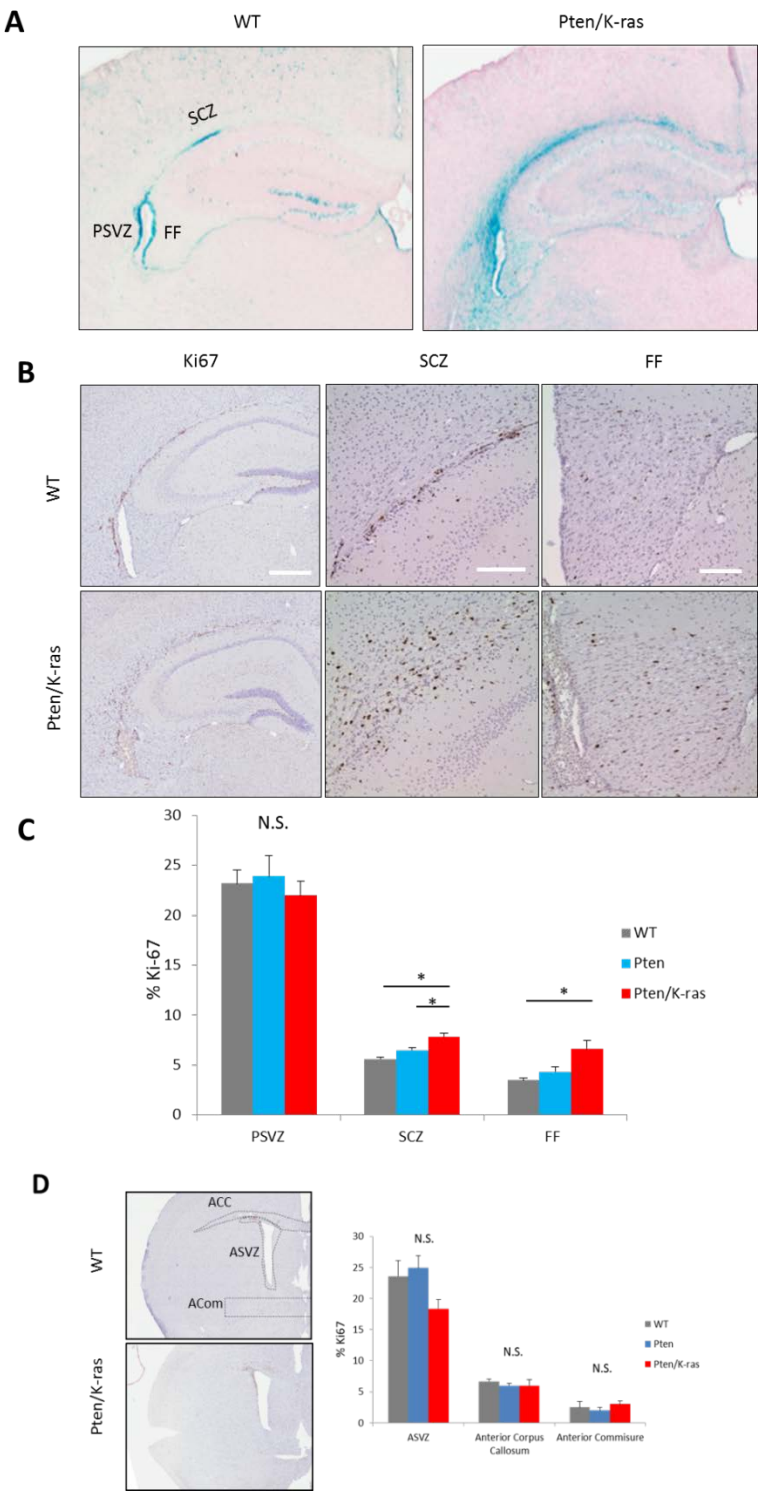

Figure 5. Increased reporter staining and proliferation in the caudal brain regions. (A) Representative coronal sections of X-gal stained 5-week-old mice. (B, C) Increased proliferation in the SCZ and fimbria fornix of mutant mice. (D) No change in proliferation in the rostral regions of mutant mice.

The composition of cell-types along the rostrocaudal axis is uniquely altered by PI3K and MAPK activation.

Olig2 is a transcription factor that is required for the production of glial progenitors as well as the maintenance and proliferation of glioma cells (Marshall et al., 2005; Ligon et al., 2007). Endogenous Olig2 expression occurs in a unique spatial patterning along the rostrocaudal axis (Menn et al., 2006). In rostral zones, Olig2 is limited to the corpus callosum, lining the dorsal wall of the SVZ (Figure 6A). In contrast, in caudal planes, Olig2 expression is seen on both sides of the collapsed walls of the SCZ (Figure 6C). Since we observed high Olig2 reactivity in the tumors, we interrogated the Olig2 composition in the SCZ and SVZ through immunofluorescence. We stained for Olig2, Ki-67, and doublecortin (DCX), and neuroblast marker, to determine how our mutations shift the balance between neuronal and glial progenitors. We selected 5 week old mice for this study since 5 weeks of age was the earliest tumors were detected. We observed noticeable differences in progenitor composition along the rostrocaudal axis. In rostral zones, we found ectopic Olig2 expression in the lateral wall and the dorsolateral corner of the SVZ (Figure 5A). These regions are normally neurogenic, as defined by the expression of DCX, but shift towards a glial fate in response to our mutations. However, the adjacent rostral white matter showed no difference in proliferation or progenitor composition (Figure 6B).

In contrast, the caudal regions of the brain showed a different response to *Pten* deletion and *K-ras* activation. Expansion of Olig2 expression was detected along both walls of the SCZ (Figure 6C). Importantly, the caudal plane of the corpus callosum showed stark enhancement of both Olig2 and DCX expression, as well as proliferation (Figure 6D). Our results highly key

differences between the SCZ and the SVZ, and suggest that mutations uniquely affect the cellular composition of these two zones.

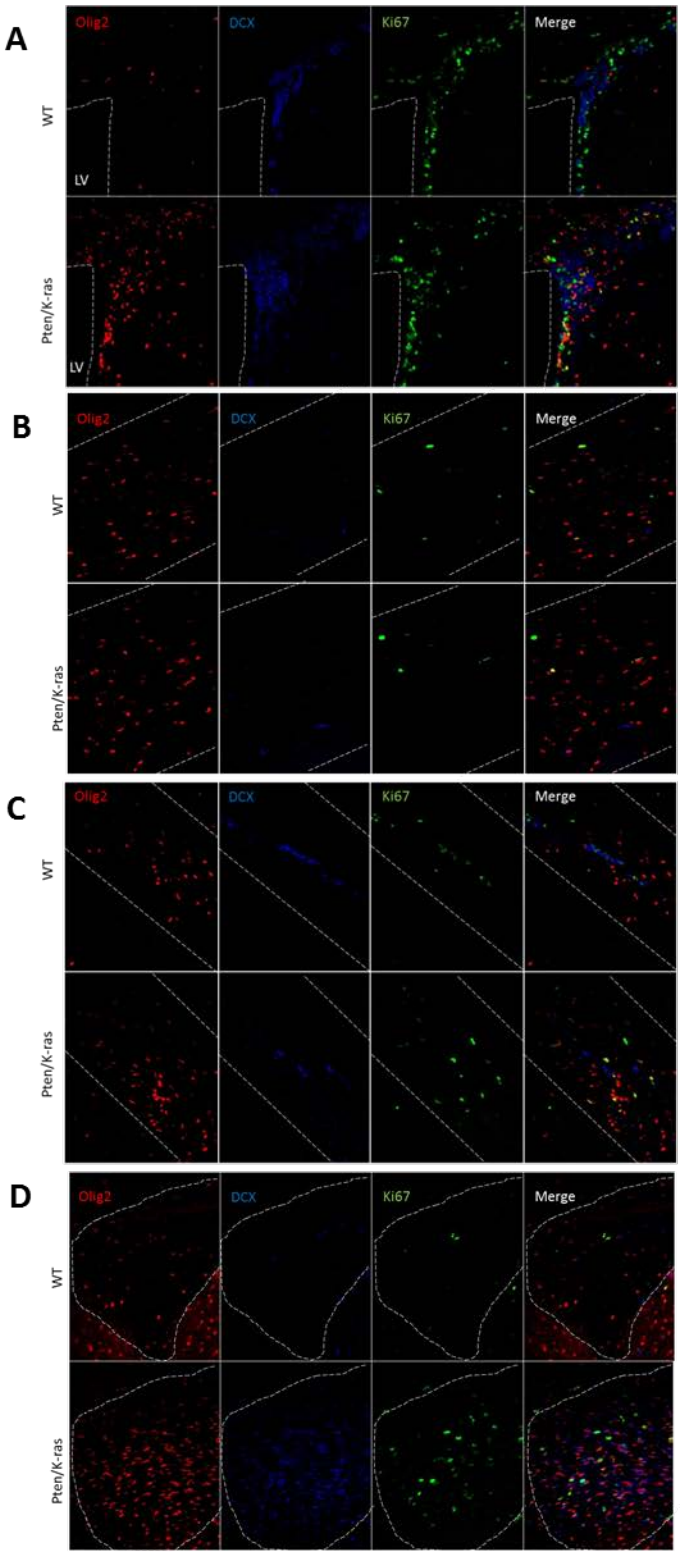

Figure 6. Comparison of Olig2 and DCX expression along the rostrocaudal axis. (A) The rostral SVZ exhibits ectopic expression of Olig2. (B) No changes in expression in the adjacent white matter. (C) The SCZ shows expansion of existing Olig2 progenitors. (D) Increase in Olig2 and DCX double positive cells in the caudal corpus callosum.

DISCUSSION

Previous studies have shown that GFAP-expressing adult neural stem cells harbor the potential to initiate GBM-like tumors upon combinations of *Rb, p53, Nf1,* and *Pten* deletions (Alcantara Llaguno et al., 2009; Jacques et al., 2010; Chow et al., 2011). These models have been useful in determining the oncogenic potential of NSCs, however, these models fail to answer two important questions. Where within this extensive niche do tumors originate from, and from which NSC subtype?

Determining the location of tumor initiation is of particular importance because anatomical position can be a prognostic factor in gliomas and reflect their cell-of-origin (Simpson et al., 1993; Fontaine and Pasquis, 2010; Lai et al., 2011). This is likely due to the genetic profiles of tumor precursor cells and their stage of development during their transformation. For example, genetic signatures and growth patterns have been shown to associate with tumor location in oligodendrogliomas (Zlatescue et al., 2001). Other studies have implicated that anatomical positioning correlates to the mutational status of GBM. A recent survey of 358 human de novo GBMs demonstrated occurrence in a high frequency within or contiguous with the caudal SVZ, and that *MGMT* promoter methylated GBMs are preferentially localized to the left hemisphere (Ellingson et al., 2012). Furthermore, GBMs with mutations in isocitrate dehydrogenase 1 (IDH1) are predominantly localized to the frontal lobe and have similar gene expression profiles as lineage-committed neural precursors (Lai et al., 2011). These clinical studies provide evidence that spatial location of gliomas reflect cell of origin, gene expression, and clinical outcome.

In addition to clinical studies, various mouse models have shown that NSCs from different germinal zones in the murine nervous system respond uniquely to glioma-causing

mutations. Deletion of *Nf1* leads to increased proliferation and gliogenesis in NSCs from the brainstem, but not the cortex, due to differential expression of the mTOR component rictor (Lee et al., 2010). Brainstem NSCs express fivefold more rictor relative to cortical NSCs, therefore *Nf1* loss results in mTORC2-mediated Akt activation and p27 degradation, leading to increased NSC proliferation and glial differentiation. Subsequently, loss of *Nf1* in NSCs from the third ventricle, but not lateral ventricles, is able to induce low grade optic gliomas (Lee et al., 2012). Transcriptomal analysis of neurospheres derived from the third and lateral ventricles revealed that they represent two molecularly-distinct stem cell populations. Furthermore, transduction of mutant N-myc into NSCs of the murine cerebellum, brainstem, and forebrain, induced distinct tumors with unique gene expression signatures (Swartling et al., 2012).

Analysis of how different compartments of the SVZ respond to oncogenic mutations has not been undertaken. The NSCs in the SVZ are heterogeneous and reside in a region-specific manner (Merkle et al., 2007), raising the question if a particular subtype may undergo transformation more readily, or if they all transform uniformly. The OB is the destination of the majority of NSCs in the SVZ. It is a complex structure, with olfactory interneurons organized into different layers based on their function. Neuroblasts enter through the core and migrate radially into the granule layer to become granule cells (GCs), or continue migration to periglomerular layer where they differentiate into periglomerular cells (PGCs) (De Marchis et al., 2007). Here, they play important roles in regulating the activity of mitral and tuft cells, the primary projection neurons that relay sensory information from the olfactory epithelia directly to the cortex (Greer, 1987). Several subtypes of GCs and PGCs can be distinguished based on their morphology and expression of molecular markers (Lledo et al., 2008). GCs can be localized into the deep or superficial layers and further subdivided based on their expression of the calcium-

binding protein calretinin (CalR) (Orona et al., 1983). PGCs can be subdivided into three types of neurons based on their expression of CalR, tyrosine hydroxylase (TH), and calbindin (CalB) (Parrish-Aungst et al., 2007). Importantly, Merkle and colleagues first demonstrated that different types of OB interneurons are derived from unique locations in the SVZ. Using adenovirus-expressing Cre, they determined that the dorsal wall of the SVZ gives rise to superficial GCs and TH^+ PGCs, whereas the ventrolateral wall produces deep GCs and $CalB^+$ PGCs. NSCs in the medial wall differentiate into $CalR^+$ GCs and PGCs. Furthermore, a study using retroviral labeling of SVZ cells showed that dendritic arbors of newborn OB interneurons are specified within different domains of the SVZ along the rostrocaudal axis (Kelsch et al., 2007). GCs with dendrites that branch into the superficial external plexiform layer are derived from NSCs residing in the anterior SVZ, whereas GCs that branch deep within the layer are from the posterior SVZ, suggesting that the rostrocaudal position of SVZ progenitors also influences their mature identity. Transplantation experiments, where progenitors from one region in the SVZ are grafted to another, failed to redirect progenitor differentiation, suggesting that fate specification is highly a cell-autonomous phenomenon (Merkle et al., 2007; Kelsch et al., 2007). These studies demonstrate that progenitor cells are intrinsically directed toward specific lineages and reside in a region specific manner. Thus, this postulates that the mosaic organization of NSCs is an important factor in gliomagenesis.

We previously determined that loss of *Pten* in SVZ NSCs resulted in enhanced proliferation without tumorigenesis or the disruption of normal neural circuitry (Supplemental Figure 1) (Gregorian et al., 2009). We reasoned that additional activation of MAPK would boost NSCs towards oncogenesis since these two pathways have been implicated to cooperate in MPNST (Chapter 2) and GBM (TCGA 2008). We found that activation of both pathways was

sufficient to induce malignant astrocytomas in the adult mouse brain. Tumors were observed throughout the frontal cortex, extending from the white matter into the surrounding brain parenchyma. Since we observed tumors throughout the mouse forebrain, we sought to determine where tumors first arose and examined the developmental pattern of our model. In both sagittal and coronal sections, we observed tumors forming in the caudal white matter during the second month of life. Subsequent analysis of mice at later time points indicated additional tumorigenesis in the rostral white matter, revealing a caudorostral glioma developmental pattern. Since the SVZ spans the majority of the frontal cortex in the adult mouse, our results suggest that stem/progenitors residing in the caudal extension of the SVZ are the first to transform due to PI3K and MAPK activation.

Our lovastatin and rapamycin treatment results provide further evidence of a directional progression in our model. Lovastatin inhibits the rate-limiting enzyme in cholesterol biosynthesis, HMG-CoA reductase, and is used to treat hyperlipidemia (Corvol et al., 2003). Lovastatin can also prevent Ras isoprenylation and activity (Mendola et al., 1990; Sebti et al., 1991), and has been shown to rescue the learning the deficits in $Nf1^{+/-}$ mice by reducing MAPK activity (Costa et al., 2001; Costa, Federov et al. 2002; Li et al., 2005). Therefore, we reasoned that lovastatin may be a promising anti-glioma therapeutic. Similar to our MPNST treatment results in Chapter 2, we saw little efficacy when administered individually, but remarkable success when combined with rapamycin. Two of the five treated mice were tumor-free upon inspection, while the remaining three showed well-defined tumors in the corpus callosum. Compared to vehicle treated controls, combination treated tumors were located more posteriorly along the rostrocaudal axis of the corpus callosum, supporting our hypothesis that tumors initiate from the SCZ. Our treatment strategy also demonstrated long-term efficacy, as 10-week-old

mice survived, on average, twice as long as controls. Surprisingly, lovastatin and rapamycin administration was unable to prevent or impede MPNST formation, despite effectively controlling brain gliomas.

It should also be noted that we never found tumors in the OB or the RMS. Yet surprisingly, we observed β-galactosidase reactivity in the OB, indicating that a subpopulation of SVZ progenitors is able to withstand genetic manipulation and follow normal integration and differentiation (Supplemental Figure 3). These results, with the MPNST resistance, demonstrate that oncogenic properties are defined by a complex interplay between genetic lesions and initiating cell-types.

Our results highlight a population of stem/progenitors residing in the caudal extension of the SVZ. During rodent brain development, the caudal regions of the lateral ventricles collapse due to hippocampal growth and expansion. The two opposing walls of the SVZ become sequestered together between the hippocampus and corpus callosum, giving rise to the SCZ. The SVZ and SCZ are similar in that they both contain multi-potent stem cells that can differentiate into neurons, oligodendrocytes, and astrocytes. *In vitro* studies have shown that stem/progenitors from this both regions can form neurospheres and differentiate into all three lineages (Seri et al., 2006). *In vivo* studies using retroviral labeling of SCZ stem/progenitors also reveal that they give rise to migrating neuroblasts that populate the olfactory bulb, and immature glia in the corpus callosum, striatum, and fimbria fornix (Menn et al., 2006). Despite these similarities, there are key differences between the two neurogenic zones. We and others have demonstrated that cells isolated from the SCZ produce fewer neurospheres than the SVZ (Supplemental Figure 4) (Seri et al., 2006). It was later reported that the rostral SVZ produces a greater number of neurons compared to the SCZ *in vivo* (Menn et al., 2006). Furthermore, it was

recently discovered that an age-dependent decline in neurogenesis occurs much more rapidly in the SCZ compared to the SVZ (Luo et al., 2006; Kim et al., 2012). Although few in number, these studies provide evidence that the SVZ and SCZ are unique and distinct germinal zones.

In the neonatal and adult SVZ, neurogenesis and gliogenesis occur simultaneously (Kriegstein and Alvarez-Bullya, 2009). The regulation of Olig2 expression in neuroglial progenitors is a critical mechanism that controls the balance between gliogenesis and neurogenesis in the postnatal SVZ (Cai et al., 2007 ; Hack et al., 2005). A number of studies have shown that Olig2 is regulated by ERK activity (Jackson et al, 2006; Kessaris et al., 2004; Hu et al., 2008; Lee J et al., 2010). Furthermore, a recent study showed that ERK activation via *Nf1* deletion can induce Olig2 expression in SVZ progenitors, thereby shifting the balance towards gliogenesis at the expense of neurogenesis (Wang et al., 2012). These findings may explain why we observe such a contrast in transformation kinetics between the SVZ and SCZ. The SCZ is innately gliogenic, expressing basal levels of Olig2 that directs precursors towards mature glia in the nearby white matter (Marshall et al., 2005; Menn et al., 2006; Seri et al., 2006). In contrast, the anterior SVZ is robustly abundant with DCX positive neuroblasts and devoid of Olig2 positive glial progenitors (Doetsch, 2003). Therefore, we postulate that glial progenitors in the SCZ have a transformation advantage over neural progenitors in the SVZ due to their innate glial status. Interestingly, heterotypic microtransplantations of SVZ grafts into the SCZ resulted in a majority of the cells merging into the RMS and maturing into granule neurons in the OB (Seri et al., 2006). Therefore, it will be interesting to characterize the specific markers that confer SCZ and SVZ cells their unique properties, and to investigate whether these markers are detectable in gliomas.

It would be interesting to determine which GBM subtype our model reflects. A recent study deleted *Pten* and *p53* in PDGFRA positive glial progenitors and compared gene expression of the resulting gliomas to the four GBM subtypes. They found that their model resembled the Proneural subtype, establishing the relationship between glial progenitors and Proneural GBM (Lei et al., 2011). In our model, we observe high phospho-PDGFRA reactivity in the SCZ and tumors (Supplemental Figure 5), therefore we hypothesize that our model would reflect the Proneural subtype. However, we also postulate that our model may harbor properties similar to other subtypes. The presence of tumors stemming from the rostral SVZ raises the question if these tumors retain their neural gene expression and therefore would be similar to the Neural subtype, or if the ectopic Olig2 expression directs them towards the Proneural group. Further studies are required to determine the gene expression profiles of the tumors from our model.

Our study highlights the impact that NSC diversity has on gliomagenesis. We provide the first evidence that the SVZ and SCZ are distinct germinal zones harboring different oncogenic properties. First, we show that tumors originate in the caudal white matter and exhibit a caudorostral progression. This is supported by our treatment results, in which we slow the progression of gliomas and observe tumors only in the caudal regions of the white matter. Secondly, we show increased reporter staining in the SCZ, prior to the SVZ, and that our genetic perturbations in GFAP-expressing NSCs do not result in a uniform increase of proliferation among stem/progenitors, but rather affect the SCZ separately from the SVZ. Finally, we show that the SVZ and SCZ are innately different in their composition of neural and glial progenitors, and that activation of the PI3K and MAPK pathways uniquely alter the cellular make-up of the two niches. This study demonstrates that transformation among neural stem cells is not uniform,

and reveals a critical role of the SCZ in gliomagenesis, imploring for further investigation of SCZ progenitors.

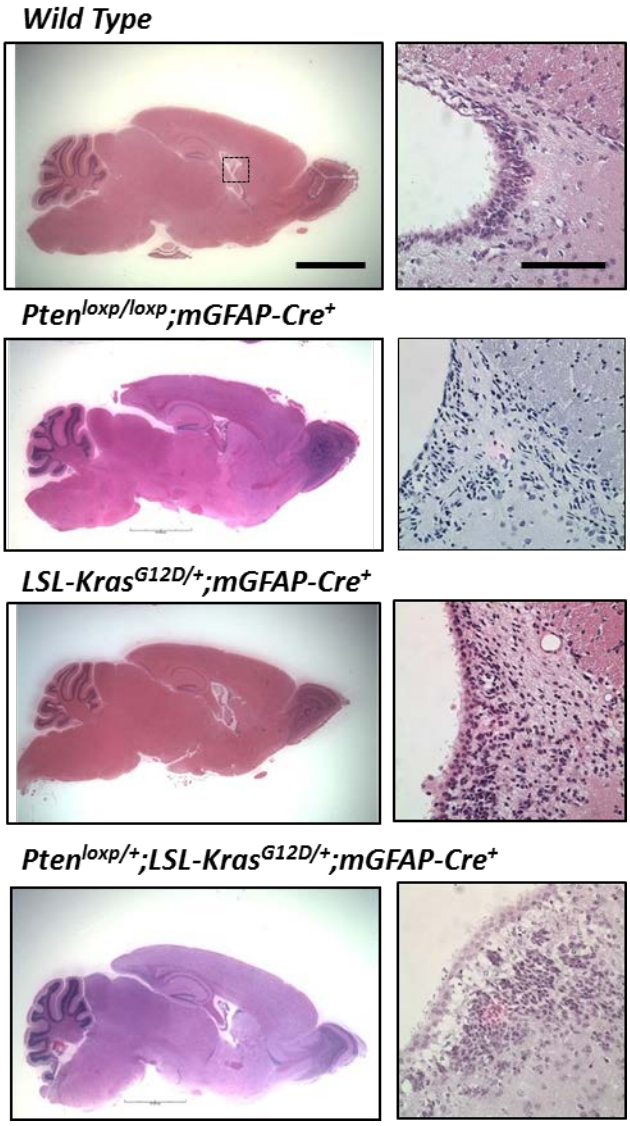

Supplementary Figure 1. Sagittal sections of non-gliomagenic geneotypes. Deletion of *Pten* or activation of *K-ras* leads to increased cellularity in the SVZ (right), without tumorigenesis. Mice are viable and indistinguishable from WT littermates. Heterozygous deletion of *Pten* with activation of *K-ras* induces NF1 phenotype (Chapter 2), without CNS tumorigenesis. Scale bar: 3 mm, 75µm.

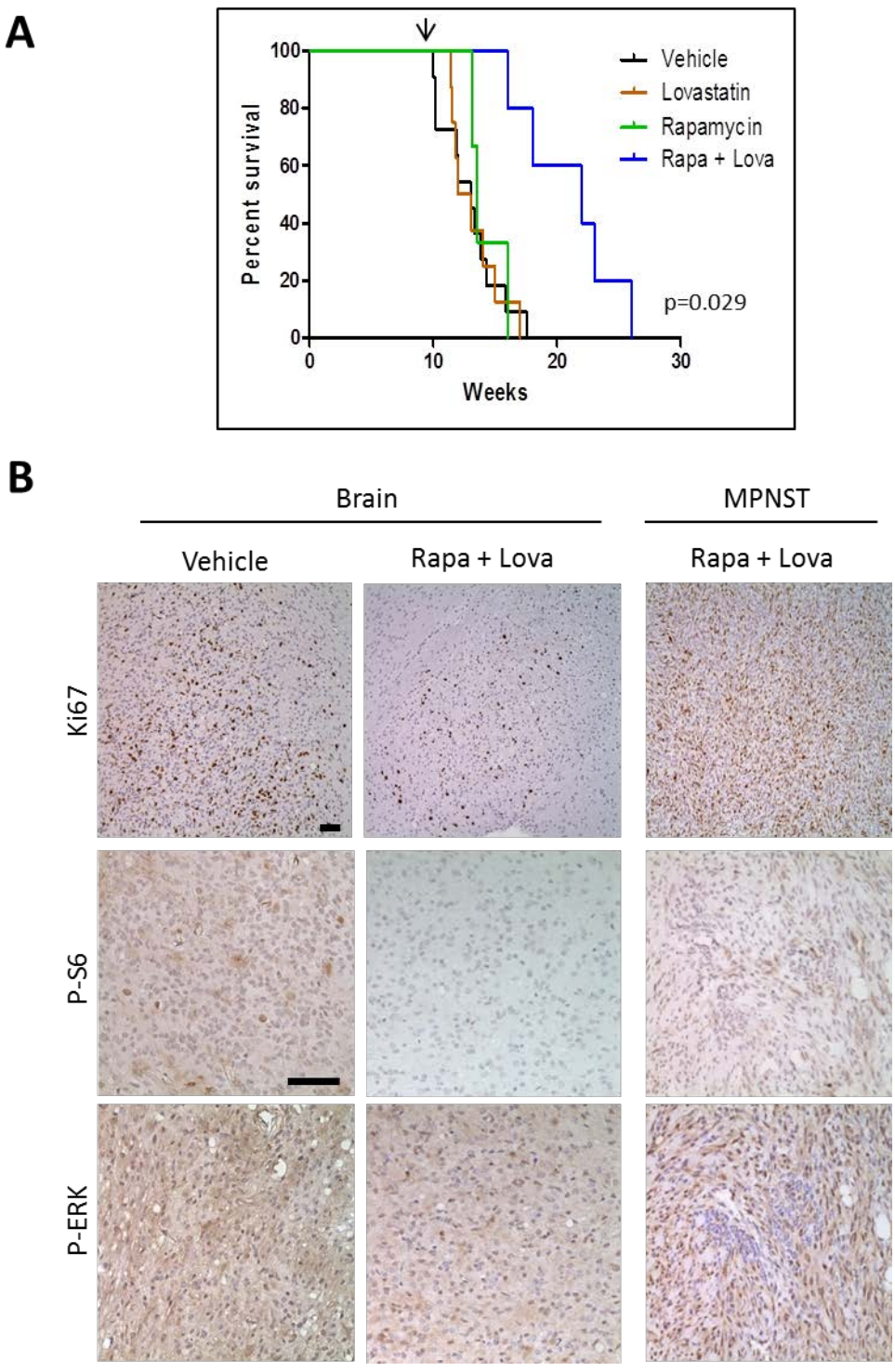

Supplemental Figure 2. Treatment of 10-week-old mice with rapamycin and lovastatin increases survival but is not effective against MPNST. (A) Survival curve of treated mice. (B) Immuostaining for Ki-67 and downstream effectors of the PI3K and MAPK pathways. Scale bars: 50 µm.

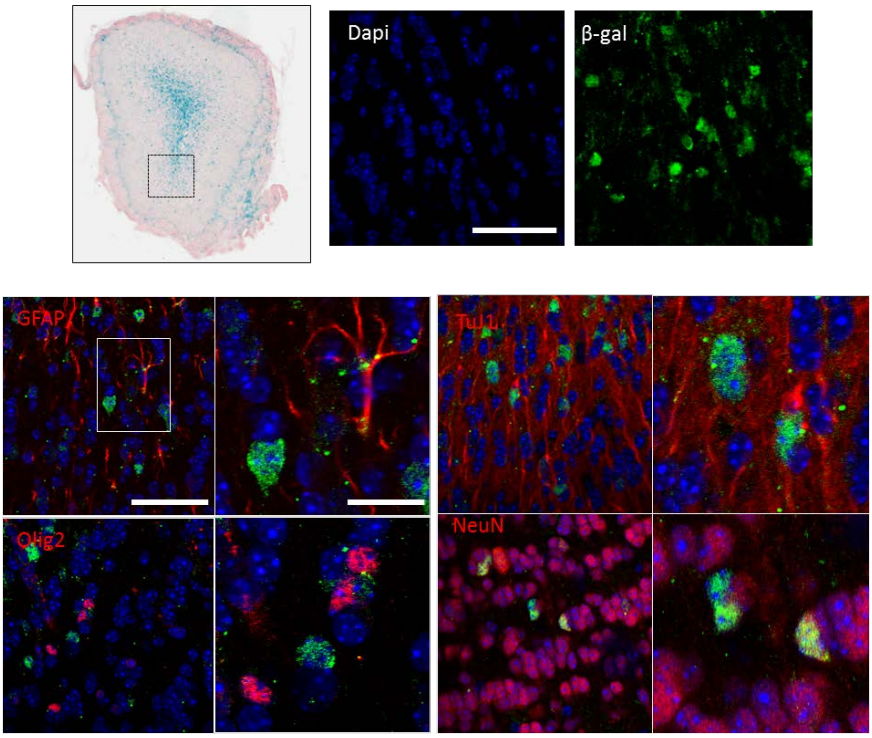

Supplementary Figure 3. Lineage tracing of SVZ progenitors in the OB of mutant mice. A subpopulation of SVZ stem cells are able to integrate and differentiate normally in the mutant OB despite genetic manipulation. β-galactosidase positive cells (green) are able to repress glial markers GFAP and Olig2(red, left) and express neuronal marker TuJ1 and NeuN (red, right).

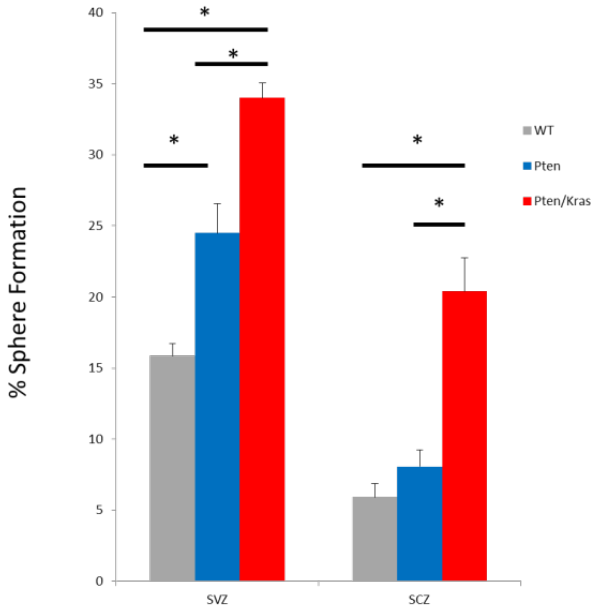

Supplementary Figure 4. Difference in self-renewal between SVZ and SCZ. NSCs from WT SVZ and SCZ have different self-renewal capacities and self-renewal responses to genetic manipulations.

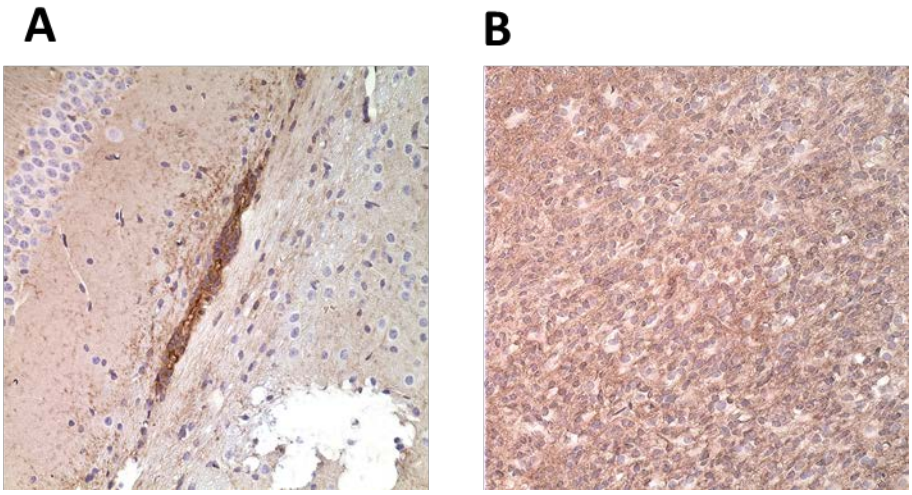

Supplementary Figure 5. Phospho-PDGFRA staining in the brain. (A) The pre-tumorigenic SCZ and (B) brain tumors show high PDGFR activity.

Experimental Procedures

Animals

Pten$^{loxp/loxp}$;*mGFAP-Cre*$^{+}$ transgenic mice line were generated previously (Gregorian et al. 2009) and crossed to *LSL-Kras*$^{G12D/+}$on a C57, 129/Balb/c background(Jackson, Willis et al. 2001). loxP-Stop-loxP-K-ras$^{G12D/G12D}$ (LSL-K-ras$^{G12D/G12D}$) mice are embryonically lethal. F_1 generation *Pten*$^{loxp/+}$;*LSL-Kras*$^{G12D/+}$ males were backcrossed with *Pten*$^{loxp/loxp}$;*mGFAP-Cre*$^{+}$ females to produce F_2 generation experimental animals. Animals were genotyped by standard genomic PCR techniques (Lesche, Groszer et al. 2002). *Pten*$^{loxp/loxp}$;*mGFAP-Cre*$^{+}$ mice were crossed to ROSA26 (Soriano, 1999) mice for reporter analysis as described previously (Gregorian et al., 2009). Mice were observed daily for evidence of illness or tumor formation. If loss 10% of body weight or had difficulty feeding and grooming, mice were sacrificed. Moribund mice with possible internal tumors were also sacrificed. Animals were housed in a temperature-, humidity-, and light-controlled room (12-h light/dark cycle), and allowed free access to food and water. All experiments were conducted according to the research guidelines of the UCLA Chancellor's Animal Research Committee.

Polymerase Chain Reaction (PCR)

The specificity of *Pten* excision and Cre expression was evaluated by PCR using DNA from tail clip biopsy as described previously (Gregorian et al., 2009). The *K-ras* and *Lox-K-ras G12D* alleles were detected via combination of 3'universal with either 5'wt and 3'mut, The yielding a 265-bp and a 305-bp product, respectively. dt5' new (5'wt) 5'GTC GAC AAG CTC ATG CGG G 3' , Uni'new (3'universal) 5' CGC AGA CTG TAG AGC AGC G 3', and SD5'-new (5'mut) 5' CCA TGG CTT GAG TAA GTC TGC 3'. PCR was performed in 20 µl reactions using standard procedures for forty cycles; each cycle consisted of denaturing at 94˚C for 30", annealing at 60˚C

for 1:30', and extension at 72˚C for 1', followed by a single 5' extension at 72˚C. The PCR products were analyzed on 2% agarose gels.

Histology and Immunohistochemistry of Tissue Sections

All tumors were graded according to World Health Organization (WHO) histopathological criteria (Kleihues, Louis et al. 2002). IHC staining was performed on age-matched control and mutant sections. 5 μm sections that were prepared from paraffin-embedded blocks were placed on charged glass slides. The slides were deparaffinized with xylene and rehydrated in descending grades (100%–70%) of ethanol. The endogenous peroxidase activity was inactivated in 3% hydrogen peroxide (H_2O_2). After washing in deionized water, antigen retrieval was performed by incubating the slides in 0.01 M citric acid buffer (pH 6.0) at 95°C for 13.5 min. Slides were then allowed to cool for 30 min in citric acid buffer. After washing in deionized water, the slides were then transferred to either PBS (pH 7.4) or TBST for 5 min. For DAB staining, slides were first blocked with 5% normal donkey serum then incubated with primary antibody overnight at 4°C. Following three 5 min washes in either PBS or TBST, slides were incubated with biotinylated secondary antibody (1:200, Jackson Immunoresearch) for 30 min at room temperature. Amplification was performed with a horseradish peroxidase system (Vectastain ABC kit, Vector, PK-6100) using a liquid DAB peroxidase substrate (Biogenex, HK130-5K). Slides were counterstained in Gill's hematoxylin, dehydrated, cleared, and cover-slipped. Negative control slides were run without primary antibody. Primary antibodies used were PTEN (1:100, Cell Signaling), P-AKT (1:50; Cell Signaling); P-S6 (1:100 Cell Signaling); P-ERK (1:100, Cell Signaling); Ki-67 (1:500; Vector); GFAP (1:500; Dako); Olig2 (1:200; IBL); Nestin (1:5000; Novus); DCX (1:500; Santa Cruz); P-PDGFRA (1:300; Santa Cruz).

For fluorescence double staining, the section was treated as above and first stained with the first antibody followed by Alexa Fluor® conjugated secondary antibody (Invitrogen). After staining, slides were incubated in Dapi (Invitrogen) for 5 minutes, washed in TBST, and coverslipped using Prolong mounting medium (Invitrogen).

X-gal staining.

Mice were prepared and stained as previously described (Soriano, 1999). *Pten*$^{loxp/loxp}$*; K-ras*$^{G12D/+}$*; mGFAP-Cre*77.6^{+};ROSA26 mice were intracardially perfused with a fixative solution of 2% formalin , 0.2% glutaraldehyde in PBS. The brains were cryoprotected in 30% sucrose in PBS until they lost buoyancy. They were embedded in OCT, sectioned at 30um, then stained free-floating in X-gal solution for 4 hours. Sections were washed in PBS, mounted on to charged glass slides and coverslipped with 50% glycerol.

Ki-67 Quantification

Slides were digitally scanned at 20x magnification using an Aperio XL system (Aperio, Vista, CA), and images were quantified using the Definiens imaging software.

Rapamycin and Lovastatin Treatment

Rapamycin powder (LC Laboratories, Woburn, MA) was reconstituted in 100% ethanol to a stock solution of 10 mg/mL and was stored at -20ºC. Working solution was made each time by diluting the stock solution to 1 mg/mL with vehicle (5.68% Tween-80, 5.68% polyethylene glycol 400 in water). Rapamycin (4 mg/kg) in vehicle was administered via intraperitoneal injection daily. Lovastatin powder (Sigma) was reconstituted in ethanol at 55ºC (50 mg/mL) and diluted to a final concentration of 4 mg/mL in water at pH 7.5. Lovastatin (10 mg/kg) was injected subcutaneously daily.

Chapter 3 References

Alcantara Llaguno S, Chen J, Kwon CH, Jackson EL, Li Y, Burns DK, Alvarez-Buylla A, Parada LF (2009). Malignant astrocytomas originate from neural stem/progenitor cells in a somatic tumor suppressor mouse model. Cancer Cell. *15*: 45-56.

Cai J, Chen Y, Cai WH, Hurlock EC, Wu H, Kernie SG, Parada LF, Lu QR (2007). A crucial role for Olig2 in white matter astrocyte development. Development. *134*: 1887-99.

Chow LM, Endersby R, Zhu X, Rankin S, Qu C, Zhang J, Broniscer A, Ellison DW, Baker SJ (2011). Cooperativity within and among Pten, p53, and Rb pathways induces high-grade astrocytoma in adult brain. Cancer Cell. *19*: 305-16.

Corvol JC, Bouzamondo A, Sirol M, Hulot JS, Sanchez P, Lechat P (2003). Differential effects of lipid-lowering therapies on stroke prevention: a meta-analysis of randomized trials. Arch Intern Med.*163*:669-76.

Curtis MA, Kam M, Nannmark U, Anderson MF, Axell MZ, Wikkelso C, Holtås S, van Roon-Mom WM, Björk-Eriksson T, Nordborg C, Frisén J, Dragunow M, Faull RL, Eriksson PS (2007). Human neuroblasts migrate to the olfactory bulb via a lateral ventricular extension. Science. *315*: 1243-9.

De Marchis S, Bovetti S, Carletti B, Hsieh YC, Garzotto D, Peretto P, Fasolo A, Puche AC, Rossi F (2007). Generation of distinct types of periglomerular olfactory bulb interneurons during development and in adult mice: implication for intrinsic properties of the subventricular zone progenitor population. J Neurosci. *27*: 657-64.

Doetsch F, Alvarez-Buylla A (1996). Network of tangential pathways for neuronal migration in adult mammalian brain. Proc Natl Acad Sci U S A. *93*: 14895-900.

Doetsch F (2003). The glial identity of neural stem cells. Nat Neurosci *6*:1127-34.

Ellingson BM, Cloughesy TF, Pope WB, Zaw TM, Phillips H, Lalezari S, Nghiemphu PL, Ibrahim H, Naeini KM, Harris RJ, Lai A (2012). Anatomic localization of O6-methylguanine DNA methyltransferase (MGMT) promoter methylated and unmethylated tumors: a radiographic study in 358 de novo human glioblastomas. Neuroimage. *59*: 908-16.

Fontaine D, Paquis P (2010). Glioblastoma: clinical, radiological and biological prognostic factors. Neurochirurgie. *56*: 467-76.

Garcia AD, Doan NB, Imura T, Bush TG, Sofroniew MV (2004). GFAP-expressing progenitors are the principal source of constitutive neurogenesis in adult mouse forebrain. Nat Neurosci. *7*: 1233-41.

Gonzalez-Perez O, Alvarez-Buylla A (2011). Oligodendrogenesis in the subventricular zone and the role of epidermal growth factor. Brain Res Rev.*67*:147-56.

Greer CA (1987). Golgi analyses of dendritic organization among denervated olfactory bulb granule cells. J Comp Neurol. *257*: 442-52.

Hack MA, Saghatelyan A, de Chevigny A, Pfeifer A, Ashery-Padan R, Lledo PM, Götz M (2005). Neuronal fate determinants of adult olfactory bulb neurogenesis. Nat Neurosci. *8*: 865-72.

Hu JG, Fu SL, Wang YX, Li Y, Jiang XY, Wang XF, Qiu MS, Lu PH, Xu XM (2008). Platelet-derived growth factor-AA mediates oligodendrocyte lineage differentiation through activation of extracellular signal-regulated kinase signaling pathway. Neuroscience. *151*:138-47.

Huse JT, Holland E, DeAngelis LM (2013). Glioblastoma: molecular analysis and clinical implications. Annu Rev Med. *64*: 59-70.

Imura T, Kornblum HI, Sofroniew MV (2003). The predominant neural stem cell isolated from postnatal and adult forebrain but not early embryonic forebrain expresses GFAP. J Neurosci. *23*: 2824-32.

Jackson EL, Garcia-Verdugo JM, Gil-Perotin S, Roy M, Quinones-Hinojosa A, VandenBerg S, Alvarez-Buylla A (2006). PDGFR alpha-positive B cells are neural stem cells in the adult SVZ that form glioma-like growths in response to increased PDGF signaling. Neuron. *51*: 187-99.

Jacques TS, Swales A, Brzozowski MJ, Henriquez NV, Linehan JM, Mirzadeh Z, O' Malley C, Naumann H, Alvarez-Buylla A, Brandner S (2010). Combinations of genetic mutations in the adult neural stem cell compartment determine brain tumour phenotypes. EMBO J. *29*: 222-35.

Kelsch W, Mosley CP, Lin CW, Lois C (2007). Distinct mammalian precursors are committed to generate neurons with defined dendritic projection patterns. PLoS Biol. *5*: e300.

Kessaris N, Jamen F, Rubin LL, Richardson WD (2004). Cooperation between sonic hedgehog and fibroblast growth factor/MAPK signalling pathways in neocortical precursors. Development. *131*: 1289-98.

Kriegstein A, Alvarez-Buylla A (2009). The glial nature of embryonic and adult neural stem cells. Annu Rev Neurosci. *32*:149-84.

Lai A, Kharbanda S, Pope WB, Tran A, Solis OE, Peale F, Forrest WF, Pujara K, Carrillo JA, Pandita A, Ellingson BM, Bowers CW, Soriano RH, Schmidt NO, Mohan S, Yong WH, Seshagiri S, Modrusan Z, Jiang Z, Aldape KD, Mischel PS, Liau LM, Escovedo CJ, Chen W, Nghiemphu PL, James CD, Prados MD, Westphal M, Lamszus K, Cloughesy T, Phillips HS (2011). Evidence for sequenced molecular evolution of IDH1 mutant glioblastoma from a distinct cell of origin. J Clin Oncol. *29*: 4482-90.

Lee da Y, Yeh TH, Emnett RJ, White CR, Gutmann DH (2010). Neurofibromatosis-1 regulates neuroglial progenitor proliferation and glial differentiation in a brain region-specific manner. Genes Dev. *24*: 2317-29.

Lee da Y, Gianino SM, Gutmann DH (2012). Innate neural stem cell heterogeneity determines the patterning of glioma formation in children. Cancer Cell. *22*:131-8.

Lee JS, Padmanabhan A, Shin J, Zhu S, Guo F, Kanki JP, Epstein JA, Look AT (2010). Oligodendrocyte progenitor cell numbers and migration are regulated by the zebrafish orthologs of the NF1 tumor suppressor gene. Hum Mol Genet. *19*: 4643-53.

Lei L, Sonabend AM, Guarnieri P, Soderquist C, Ludwig T, Rosenfeld S, Bruce JN, Canoll P (2011). Glioblastoma models reveal the connection between adult glial progenitors and the proneural phenotype. PLoS One. *6*: e20041.

Li W, Cui Y, Kushner SA, Brown RA, Jentsch JD, Frankland PW, Cannon TD, Silva AJ (2005). The HMG-CoA reductase inhibitor lovastatin reverses the learning and attention deficits in a mouse model of neurofibromatosis type 1. Curr Biol.*15*: 1961-7.

Ligon KL, Huillard E, Mehta S, Kesari S, Liu H, Alberta JA, Bachoo RM, Kane M, Louis DN, Depinho RA, Anderson DJ, Stiles CD, Rowitch DH (2007). Olig2-regulated lineage-restricted pathway controls replication competence in neural stem cells and malignant glioma. Neuron.*53*: 503-17.

Lim SK, Llaguno SR, McKay RM, Parada LF (2011). Glioblastoma multiforme: a perspective on recent findings in human cancer and mouse models. BMB Rep. *44*: 158-64.

Lledo PM, Merkle FT, Alvarez-Buylla A (2008). Origin and function of olfactory bulb interneuron diversity. Trends Neurosci. *31*: 392-400.

Louis DN, Ohgaki H, Wiestler OD, Cavenee WK, Burger PC, Jouvet A, Scheithauer BW, Kleihues P (2007). The 2007 WHO classification of tumours of the central nervous system. Acta Neuropathol. *114*: 97-109.

Luskin MB (1993). Restricted proliferation and migration of postnatally generated neurons derived from the forebrain subventricular zone. Neuron. *11*: 173-89.

Marshall CA, Novitch BG, Goldman JE (2005). Olig2 directs astrocyte and oligodendrocyte formation in postnatal subventricular zone cells. J Neurosci *25*: 7289-98.

Mendola CE, Backer JM (1990). Lovastatin blocks N-ras oncogene-induced neuronal differentiation. Cell Growth Differ. *1*: 499-502.

Menn B, Garcia-Verdugo JM, Yaschine C, Gonzalez-Perez O, Rowitch D, Alvarez-Buylla A (2006). Origin of oligodendrocytes in the subventricular zone of the adult brain. J Neurosci. *26*: 7907-18.

Merkle FT, Mirzadeh Z, Alvarez-Buylla A (2007). Mosaic organization of neural stem cells in the adult brain. Science. *317*:381-4.

Ohgaki H, Kleihues P (2013). The definition of primary and secondary glioblastoma. Clin Cancer Res *19*: 764-72.

Orona E, Scott JW, Rainer EC (1983). Different granule cell populations innervate superficial and deep regions of the external plexiform layer in rat olfactory bulb. J Comp Neurol. *217*: 227-37.

Parrish-Aungst S, Shipley MT, Erdelyi F, Szabo G, Puche AC (2007). Quantitative analysis of neuronal diversity in the mouse olfactory bulb. J Comp Neurol. *501*: 825-36.

Paugh BS, Qu C, Jones C, Liu Z, Adamowicz-Brice M, Zhang J, Bax DA, Coyle B, Barrow J, Hargrave D, Lowe J, Gajjar A, Zhao W, Broniscer A, Ellison DW, Grundy RG, Baker SJ (2010). Integrated molecular genetic profiling of pediatric high-grade gliomas reveals key differences with the adult disease. J Clin Oncol. *28*: 3061-8.

Petreanu L, Alvarez-Buylla A (2002). Maturation and death of adult-born olfactory bulb granule neurons: role of olfaction. J Neurosci. *22*: 6106-13.

Sebti SM, Tkalcevic GT, Jani JP (1991). Lovastatin, a cholesterol biosynthesis inhibitor, inhibits the growth of human H-ras oncogene transformed cells in nude mice. Cancer Commun. *3*:141-7.

Seri B, Herrera DG, Gritti A, Ferron S, Collado L, Vescovi A, Garcia-Verdugo JM, Alvarez-Buylla A (2006). Composition and organization of the SCZ: a large germinal layer containing neural stem cells in the adult mammalian brain. Cereb Cortex *16*: 103-11.

Simpson JR, Horton J, Scott C, Curran WJ, Rubin P, Fischbach J, Isaacson S, Rotman M, Asbell SO, Nelson JS, et al. (1993). Influence of location and extent of surgical resection on survival of patients with glioblastoma multiforme: results of three consecutive Radiation Therapy Oncology Group (RTOG) clinical trials. Int J Radiat Oncol Biol Phys. *26*: 239-44.

Soriano, P. (1999). Generalized lacZ expression with the ROSA26 Cre reporter strain. Nat Genet 21(1): 70-1.

Swartling FJ, Savov V, Persson AI, Chen J, Hackett CS, Northcott PA, Grimmer MR, Lau J, Chesler L, Perry A, Phillips JJ, Taylor MD, Weiss WA (2012). Distinct neural stem cell populations give rise to disparate brain tumors in response to N-MYC. Cancer Cell. *21*: 601-13.

Verhaak RG, Hoadley KA, Purdom E, Wang V, Qi Y, Wilkerson MD, Miller CR, Ding L, Golub T, Mesirov JP, Alexe G, Lawrence M, O'Kelly M, Tamayo P, Weir BA, Gabriel S, Winckler W, Gupta S, Jakkula L, Feiler HS, Hodgson JG, James CD, Sarkaria JN, Brennan C, Kahn A, Spellman PT, Wilson RK, Speed TP, Gray JW, Meyerson M, Getz G, Perou CM, Hayes DN; Cancer Genome Atlas Research Network (2010). Integrated genomic analysis identifies clinically relevant subtypes of glioblastoma characterized by abnormalities in PDGFRA, IDH1, EGFR, and NF1. Cancer Cell. *17*: 98-110.

Wang Y, Kim E, Wang X, Novitch BG, Yoshikawa K, Chang LS, Zhu Y (2012). ERK inhibition rescues defects in fate specification of Nf1-deficient neural progenitors and brain abnormalities. Cell. *150*: 816-30.

Zlatescu MC, TehraniYazdi A, Sasaki H, Megyesi JF, Betensky RA, Louis DN, Cairncross JG (2001). Tumor location and growth pattern correlate with genetic signature in oligodendroglial neoplasms. Cancer Res. *61*: 6713-5.

Chapter 4:

Concluding Remarks

Summary

Cancers of the nervous system continue to be a significant cause of disfigurement, morbidity, and death. They are the most common form of pediatric solid tumors, in part due to the hereditary disorder of Neurofibromatosis Type 1. Genetic profiling of NF1 patients has provided insight into the role of the *NF1* gene in pathogenesis, however knocking out *Nf1* in a variety of cell populations in the mouse has not recapitulated the full spectrum of the disease, suggesting that other genetic events are likely. We are the first study to provide functional evidence that PTEN is important in controlling neurofibroma onset and subsequent malignant progression. Because no good treatment options exist for MPNSTs, the implications from our study are crucial. Our results provide a new signaling pathway responsible for the progression of an otherwise untreatable disease. Since then there have been other groups that have generated MPNST models in similar fashion by deleting *Pten* either in combination with *Nf1* deletion or with over-expression of EGFR (Keng et al., 2012a, b). Additionally, surveys of human MPNSTs have found alterations in PTEN and its controlled signaling pathway, confirming that this event occurs in human disease (Bradtmöller et al., 2012; Masliah-Planchon et al., 2013). These results provide a new hope for NF1 and MPNST patients, as new inhibitors of the PI3K/AKT/mTOR pathway are being developed (Welker and Kulik, 2013).

Like MPNSTs, few good treatment options exist for malignant brain gliomas. However, advancement in genetic analysis and the generation of mouse models have provided valuable insight into the mutations and cell-types that cause disease. Experiments in mice have shown that not only can NSCs give rise to tumors, but that differentiated neurons and astrocytes can as well (Friedmann-Morvinski et al., 2012). While these studies show that oncogenic potential exists among all cell-types in the brain, they also raise the question of which cell is most likely to

transform and produce a tumor. By mutating the entire GFAP stem cell population, and performing age-dependent analysis, we show that transformation is not uniform among stem cells. We demonstrate that progenitors in the SCZ are a likely cell-of-origin for gliomas, as they have an oncogenic advantage over those in the SVZ, perhaps due to their innate gliogenic identity. Our results highlight the importance of glial progenitor involvement in gliomas, and call for the investigation gliogenic zones in the human brain. In conclusion, the results from this dissertation have direct implications regarding new treatment strategies and new cellular origins of cancers of the nervous system.

Chapter 4 References

Bradtmöller M, Hartmann C, Zietsch J, Jäschke S, Mautner VF, Kurtz A, Park SJ, Baier M, Harder A, Reuss D, von Deimling A, Heppner FL, Holtkamp N(2012). Impaired Pten expression in human malignant peripheral nerve sheath tumours. PLoS One. *7*: e47595.

Friedmann-Morvinski D, Bushong EA, Ke E, Soda Y, Marumoto T, Singer O, Ellisman MH, Verma IM (2012). Dedifferentiation of neurons and astrocytes by oncogenes can induce gliomas in mice. Science. 338:1080-4.

Keng VW, Rahrmann EP, Watson AL, Tschida BR, Moertel CL, Jessen WJ, Rizvi TA, Collins MH, Ratner N, Largaespada DA (2012). PTEN and NF1 inactivation in Schwann cells produces a severe phenotype in the peripheral nervous system that promotes the development and malignant progression of peripheral nerve sheath tumors. Cancer Res. *72*: 3405-13.

Keng VW, Watson AL, Rahrmann EP, Li H, Tschida BR, Moriarity BS, Choi K, Rizvi TA, Collins MH, Wallace MR, Ratner N, Largaespada DA (2012). Conditional Inactivation of Pten with EGFR Overexpression in Schwann Cells Models Sporadic MPNST. Sarcoma. *2012*: 620834.

Masliah-Planchon J, Pasmant E, Luscan A, Laurendeau I, Ortonne N, Hivelin M, Varin J, Valeyrie-Allanore L, Dumaine V, Lantieri L, Leroy K, Parfait B, Wolkenstein P, Vidaud M, Vidaud D, Bièche I (2013). MicroRNAome profiling in benign and malignant neurofibromatosis type 1-associated nerve sheath tumors: evidences of PTEN pathway alterations in early NF1 tumorigenesis. BMC Genomics. *14*: 473.

Welker ME, Kulik G (2013). Recent syntheses of PI3K/Akt/mTOR signaling pathway inhibitors. Bioorg Med Chem. *21*: 4063-91.

APPENDIX

Development/Plasticity/Repair

Pten Deletion in Adult Neural Stem/Progenitor Cells Enhances Constitutive Neurogenesis

Caroline Gregorian,[1] Jonathan Nakashima,[1] Janel Le Belle,[1] John Ohab,[2] Rachel Kim,[1] Annie Liu,[1] Kate Barzan Smith,[1] Matthias Groszer,[1,3] A. Denise Garcia,[4] Michael V. Sofroniew,[4] S. Thomas Carmichael,[2] Harley I. Kornblum,[1,5] Xin Liu,[1,3] and Hong Wu[1]

Departments of [1]Molecular and Medical Pharmacology, [2]Neurology, [3]Pathology and Laboratory Medicine, and [4]Neurobiology, [5]The Semel Institute, David Geffen School of Medicine, University of California, Los Angeles, Los Angeles, California 90095

Here we show that conditional deletion of *Pten* in a subpopulation of adult neural stem cells in the subependymal zone (SEZ) leads to persistently enhanced neural stem cell self-renewal without sign of exhaustion. These *Pten* null SEZ-born neural stem cells and progenies can follow the endogenous migration, differentiation, and integration pathways and contribute to constitutive neurogenesis in the olfactory bulb. As a result, *Pten* deleted animals have increased olfactory bulb mass and enhanced olfactory function. *Pten* null cells in the olfactory bulb can establish normal connections with peripheral olfactory epithelium and help olfactory bulb recovery from acute damage. Following a focal stroke, *Pten* null progenitors give rise to greater numbers of neuroblasts that migrate to peri-infarct cortex. However, in contrast to the olfactory bulb, no significant long-term survival and integration can be observed, indicating that additional factors are necessary for long-term survival of newly born neurons after stroke. These data suggest that manipulating PTEN-controlled signaling pathways may be a useful step in facilitating endogenous neural stem/progenitor expansion for the treatment of disorders or lesions in regions associated with constitutive neurogenesis.

Key words: SEZ; PTEN; neurogenesis; olfactory; neural repair; poststroke

Introduction

The adult CNS contains self-renewing stem cells capable of generating new neurons, astrocytes, and oligodendrocytes, a process evolutionarily conserved in birds, rodents, primates, and humans (Doetsch, 2003). The subependymal zone (SEZ) is one of at least two areas of adult neurogenesis where glial fibrillary acidic protein (GFAP) expressing cells act as slow-dividing neural stem cells (NSCs) capable of generating neuroblast precursors (Doetsch, 2003; Garcia et al., 2004; Lledo et al., 2006). The neuroblasts migrate into the rostral migratory stream (RMS) and then into the olfactory bulb (OB) where they differentiate into granule and periglomerular neurons (Luskin, 1993; Lois et al., 1996; Petreanu and Alvarez-Buylla, 2002; Hack et al., 2005; Curtis et al., 2007). Since the majority of granule neurons in the OB are generated postnatally (Petreanu and Alvarez-Buylla, 2002), it is believed that continued neoneurogenesis from the SEZ is critical for maintaining the homeostasis of the OB and therefore the olfactory functions (Goldman, 1998).

NSC-mediated neoneurogenesis is also believed to participate in the process of neural repair. Recent findings suggest endogenously generated new neurons participate in the formation of circuitry and at least some functional recovery following neurological damage such as stroke (Yamashita et al., 2006). Therefore, understanding the molecular mechanisms and pathways capable of activating and expanding neural stem/precursor cell (NS/PC) populations, stimulating their migration toward damaged or diseased areas, enhancing their survival, and promoting their maturation and integration into the existing neural circuitries may ultimately lead to repair and improve damaged neuronal functions (Peterson, 2002; Emsley et al., 2005).

Phosphatase and tensin homolog deleted on chromosome 10 (*PTEN*) encodes a phosphatase and is a potent antagonist of phosphatidylinositol-3-kinase (PI3K) (Liaw et al., 1997; Nelen et al., 1997; Li et al., 1998) and its regulated pathways (Lee et al., 1999; Maehama et al., 2001; Vivanco and Sawyers, 2002). Utilizing Cre-Lox technology, our group as well as others have generated mouse models with conditional deletion of the murine homolog of the *PTEN* gene (*Pten*) in the brain at different developmental stages (Backman et al., 2001; Groszer et al., 2001; Kwon et al., 2001; Marino et al., 2002; Fraser et al., 2004; Stiles et al., 2004; Yue et al., 2005). By deleting *Pten* in the embryonic NSCs, we showed PTEN negatively regulates NSC proliferation, survival, and self-renewal, both *in vivo* and *in vitro* (Groszer et al.,

Received July 3, 2008; revised Nov. 8, 2008; accepted Dec. 17, 2008.

This work was supported by Miriam and Sheldon Adelson Program in Neural Repair and Rehabilitation (to H.W., S.T.C., M.V.S., H.I.K.), National Institutes of Health Grants NS047386 (to M.V.S.) and MH65756 (to H.I.K., H.W.), Brain Tumor Society (to X.L., H.W.), and Henry Singleton Brain Cancer Research Program and James S. McDonnell Foundation Award (to H.W.). C.G. and K.B.S. are predoctoral trainees supported by United States Department of Health and Human Services Ruth L. Kirschstein Institutional National Research Service Award T32 CA09056. We thank Dr. Guoping Fan and members of our laboratories for helpful comments on this manuscript.

The authors declare no competing financial interests.

Correspondence should be addressed to Dr. Hong Wu, Department of Molecular and Medical Pharmacology, CHS 23-214, University of California, Los Angeles School of Medicine, 650 CE Young Drive South, Los Angeles, CA 90095-1735. E-mail: hwu@mednet.ucla.edu.

M. Groszer's present address: Wellcome Trust Centre for Human Genetics, University of Oxford, Roosevelt Drive, Oxford OX3 7BN, UK.

DOI:10.1523/JNEUROSCI.3095-08.2009

 0270-6474/09/291874-13$15.00/0

2001, 2006). Our recent results demonstrate that *Pten* null NS/PCs have enhanced self-renewal capacity, accelerated G0-G1 cell cycle entry, shortened cell cycle, and decreased growth factor dependency (Groszer et al., 2006). Therefore, loss of PTEN is sufficient to increase the pool of self-renewing NSCs and promote their escape from the homeostatic mechanisms of proliferation control while cell fate commitments of the *Pten* null NS/PCs are largely undisturbed (Groszer et al., 2001, 2006).

Because PTEN loss can lead to enhanced embryonic NSC self-renewal, proliferation, and survival, its transient inactivation may be a promising approach for "boosting" the limited adult NSC population, a critical step toward treating certain neurodegenerative diseases. However, such an approach would have to be vigorously tested *in vivo* to ensure that (1) the PTEN-PI3K pathway plays a similar role in adult NSCs, and (2) perturbation of PTEN-PI3K pathway alone in NSCs is not tumorigenic. To address these issues and further explore the role of PTEN in regulating adult neurogenesis and repair *in vivo*, we deleted *Pten* in a subpopulation of adult NS/PCs in the SEZ by crossing *Pten* conditional knock-out mice ($Pten^{loxp/loxp}$) (Lesche et al., 2002) with a murine *GFAP-Cre*$^+$ (*mGFAP-Cre*$^+$) transgenic line.

Materials and Methods

Animals. *mGFAP-Cre*$^+$ transgenic mice line 77.6 were generated using a 15 kb promoter cassette containing the full-length sequence of the murine GFAP gene as described previously for line 73.12 (Garcia et al., 2004) and crossed to $Pten^{loxp/loxp}$ mice (Lesche et al., 2002) on a 129/BALB/c background. F_1 generation compound heterozygous animals were backcrossed with $Pten^{loxp/loxp}$ mice to produce F_2 generation experimental animals. Animals were genotyped by standard genomic PCR techniques (Lesche et al., 2002). $Pten^{loxp/loxp}$;*mGFAP-Cre*$^+$ mice were crossed to ROSA26 mice (Soriano, 1999) for reporter analysis. In addition to the SEZ, 77.6 mice exhibited only a scattered mosaic pattern of Cre/β-gal expression in subpopulations of GFAP$^+$ astrocytes in the adult brain. Animals were housed in a temperature-, humidity-, and light-controlled room (12 h light/dark cycle), and allowed *ad libitum* access to food and water. All experiments were conducted according to the research guidelines of the University of California at Los Angeles Chancellor's Animal Research Committee. $Pten^{loxp/loxp}$ and $Pten^{loxp/loxp}$;*mGFAP-Cre*$^+$ animals are herein to referred to as control and mutant, respectively.

PCR. The specificity of *Pten* excision was evaluated by PCR using DNA from tail clip biopsy. For *Pten* PCR, the loxp (650 bp), wild-type (500 bp), and exon 5 (300 bp) fragments are amplified simultaneously by using three primers TCCCAGAGTTCATACCAGGA (Pten6637-F), GCAATGGCCAGTACTAGTGA-AC (Pten6925-R), and AATCTGTG-CATGAAGGGAAC (Pten7319-R). PCR was performed in 20 μl reactions using standard procedures for forty cycles; each cycle consisted of denaturing at 94°C for 45 s, annealing at 60°C for 30 s, and extension at 72°C for 1 min, followed by a single 5 min extension at 72°C. The PCR products were analyzed on 2% agarose gels.

5-Bromo-2′-deoxyuridine labeling. 5-Bromo-2′-deoxyuridine (BrdU; Sigma, B5002) was given as either a single intraperitoneal injection of 200 mg/kg followed by perfusion with 4% paraformaldehyde after 2 h, or as four intraperitoneal injections of 200 mg/kg every 12 h followed by perfusion after 14 d. Staining with anti-BrdU antibody (1:1000 BD Biosciences, 51–75512) was performed according to manufacturer's suggestions.

Neurosphere cultures. Neurosphere cultures were prepared as described previously (Groszer et al., 2006). Briefly, 8-week-old SEZs were dissected, minced with a razor blade, dissociated by enzymatic digestion with Accumax followed by light trituration with a fire-polished glass pipette, and passed through a 70 μM nylon mesh. For moderate density cultures, cells were resuspended at 10,000 cells/ml (10K) in Neurobasal medium (Invitrogen), supplemented with B-27 (Invitrogen), Heparin (Sigma), 20 ng/ml basic fibroblast growth factor (bFGF, Peprotech), and 20 ng/ml epidermal growth factor (EGF, Invitrogen). For clonal/low density cultures, tertiary neurospheres were dissociated into a single cell suspension as described above and the cells were plated at 1000 cells/ml (1K) in T25 tissue culture flasks. Clonal cultures were passaged every 2 weeks. At passage 1, 4, 8, 16, and 24, cells were also plated into 96 well plates at clonal density and after 10 d clonal neurospheres were counted and differentiated. All neurospheres in the 96-well clonal plates which measured >40 μM in diameter were counted using the Microcomputer Imaging Device Program (MCID).

Immunocytochemistry of neurospheres. Immunocytochemistry of neurosphere cultures was performed as described previously (Groszer et al., 2001). Briefly, following neurosphere counting, at least 20 randomly chosen clonal neurospheres were transferred from the 96-well plates onto poly-L-lysine (BD Biosciences) and laminin-coated glass coverslips (one sphere per coverslip) for differentiation in Neurobasal medium in the absence of growth factors. After five days, the differentiated neurospheres were fixed in 4% paraformaldehyde and immunostained with rabbit anti-TUJ1 (1: 1000; Covance, MMS-435P) for neurons.

Image analysis and quantification. BrdU-immunostained (BrdU$^+$) nuclei were visualized with a Leica light microscope (40× objective) equipped with a charge-coupled device digital camera. For 14 d postinjection, comparable sections of immunostained profiles contained in the GCL and RMS were counted in 5 μm thick serial sections at 100 μm intervals. For the 2 h postinjection period, the numbers of BrdU$^+$ nuclei were counted in coronal sections of SEZ and OB. The respective areas of these layers/regions were determined with nuclei were visualized with Ariol SL-50 scanner and analysis system (Applied Imaging/Genetix) software and the quantified values were converted to densities (number of BrdU$^+$ profiles per mm^3); $n = 6$. The structure volumes and RMS were measured as described previously (Petreanu and Alvarez-Buylla, 2002; Tsai et al., 2006).

Histology and immunohistochemistry of tissue section. All IHC staining was performed on 5 μm sections that were prepared from paraffin-embedded blocks and placed on charged glass slides. The slides were deparaffinized with xylene and rehydrated in descending grades (100%–70%) of ethanol. The endogenous peroxidase activity was inactivated in 3% hydrogen peroxide (H_2O_2). After washing in deionized water, antigen retrieval was performed by incubating the slides in 0.01 M citric acid buffer, pH 6.0, at 95°C for 13.5 min. Slides were then allowed to cool for 30 min in citric acid buffer. After washing in deionized water, the slides were transferred to either PBS, pH 7.4, or TBST for 5 min. For DAB staining, slides were first blocked with 5% normal goat serum then incubated with primary antibody overnight at 4°C. Following three 5 min washes in either PBS or TBST, slides were incubated with biotinylated secondary antibody (1:200, Biogenex) for 30 min at room temperature. Amplification was performed with a horseradish peroxidase system (Vectastain ABC kit, Vector, PK-6100) using a liquid DAB peroxidase substrate (Biogenex, HK130–5K). Slides were counterstained in Gill's hematoxylin, dehydrated, cleared, and coverslipped. Negative control slides were run without primary antibody. For fluorescence double staining, the section was treated as above and first stained with the first antibody followed by signal amplification with TSA Plus Fluorescence Systems (PerkinElmer, NEL-7448). After biotin blocking, the section was stained with the second antibody and signal was amplified with TSA system with different fluorescence. Primary antibodies used were rabbit anti-PTEN (1:100; Cell Signaling, 9552); rabbit anti-pS6 (1:100; Cell Signaling 2155); rabbit anti-pAKT (1:100; Cell Signaling, 9172); rat anti-GFAP (1:1000; ZYMED Laboratories, 18–0063); goat anti-Nestin (1:50; R&D Systems, AF2736); rabbit anti-Cre (1:3000; Covance PRB-106C); goat anti-doublecortin (1:500; Santa Cruz, sc8066); mouse anti-NeuN (1:1000; Chemicon, MAB377); rabbit anti-β-galactosidase (1:1000; MP Biochemicals, 55976); rabbit anti-ki-67 (1:100; Vector, VP-RM04). 4′,6-diamidino-2-phenylindole (DAPI; Invitrogen, D-1306) used as a fluorescent counterstain.

Olfactory habituation test. This task measures the ability of mice to detect a novel odorant and to habituate responding to that odorant over repeated presentations. Previous studies (Trinh and Storm, 2004) demonstrated that a high number of sniffs upon initial exposure of an odorant indicated that the animal detected a novel odorant. Each mouse was housed individually and handled daily for five days before the beginning of any behavioral manipulation. Individual mice were then exposed to an

odorant for three successive 2 min trials separated by 1 min intervals. The first odorant was always sterile water to habituate the animal to the introduction of a novel object (cotton swab) in the home cage. Following this pre-exposure phase, a cotton swab saturated with an odorant was introduced into the home cage for another three successive 2-min trial separated by 1 min intervals. The total number of contacts that the mouse made with the cotton swab for each of three 2 min exposures as well as the total amount of time spent in contact with the cotton swab was recorded. The odorants used were isoamyl acetate, isomenthone, hexyl alcohol, limonene, and anisole (Sigma). For data collection and analysis, all experiments were recorded using a camcorder. The number of sniffs and the duration of each sniff were analyzed in a blind setting by viewing recordings in real time. To be consistent and unbiased in analysis, a full sheet of plain paper with a 1 in^2 box was cut out and placed onto the screen with the cotton swab directly in the middle of the box, thus blocking the rest of the screen. Every time the nose of the mouse entered the box, it was scored as a sniff; the duration of each sniff was recorded as the amount of time the nose of the mouse remained in the box. Time intervals were divided into five categories of time as follows: less then 1, 2–5, 6–9, 10–12, and >12 s. A total of 14 control and 12 mutant sexually naive male mice at 10–12 months of age were used in behavior experiments.

Chemical ablation of olfactory epithelium. Control and mutant sexually naive 14- to 16-week-old male mice ($n = 8$) were housed individually and given intraperitoneal injections of dichlobenil (2.6-dichlobenzonitrile, Sigma, 25 μg/g body weight) in DMSO (dimethyl sulfoxide, 2 μl/g body weight) for 7 d (Yoon et al., 2005). An additional cohort of control and mutant mice ($n = 5$) were given DMSO (vehicle, 2 μl/g body weight) and evaluated for ability to detect novel odors using the odorant habituation test at 2, 3, and 4 weeks after the last injection.

Stroke model. Stroke was produced in 2- to 5-month-old control and mutant animals. Briefly, stroke was produced using a distal, branch artery occlusion of the middle cerebral artery (Ohab et al., 2006; Tsai et al., 2006). The middle cerebral artery was exposed over the surface of the frontoparietal cortex through a small craniotomy, and a parietal branch coagulated and transected. Both jugular veins in the neck were occluded for 15 min and then released. This produces a small stroke in he vibrissal (barrel) somatosensory field of the cortex.

Stereology. Stereological quantification was performed using serial sections through the anterior SEZ, OB, and peri-infarct cortex using unbiased counting with the optical fractionator as described previously (Tsai et al., 2006).

Statistical analysis. Unless otherwise noted, all data were subjected to statistical analysis by using two-sample *t* testing assuming unequal variances (Excel Data Analysis Tool Pak, Microsoft) to determine the differences between the control and mutant groups. A *p* value of 0.05 or less was considered significant.

Results

Generation of *mGFAP-Cre*$^+$ line for conditionally targeting adult neural stem/progenitor cells

Previous studies have made a compelling case that the majority of multipotent NSCs responsible for neoneurogenesis in the adult mouse brain express GFAP (Doetsch et al., 1999; Groszer et al., 2001; Imura et al., 2003; Garcia et al., 2004). To further explore the role of PTEN in regulating adult neurogenesis and repair *in vivo*, we generated a new m*GFAP-Cre*$^+$ transgenic line 77.6 using the *mGFAP* gene cassette (Garcia et al., 2004) (for details, please see Materials and Methods). Immunohistochemistry (IHC) of 77.6 mice crossed to *Rosa26-LacZ* reporter mice (Soriano, 1999) showed Cre expression in a small subpopulation of SEZ cell in adult brain (Fig. 1*a*,*b*) and β-Gal expression in many more cells corresponding to Cre^+ cells and their progenies (Fig. 1*e*). These $Cre^+/\beta\text{-Gal}^+$ cells represent adult NSCs since their progenies can migrate and differentiate along the RMS (Fig. 1*f*) and reach the granule cell layer (GCL) in the OB (Fig. 1*h*). In addition, we used double-labeling immunohistochemistry to compare expression of Cre with GFAP and Nestin, intermediate filaments whose dynamic regulation by neural progenitors and astrocytes at different stages of development has been well documented (Garcia et al., 2004; Lagace et al. 2007). Three dimensional analysis of SEZ cells using scanning confocal laser microscopy showed that Cre^+ cells in the SEZ express GFAP (Fig. 1*c*) and Nestin (Fig. 1*d*). Cells that were Cre positive/GFAP negative or Cre positive/Nestin negative were not found (data not shown). Furthermore, neither Cre nor LacZ reporter expression could be detected in embryonic brains (data not shown), suggesting Cre is not expressed during embryonic development, and only postnatally in progenitor cells. In contrast to the previously reported *mGFAP* lines 7.1 (Bush et al., 1998; Imura et al., 2003) and 73.12 (Garcia et al., 2004), *mGFAP-Cre*$^+$ line 77.6-mediated reporter expression in progenitor cells was limited to the SEZ region and no Cre or LacZ reporter expression could be detected in $GFAP^+$ NSC populations in the hippocampus. Therefore, *mGFAP-Cre*$^+$ line 77.6 was chosen for this study because we hypothesized that the limited Cre transgene expression in NSCs of line 77.6 would circumvent increased brain size, altered brain histoarchitecture and premature lethality caused by global *Pten* deletion from NSCs in previous conditional knock-out models (Groszer et al., 2001; Yue et al., 2005).

Pten deletion in the adult NSC leads to increased self-renewal without tumorigenesis or premature senescence

To explore PTEN′s role in regulating adult NSCs, $Pten^{loxp/loxp}$ (Lesche et al., 2002) mice were crossed with *mGFAP-Cre*$^+$ line 77.6 mice. $Pten^{loxp/loxp}$;*mGFAP-Cre*$^+$ mutants are viable and fertile, yielding Mendelian offspring distributions (data not shown). Importantly, no tumors or aberrant neurological phenotypes were detected in mutant animals up to two years of age.

Previously, we found that deletion of *Pten* in embryonic NSC resulted in an enhanced ability to self-renew *in vitro* compared with control spheres (Groszer et al., 2006). To assess the function of PTEN in controlling adult NSC self-renewal and proliferation, we compared neurosphere forming activity of *Pten* deleted brain (Mutant) with that of their wild-type littermates (Control) in a serial clonal passaging experiment. Similar to *Pten* deletion in the embryonic neural stem cells, spheres formed from *Pten* deleted adult brain were generally bigger (supplemental Fig. 1*a*, available at www.jneurosci.org as supplemental material). Importantly, by passage 4 >90% of spheres isolated from the mutant cultures carried *Pten* bi-allele deletion and were positive for the Cre transgene (supplemental Fig. 1*b*, available at www.jneurosci.org as supplemental material). At each passage, *mGFAP-Cre*-mediated *Pten* deletion in adult NSCs resulted in increased clonal neurosphere number, a measurement of neural stem cell self-renewal capacity (Fig. 2*a*). Serial clonal passaging of cells over 48 weeks (24 passages), at a density at which nearly all spheres are derived from a single cell, resulted in the eventual senescence of wild-type cultures while the mutant cells maintained high rates of self-renewal. This enhanced neurosphere formation was also reflected in the total cell numbers attained at each passage (Fig. 2*b*). Previous study has suggested that progenitors tend to lose their neurogenic potential and become more glial-restricted over time (Seaberg et al., 2005). Following *in vitro* differentiation, the clonal neurospheres from mutant mice maintained a significantly enhanced neurogenesis even at late passages, whereas the wild-type cultures produced fewer neurons than their mutant counterpart at every passage and their ability to generate neurons declined substantially with time in culture (Fig. 2*c*), similar to our previous studies on *Pten* deleted embryonic NSCs (Groszer et al., 2001). Together, these data indicate that *Pten* deletion persistently en-

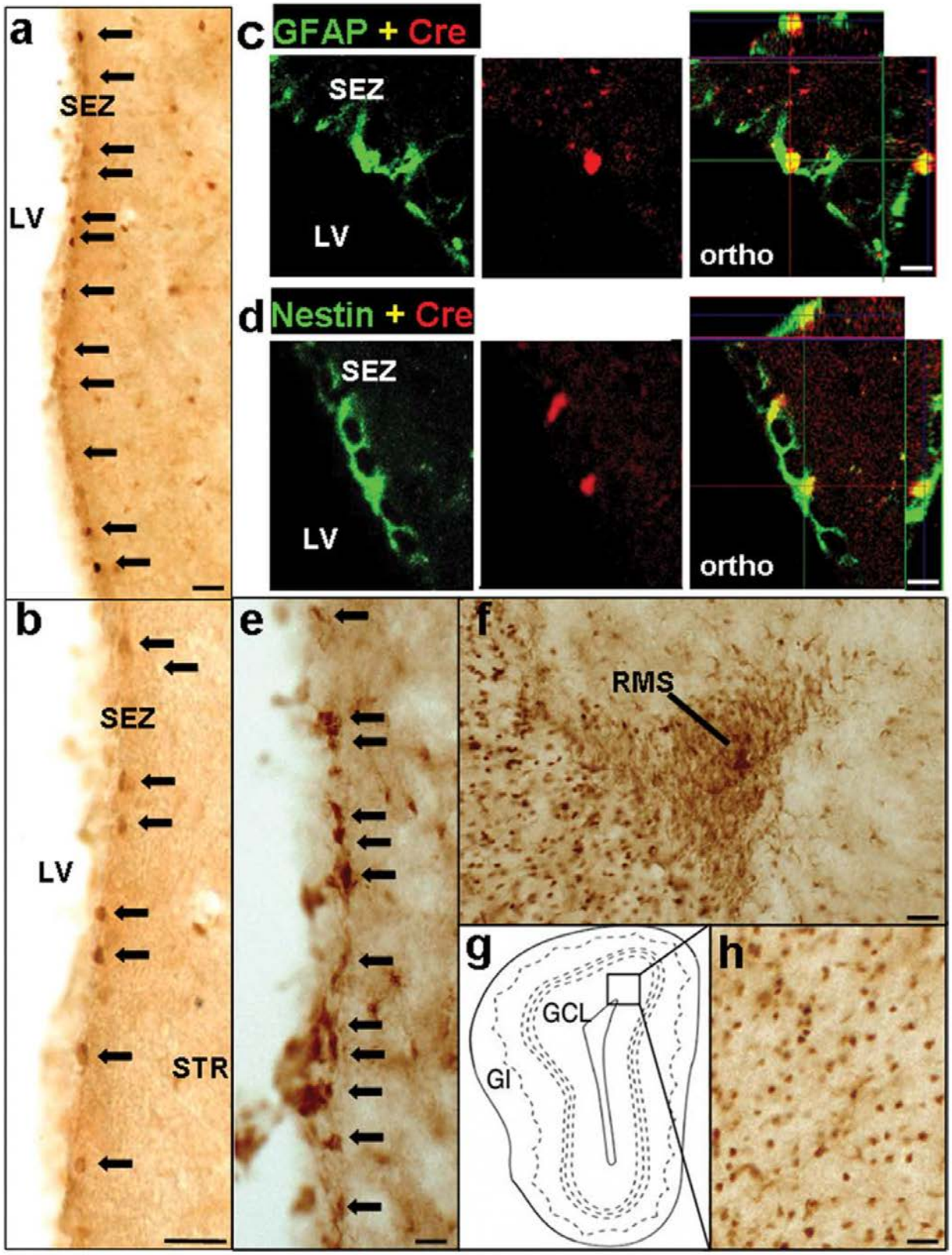

Figure 1. *mGFAP-Cre* line for conditionally targeting adult neural stem/progenitor cells. ***a***, ***b***, ***e***, ***f***, ***h***, Survey images of coronal sections of the SEZ (***a***, ***b***, ***e***), RMS (***f***), and OB (***h***) stained by bright-field immunohistochemistry. A small number of cells in the SEZ express Cre (***a***, low mag; ***b***, high mag). Scale bars, 80 μm. ***c***, ***d***, Confocal micrographs of single optical slices through cells in the SEZ that are double stained by immunofluorescence for Cre and GFAP (***c***) or Cre and Nestin (***d***). Individual channels and orthogonal analysis show that all Cre-expressing (*Figure legend continues*.)

hances self-renewal of adult NSC, while maintaining their capacity to produce neurons, without any evidence of stem cell exhaustion.

Pten deletion leads to expansion of neural stem and progenitor cells in the SEZ region

At the tissue level, *Pten* deletion led to a robust increase in GFAP$^+$ cells (Fig. 3*a*, second right) in the SEZ. Cells with hyperphosphorylation of S6 (P-S6) (Fig. 3*a*, third right) and AKT (P-AKT; supplemental Fig. 2*a*, available at www.jneurosci.org as supplemental material), surrogate markers for PTEN loss and PI3K activation that have been implicated in neuron survival and cell cycle control (Datta et al., 1999), could be easily visualized in the same region. GFAP expression and numbers of GFAP$^+$ cells did not appear different from controls in neighboring structures and other parts of forebrain except the SEZ region (data not shown), further supporting SEZ-specific *Pten* deletion. Importantly, these P-S6$^+$ cells also express GFAP (Fig. 3*a*) and/or Doublecortin (DCX), a marker for immature and migrating neuroblast progenitors (supplemental Fig. 2*b*, available at www.jneurosci.org as supplemental material), suggesting that PTEN loss or PI3K-AKT activation leads to the expansion of adult NSC and progenitors in SEZ region.

Consistent with NSC expansion, the volume of the mutant SEZ is significantly increased when compared with controls (Fig. 3*b*) (0.021 ± 0.0011 vs 0.032 ± 0.008 mm^3 ± SEM; $p < 0.01$), which was accompanied by a greater number of Ki-67$^+$ (Fig. 3*c*) (6832.12 ± 231.8 vs 8376.98 ± 122.8 cells ± SEM; $p < 0.01$) and DCX$^+$ neuroblasts (Feng and Walsh, 2001). Figure 3*d* shows a statistically significant increase in DCX volume in *Pten*$^{loxp/loxp;}$*mGFAP-Cre*$^+$ SEZ (Fig. 3*d*) (0.019 ± 0.0012 vs 0.062 ± 0.0064 mm^3 ± SEM; $p < 0.01$). These results indicated that *Pten* null NSCs can readily proliferate and differentiate into DCX$^+$ neuroblasts, the precursors for adult neurogenesis.

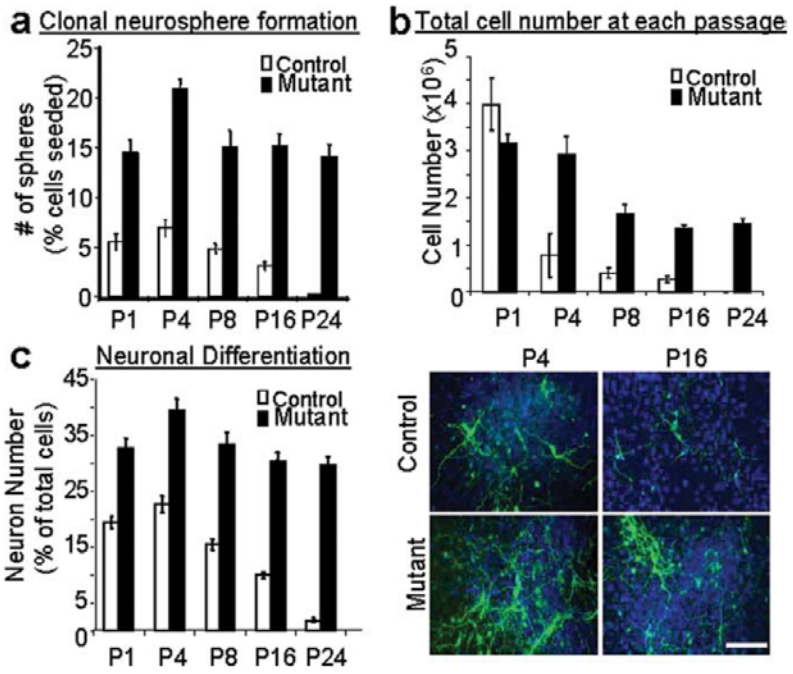

Figure 2. *Pten* deletion in clonal neurosphere cultures enhances stem cell self-renewal and neurogenesis over long-term serial clonal passages compared with the gradual senescence and decreased neurogenesis in wild-type cultures. ***a***, Neurosphere cultures generated from the adult SVZ of *Pten* knock-out (Mutant) and wild-type (Control) mice were cultured at clonal density (1000 cells/ml), passaged, and reseeded at clonal density every 2 weeks. Clonal neurosphere numbers, representative of the number of stem cells present in the culture, were significantly higher in mutant cultures at all passages ($p < 0.001$). ***b***, The clonal neurospheres were then dissociated and the total cell number was counted at each passage followed by reculturing at clonal density. After the first passage, mutant cultures consistently produced higher total cell numbers even after long-term serial clonal passaging while control cultures produced decreased cell numbers with time, eventually senescing by passage 24. Data are means ± SEM; $n = 4$. ***c***, Immunocytochemistry for TUJ1$^+$ cells (green) and the counterstain Hoescht (blue) are shown at passage 4 and 16 indicating the clonal neurospheres from mutant mice maintained their robust neurogenesis even at late clonal passages while the ability to generate neurons was dramatically attenuated in control cultures over time. Scale bar, 60 μm. $n = 4$.

SEZ-born *Pten* null progenitors and their progenies follow the endogenous migration pathway

SEZ-born progenitors are known to migrate to the OB via the well-defined RMS. Because PTEN has been implicated in controlling cell chemotaxis (Funamoto et al., 2002; Iijima and Devreotes, 2002) as well as migration (Tamura et al., 1998; Liliental et al., 2000; Raftopoulou et al., 2004; Yue et al., 2005), we determined whether the progenies of SEZ-born *Pten* null progenitors could respond to normal environmental cues and migrate into and along the RMS. To mark the SEZ-born progenitors and their differentiated progenies, we pulse labeled control and mutant mice with BrdU and quantified the number of BrdU$^+$ cells in the RMS after 5 d of chase. As shown in Figure 4*a*, a significant increase in the number of BrdU$^+$ cells was found in the mutant RMS (Fig. 4*a*) (22998 ± 968 vs 33386 ± 786 cells per mm^3 ± SEM; $p < 0.05$). Furthermore, the BrdU$^+$ cells were also positive for P-S6 staining (Fig. 4*a*), indicating that SEZ-born *Pten* null progenitors exhibited enhanced cell proliferation but could follow the endogenous migration pathway into the RMS.

We then tested whether the migrating *Pten* null progenitors within the RMS express similar markers as controls. Neuroblasts in mutant RMS are *Pten*$^-$ (supplemental Fig. 3, available at www.jneurosci.org as supplemental material) and DCX$^+$ (Fig. 4*b*) with many more DCX$^+$ neuroblasts in the RMS of *Pten*$^{loxp/loxp}$; *mGFAP-Cre*$^+$ mice (Fig. 4*b*) (2642 ± 126 vs 3894 ± 60 cells per mm^2 ± SEM; $p < 0.05$).

During migration, neuroblasts are restricted to the RMS with few cells diverging from the path (Doetsch and Alvarez-Buylla, 1996). Although it seemed that a greater number of

←

(*Figure legend continued.*) cells in the SEZ also express GFAP (***c***) and Nestin (***d***). Orthogonal images (ortho) show three-dimensional analysis of individual cells at specific sites marked by intersecting *x*, *y*, and *z* axes. Scale bars, 20 μm. Many cells express the reporter protein β-gal (***e***) in the neurogenic proliferative regions of the SEZ. Migrating neuroblasts in the RMS (***f***) and granule neurons in the OB (***h***) also express β-gal. Box in *g* indicates the region shown in ***h***. Arrows in ***a***, ***b***, and ***e*** indicate representative Cre or β-gal-positive cells in SEZ. SEZ, Subependymal zone; LV, left ventricle; STR, striatum; RMS, rostral migratory stream; OB, olfactory bulb; GCL, granule cell layer; GI, glomeruli.

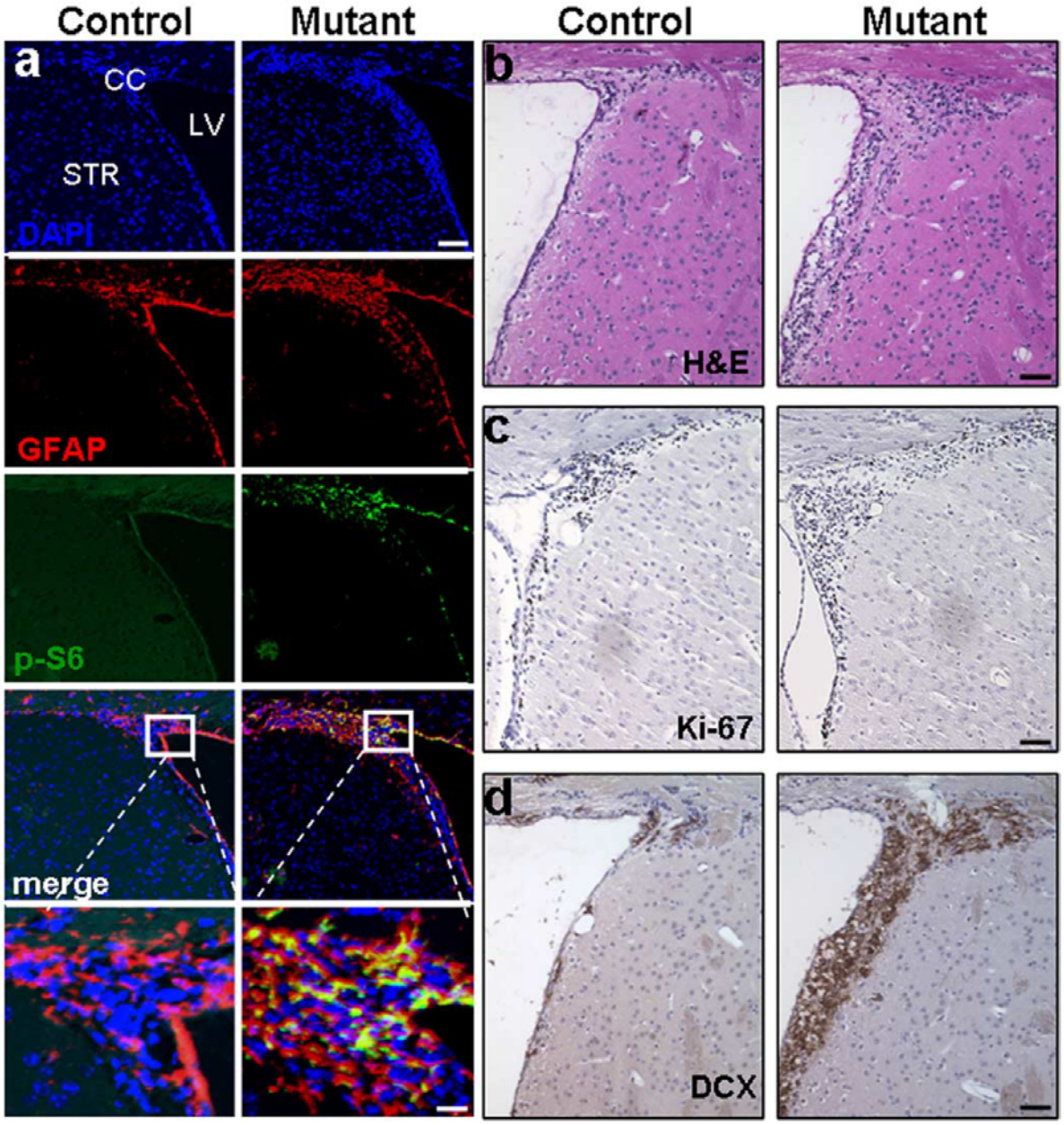

Figure 3. *mGFAP-Cre*-mediated *Pten* deletion leads to expansion of adult neural stem cells and their progenies *in vivo*. Survey images of coronal sections of control and mutant SEZ. ***a***, Compared with littermate controls, mutant mice showed increased GFAP and P-S6-positive (labeled cells which co-localized in the SEZ. DAPI counter stain is used to visualize nuclei. Scale bars: top, 150 μm; bottom, 25 μm. ***b–d***, Images of H&E (***b***), Ki-67 (***c***), and DCX (***d***) expression demonstrate increased proliferation in mutant SEZ compared with control regions. Scale bar, 60 μm. $n = 5$. SEZ, Subependymal zone; LV, lateral ventricle; CC, corpus callosum; STR, striatum; H&E, hematoxylin and eosin; DCX, doublecortin.

cells diverged from the RMS in the $Pten^{loxp/loxp}$;$mGFAP\text{-}Cre^{+}$ mice, the ratio of diverging DCX^{+} cells to the total number of cells in the mutant RMS was not significantly different from that of controls (1.28 ± 0.004 vs 1.36 ± 0.009% of total ± SEM; $p > 0.05$). These results suggest that *Pten* null SEZ-born neuroblasts are able to recognize environmental cues and migrate along the endogenous pathway.

Deletion of *Pten* in adult SEZ leads to increased OB mass

Although OB granule cell neurons (GC) are continuously generated throughout adulthood, OB volume remains constant during adulthood (Pomeroy et al., 1990). This homeostatic stage is achieved largely via a balance between SEZ neoneurogenesis and cell death in the GCL of OB (Najbauer and Leon, 1995; Fiske and Brunjes, 2001; Petreanu and Alvarez-Buylla, 2002). Measure-

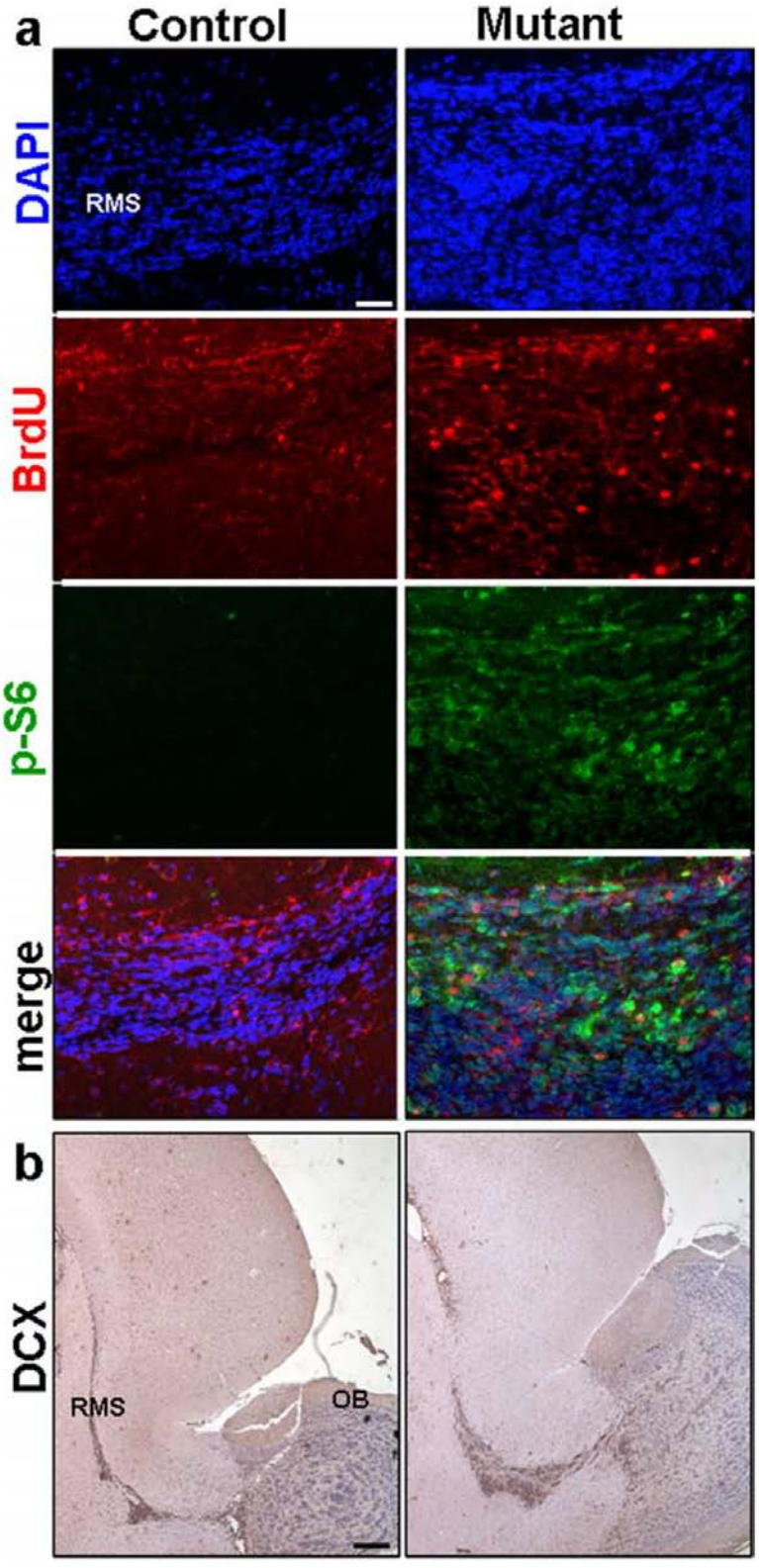

Figure 4. *Pten* deletion leads to enhanced migration of SEZ-born progenitors in RMS. ***a***, Representative images of RMS stained for BrdU, P-S6, and their colocalization revealed an increase in *Pten* null SEZ-born progenitors migrating in RMS when compared with control and shows the BrdU$^+$ population in mutant RMS is *Pten* null. Scale bar, 100 μm. ***b***, Survey images of sagittal sections of control and mutant RMS stained with DCX demonstrate an increase in the number of migrating neuroblasts in mutant RMS compared with control. DAPI counter stain is used to visualize nuclei. Scale bar, 400 μm. $n = 6$. DCX, Doublecortin; RMS, rostral migratory stream; OB, olfactory bulb.

ments taken from mutants and their littermate controls demonstrated continuous increases in size (Fig. 5*a*, upper panel) and weight of mutant OB, starting at 2.5 months of age (Fig. 5*a*, lower panel). This increased size and mass of mutant OB is consistent with previous reports that there is a surge of progenitors migrating to the OB at 3–4 months of age (Petreanu and Alvarez-Buylla, 2002). Histological analysis of mutant OB (Fig. 5*b*) and other brain regions (supplemental Fig. 4, available at www.jneurosci.org as supplemental material) revealed normal histoarchitecture.

Because SEZ-born progenitors migrate and integrate into the GCL of the OB, we hypothesized that an increase in GCL volume may contribute to the increased OB mass. Compared with control, *Pten*$^{loxp/loxp}$;*mGFAP-Cre*$^+$ GCL volume increased twofold at 3.5 months (Fig. 5*c*, columns on the left) (2.92 ± 0.071 vs 5.60 ± 0.25 mm^3 $\pm$ SEM; $p < 0.05$) while no statistically significant differences were observed in the external plexiform layer (EPL) (Fig. 5*c*, columns on the right) (1.19 ± 0.054 vs 1.10 ± 0.043 mm^3 $\pm$ SEM; $p > 0.05$), a region not influenced by SEZ-mediated neurogenesis. To further test whether increased GCL volume is due to SEZ-born granule cells incorporated into the OB, mice were injected with BrdU and killed at 2 h or 14 d after the last injection. These time points were chosen to ensure that there were no ectopic proliferating cells in the mutant OB (2 h chase) and to allow sufficient time for BrdU-labeled neuroblasts to migrate, differentiate, and incorporate into the outer layers of the OB (14 d chase). BrdU$^+$ cells could not be detected in either control or mutant OB after 2 h of chase (supplemental Fig. 5, available at www.jneurosci.org as supplemental material). However, after 14 d chase there was an approximate twofold increase in the number of BrdU$^+$ cells in the GCL of 3.5-month-old *Pten*$^{loxp/loxp}$;*mGFAP-Cre*$^+$ mice when compared with wild-type controls (Fig. 5*d*) (2.92 ± 0.07 vs 5.60 ± 0.25 cells $\pm$ SEM; $p < 0.001$). These results indicate that the increase in GCL volume was not due to ectopic cell proliferation within the OB but from an increase in the number of cells that migrated from the SEZ to the GCL via the RMS. We also observed a sig-

←

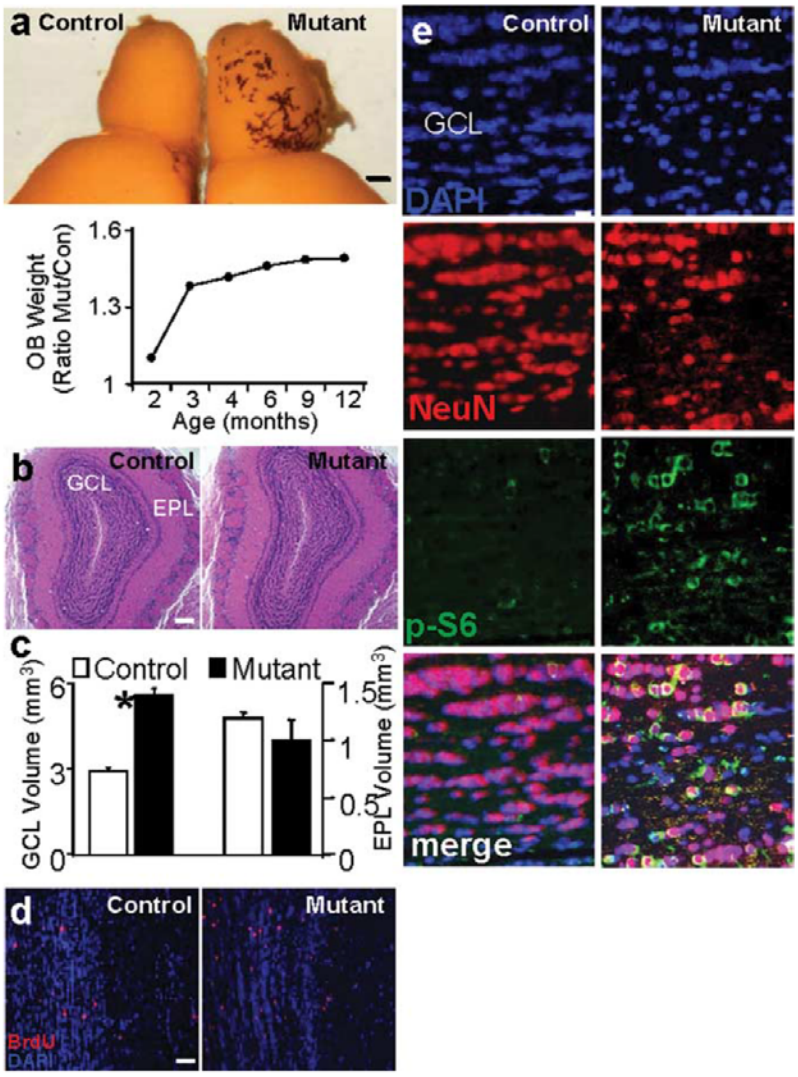

Figure 5. Increased OB mass and enhanced proliferation and migration of SEZ-born progenitors to the GCL of OB in mutant mice. ***a***, Enlarged OB of mutant mice. Photo shows a brain hemisphere from age-matched control and mutant mice. Scale bar, 1 mm. Panel below depicts the progressive increase in the ratio of mutant/control OB weight. $n = 40$. ***b***, Histological analysis of OB section from control and mutant mice reveals normal histoarchitecture. Scale bar, 500 μm. ***c***, GCL volume is significantly increased in mutant mice ($^*p < 0.05$) whereas no significant change is observed in EPL ($p > 0.05$). Data are means ± SEM; $n = 10$. ***d***, SEZ-born neuroblast migration was analyzed by BrdU pulse-labeling. Mice were injected with 200 mg/kg BrdU peritoneally, and distribution of BrdU-labeled cells was determined 2 weeks after injection. An increased number of BrdU-labeled cells within mutant GCL indicated *Pten* mutant mice had a significant increase in cell number at 2 weeks post injection. Scale bar, 100 μm. $n = 5$. ***e***, Representative GCL images show enhanced immunoreactivity for NeuN and increased NeuN/P-S6 double positive cells in mutant when compared with a matched control region. DAPI is used as counterstain to visualize nuclei. Scale bar, 10 μm. OB, Olfactory bulb; GCL, granule cell layer; EPL, external plexiform layer.

nificant decrease in the number of TUNEL$^+$ cells in the mutant GCL 2.51 ± 0.22 (control) vs 1.83 ± 0.16 (mutant) cells ± SEM; $p < 0.05$), indicating that OB enlargement in the mutant mice is a net result of increased cell proliferation and decreased cell death. Furthermore, *Pten* null NSC-derived granule neurons in the GCL were positive for both P-S6 and NeuN, a neuron-specific marker (Fig. 5*e*). Together, these results indicate that *Pten* deleted NSCs and their progenies can follow endogenous cues along the normal RMS and reach the OB. Within the OB, they can differentiate and integrate into the GCL.

Pten$^{loxp/loxp}$;*mGFAP-Cre*$^+$ mice exhibit enhanced habituation to novel odors

The life-long neurogenesis along SEZ-RMS-OB suggests that adult-born neurons play critical roles in olfactory functions (Petreanu and Alvarez-Buylla, 2002; Winner et al., 2002): adult-born neurons extend new processes and form new synapses with each other or with existing GC (Cecchi et al., 2001; Petreanu and Alvarez-Buylla, 2002), and the rates of neurogenesis are known to be positively correlated with performance on memory (Nilsson et al., 1999; Shors et al., 2001; Rochefort et al., 2002) and olfactory discrimination tasks (Gheusi et al., 2000; Enwere et al., 2004). To test whether SEZ-derived *Pten* null GCs are functional, we performed an olfactory behavioral test. This Odorant Habituation Task behavioral assay measures the ability of mice to detect a novel odorant and to habituate in responding to that odorant over repeated presentations (Trinh and Storm, 2004). We found that olfactory discrimination was intact in *Pten*$^{loxp/loxp}$;*mGFAP-Cre*$^+$ mice since the first exposure to an odorant resulted in an increase in the number of sniffs from the previous trial, proving that the mice were able to detect a novel odor (Fig. 6*a*). Furthermore, mutant mice habituate faster to a novel odorant when compared with controls, as demonstrated by a decrease in the number of sniffs during the second and third exposures of both isoamyl acetate and isomenthone (Fig. 6*a*, right panels). A similar pattern was observed with two additional odorants regardless of order of presentation (data not shown). In addition, when the duration of the sniffs was measured, *Pten*$^{loxp/loxp}$;*mGFAP-Cre*$^+$ mice exhibited a decrease in the time spent within each odorant group compared with controls (supplemental Fig. 6, available at www.jneurosci.org as supplemental material). A decrease in the time spent investigating an odorant after repeating exposure further implies that *Pten*$^{loxp/loxp}$;*mGFAP-Cre*$^+$ mice have an increased ability to recall, recognize, or habituate to the odorant when compared with control.

This enhanced odorant habituation suggests that 1) *Pten* deletion in adult NSC causes enhanced proliferation and self-renewal without interfering with the normal properties and destiny of their differentiated progenies, and 2) *Pten* null granule neurons are able to integrate into the olfactory circuitry and contribute to odor discrimination. We therefore hypothesized that perturbation of endogenous PTEN function may be beneficial for neuronal repair and postinjury recovery. To test this hypothesis, mice were treated with dichlobenil, a chemical shown to selectively destroy the olfactory sensory epithelium (Mombaerts et al., 1996; Yoon et al., 2005) in adult mice. In agreement with published reports, we observed a

severe destruction of the main olfactory epithelium (MOE) neuronal layer in animals treated with dichlobenil when compared with controls (supplemental Fig. 7, available at www.jneurosci.org as supplemental material). Post dichlobenil treatment, all mice were evaluated weekly for their ability to detect novel odors (Odorant Habituation Test as described above). Consistent with previous report (Yoon et al., 2005), all drug treated mice, regardless of genotype, lost their ability to detect odorants 2 weeks after treatment (Fig. 6*b*, top panel). However, *Pten*$^{loxp/loxp}$;*mGFAP-Cre*$^{+}$ mice showed an improvement in odorant detection 4 weeks post treatment (Fig. 6*b*, middle panel). MOE examination after 4 weeks of dichlobenil treatment showed comparable regeneration of the epithelial layer in both control and mutant mice with no significant difference in Pten (supplemental Fig. 8*b*, available at www.jneurosci.org as supplemental material) or P-S6 (supplemental Fig. 8*c*, available at www.jneurosci.org as supplemental material) staining, indicating improved behavioral test performance in the mutant animals is not due to enhanced regeneration or *Pten* deletion in mutant MOE. By 6 weeks post treatment, the *Pten*$^{loxp/loxp}$;*mGFAP-Cre*$^{+}$ mice had almost recovered to pre-treatment stage (Fig. 6*b*, bottom panel). These results suggest *Pten* null cells in the OB can establish normal connections with peripheral olfactory epithelium and enhanced NSC self-renewal and proliferation in *Pten* deleted SEZ may help OB recovery from acute damage.

Pten deletion enhances poststroke neuroblast migration

Stroke is a common cause of neuronal damage. Seven to ten days after the initial insult, SEZ-born neuroblasts proliferate and migrate to the site of injury, contributing to poststroke neurogenesis and recovery (Arvidsson et al., 2002; Parent, 2002; Jin et al., 2003; Tsai et al., 2006). We tested whether *Pten* deletion in SEZ NSCs could enhance neuroblast proliferation and migration after ischemic injury. For this, we introduced a limited stroke in the sensorimotor cortex of the brain, which closely mimics the human condition and quantified the location and number of immature neurons with the protein marker doublecortin (DCX) (Carmichael, 2005; Ohab et al., 2006). As reported in normal adult mice (Ohab et al., 2006; Tsai et al., 2006), there were no DCX^{+} cells in the cortex of either control or *Pten*$^{loxp/loxp}$;*mGFAP-Cre*$^{+}$ mice before stroke (data not shown), suggesting that *Pten* null NSCs in the SEZ do not migrate to the cortex without additional stimulation (supplemental Fig. 9, available at www.jneurosci.org as supplemental material). Conditional *Pten* deletion also had no effect on infarct size (1.57 ± 0.38 vs 1.48 ± 0.34 mm^3 $\pm$ SEM; $p > 0.05$).

One week after stroke, DCX^{+} cells were found in subcortical white matter and peri-infarct cortex of both groups (Fig. 7*a*, left panels). However, *Pten*$^{loxp/loxp}$;*mGFAP-Cre*$^{+}$ mice showed a large and statistically significant increase of DCX^{+} neuroblasts in the peri-infarct cortex at day 7 when compared with controls (Fig. 7*a*, right panels) (>4500 more immature neurons per animal in mutant vs control; $p < 0.001$), suggesting that *Pten* null NSCs and their progenies can readily respond to ischemic injury and migrate to the damaged site. Staining of P-S6 marker further supports the idea that it is *Pten* null neuroblasts which contribute to the increased DCX^{+} population in the peri-infarct site (Fig. 7*b*). These results indicate that PTEN is a potent negative regulator of NSC/progenitor proliferation and neurogenesis in response to injury.

Previous studies have shown that despite the migration of large numbers of newly born immature neurons to peri-infarct cortex in the first week after stroke, only a small percentage survive long term (Arvidsson et al., 2002; Ohab et al., 2006). To determine if PTEN plays a role in the long-term survival and differentiation of immature neurons in regions of damage after stroke, we labeled newly born cells in the first week after stroke with BrdU, and co-labeled these cells 90 d later with double staining for the mature neuronal marker NeuN. There was no difference in stereological counts of BrdU/NeuN cells between *Pten*$^{loxp/loxp}$;*mGFAP-Cre*$^{+}$ mice and littermate controls 90 d after

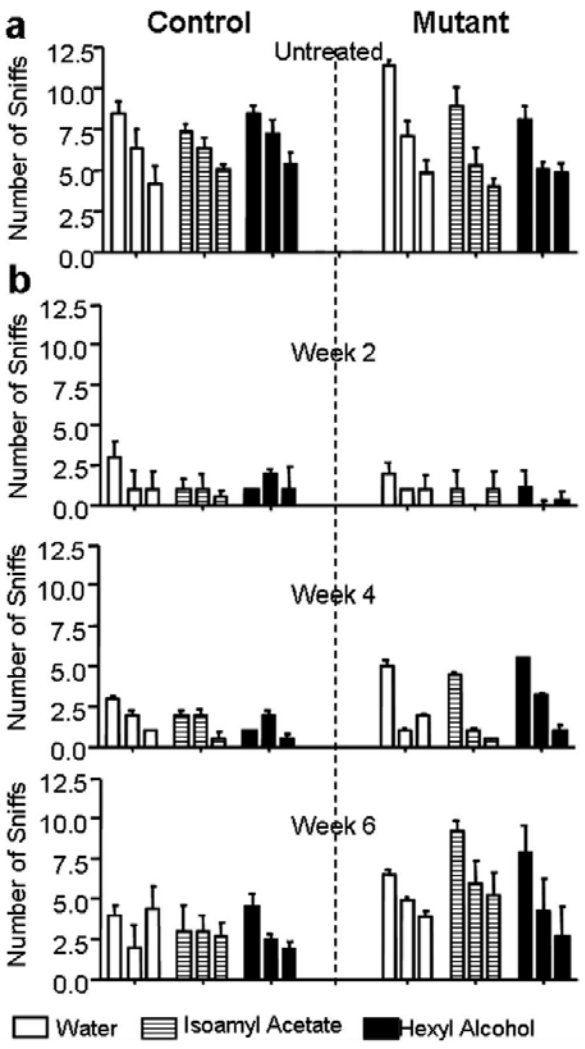

Figure 6. Enhanced olfactory habituation and recovery after epithelium injury in *Pten*$^{loxp/loxp}$;*mGFAP-Cre*$^{+}$ mice. ***a***, ***b***, Control and mutant mice were subjected to the olfactory habituation test. Pretraining of wild-type control mice to a cotton swab soaked in water habituated mice to the presence of the swab in their cage. This was manifested as a decline in the number of sniffs with subsequent exposures to the swab. During odorant testing, the cotton swab was laced with 50 μM isoamyl acetate or 50 μM hexyl alcohol and introduced on three successive trials. The fact that the control mice sniffed the isoamyl acetate- and hexyl alcohol-laced cotton swabs more times than during the third exposure to the water swab indicated that the animal was able to smell these odorants. ***a***, Compared with control, mutant mice sniffed the swabs less frequently in the second and third exposures (all three conditions) signifying they habituated to the novel odorant faster than the control. $n = 14$ (control) and 12 (mutant). ***b***, Both control and mutant mice lost their ability to detect odorants at 2 weeks post treatment, whereas the ability of mutant mice to detect odorants began recovering at 4 weeks post treatment, and their ability to detect odorants was restored to pre-treatment levels by week 6. Data are means $\pm$ SEM; $n = 8$.

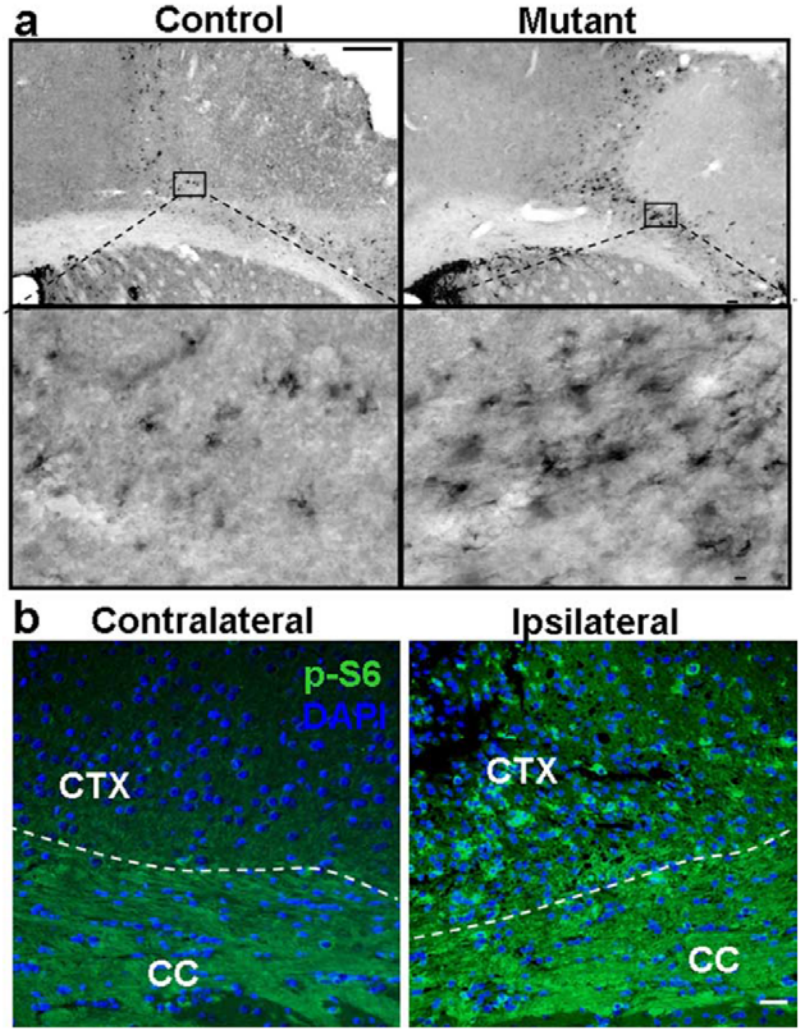

Figure 7. *Pten* deletion enhances post-stroke neuroblast migration. *a*, DCX labeling in peri-infarct cortex and SEZ. DCX^+ cells in control and mutant 7 d after stroke. Right panel shows stereological quantification of DCX^+ cells in peri-infarct cortex. Scale bars: top, 100 μm; bottom, 25 μm. $n = 6$. *b*, Representative images of P-S6 staining from both hemispheres of mutant mouse. Left panel shows hemisphere containing peri-infarct cortex which has increased staining for p-S6 in peri-infarct cortex when compared with uninjured cortex in the same animal (right panel). DAPI is used as counterstain to visualize nuclei. Scale bar, 50 μm. CTX, Cortex; CC, corpus callosum.

stroke (315 ± 123 vs 303 ± 199 cells per animal in mutant and control ± SEM, respectively; $p > 0.05$). This data indicate that although PTEN plays a prominent role in the control the initial proliferation and migration of immature neurons in poststroke neurogenesis, it does not play an autonomous role in the survival of these cells in the long term.

Discussion

Neurological disorders are the leading source of disability. Currently there are no treatments that promote repair and recovery in the brain from any major neurological disorder, including stroke, degenerative disease, and trauma. NSCs are cells that can give rise to the major components of the brain and spinal cord, thus attractive resources for repairing neurological disorders (Lindvall and Kokaia, 2006). The major challenges of NSC-mediated neuronal repair are 1) to understand the key pathways involved in controlling NSC self-renewal, proliferation, survival and differentiation, 2) to develop methodologies for manipulating these pathways toward therapeutic use, and 3) to test the potential benefit of NSCs and their progenies in human disease-relevant model systems before being used on human patients.

In this study we demonstrated that deletion of *Pten* in adult NSCs is not tumorigenic but promotes NSC expansion. Progeny from *Pten* null NSCs follow the endogenous migratory cues, differentiate, and integrate into the existing circuitry. Under conditions of acute damage, such as olfactory epithelium ablation, animals with *Pten* NSC deletion exhibited faster recovery. These data suggest that conditional manipulation of the PTEN/PI3K pathway in NSCs may be beneficial for NSC expansion, proliferation, and survival, in turn, promoting recovery and the integration of newly born neurons to existing or damaged neuronal networks associated with constitutive neurogenesis.

Stem cell self-renewal is known to be regulated by different signaling pathways, but the effect of a specific pathway may depend on the developmental stage or lineage of a stem cell population. For example, deletion of p21 in adult neural stem cells results in a transient increase in neurospheres formation with a subsequent decline in stem cell numbers; a phenomenon known as stem cell "exhaustion" (Kippin et al., 2005). Although, in a similar manner, PTEN loss leads to the "exhaustion" of adult hematopoietic stem cells (Yilmaz et al., 2006; Zhang et al., 2006; and our unpublished observation), conditional deletion of *Pten* in both embryonic and adult NSC promotes a sustained self-renewal and stem/progenitor expansion (Groszer et al., 2006; Groszer et al., 2001; and this study). Significantly, we observed that the mutant cultures maintain an enhanced self-renewal, proliferation/survival rate, over extremely long-term expansion times under clonal conditions, suggesting that the role of PTEN in regulating stem cell activity may be modulated by factors specific to the neural stem cell lineage. Therefore, further study of these lineage- or developmental stage-specific mediators of self-renewal pathways will be increasingly critical for our understanding of the underlying mechanisms of stem cell self-renewal and therapeutic manipulations.

In the current study, we demonstrated enhanced and prolonged neurogenic capacity in clonal cultures of *Pten*-deleted neural stem/progenitor cells compared with wild-type controls. In our first report of *Pten* mutant embryonic progenitors, we did not expand cultures for prolonged periods of time, and therefore did not observe this phenomenon. However, more recently, in an experiment using serial passaging of embryonic progenitors, we also observed similar results to those reported here. Although *Pten* deletion promotes neuronal survival, we do not think that

this effect, in and of itself, accounts for the observed enhancement in neurogenesis, as the observed enhancement in neuronal production appears similar between *Pten* deleted and wild-type neurospheres at early passages as well. It is possible that *Pten* deletion in some way promotes a neuronal cell fate to some extent but this is not necessarily at the expense of glial differentiation. Instead, we view the enhanced maintenance of neurogenesis as being largely due to the fact that *Pten* deletion is allowing for the maintenance of a multipotent stem cell-like pool that retains neuronal competence, whereas multiply passaged wild-type cultures do not maintain stem cells production, and become enriched for glial restricted precursors (Bhattacharyya and Svendsen, 2003; Jain et al., 2003; Seaberg et al., 2005).

Our previous studies and those by others demonstrated that *Pten* deletion in the embryonic brain leads to abnormal histoarchitecture with severe layering defects (Backman et al., 2001; Groszer et al., 2001; Marino et al., 2002; Yue et al., 2005). However, as *Pten* deletion happens in nearly 100% of the neural stem/progenitor cells, it is unclear whether the abnormal phenotypes observed are caused by intrinsic migratory defects of *Pten*-null neurons, extrinsic microenvironmental cues provided by *Pten* null radial glia, or perhaps both (Groszer et al., 2001). In this study, we demonstrated that in the presence of wild-type environmental cues, *Pten* null adult NSCs and their progenies can follow the endogenous migration pathway, undergo differentiation, and reach their normal target. This result is consistent with a previous study on *Pten* heterozygous mice showing that $Pten^{+/-}$ cells migrated to the outer layers of the OB more rapidly and incorporated at the same sites as $Pten^{+/+}$ cells (Li et al., 2002). Therefore, the extrinsic microenvironment cues plays a more predominant role in controlling the migratory behavior of SEZ-derived *Pten* null NSCs and their progenies.

Nearly 90% of the GCs in the OB are SEZ-derived and incorporated postnatally, and their survival depends on incoming activities (Rosselli-Austin and Williams, 1990; Brunjes, 1994). GCs are also known to extensively shape mitral cell response to odors (Yokoi et al., 1995), and there is evidence that the OB circuitry maximizes differences in odor representations (Friedrich and Laurent, 2001; Dulac, 2005). Animals carrying a mutation in the cyclic nucleotide gated channel are not able to transduce the signal from the olfactory receptors in the olfactory neurons (Baker et al., 1999) and have smaller GCL volume and OB mass (Petreanu and Alvarez-Buylla, 2002). The lack of electrical activity in the OB of these mice dramatically reduced the survival of newly generated neurons of the GCL, suggesting that peripheral olfactory epithelium plays a critical role in the survival of GCL neurons in the OB (Petreanu and Alvarez-Buylla, 2002). Our results showed that PTEN loss in SEZ NSCs leads to an increase in GCL volume and OB size as well as an improvement in olfactory function, suggesting that the *Pten* null SEZ-derived GCL neurons are able to integrate into the existing circuitry, receive electrical input from olfactory epithelium and are thus functional. Because olfactory ablation/repair is a multifactor-dependent process, we cannot rule out that mechanisms other than *Pten* null granular cells in the OB also contribute to the faster recovery observed in our study. Since *Pten* conditional deletion in adult NSCs also enhances the recovery of olfactory function after ablation of olfactory epithelium, our data suggest an important role for SEZ-derived neurons in reestablishment of the connection between OB and olfactory epithelium during acute damage via a currently unknown mechanism.

SEZ-born progenitors are known to play a role in postischemic injury recovery (Ohab et al., 2006). In a stroke-injury model, *Pten* conditional knock-out animals showed a robust increase in cell proliferation and DCX^+ neuroblast migration from the SEZ over long distances to the peri-infarct cortex, suggesting *Pten* null neuroblasts are responsive to chemotactic stimulation and can migrate to the injury site. Although the SEZ DCX volume did not increase in *Pten* conditional knock-out mice poststroke when compared with non-stroke animals (supplemental Fig. 10, available at www.jneurosci.org as supplemental material), the significantly enhanced proliferation and migration of *Pten* null neuroblasts to the peri-infarct cortex suggested that *Pten* null neuroblasts are primed for the signals that induce poststroke neurogenesis. *Pten* deletion might have been expected to promote neuroblast survival as it potentiates the action of the PI3K/Akt pathway, a common downstream signaling pathway for many of the neural stem cell survival and differentiation growth factors (Greenberg and Jin, 2006). Interestingly, *Pten* conditional deletion in these neuroblasts is not sufficient to promote their long-term differentiation/survival and functional integration once they have migrated into peri-infarct cortex. Thus, in addition to soluble growth factor signaling, the cellular environment of the peri-infarct cortex may exert an important degree of control over cell survival in newly born neurons after stroke.

Stem cell-based therapies, including the promotion of endogenous neurogenesis or transplantation of stem/progenitor cells, are limited in large part by the death of the progenitor pool (Goldman, 2005). In poststroke neurogenesis, despite a robust generation of newly born neurons, ninety percent of them eventually die (Ohab et al., 2006). After stem/progenitor transplantation, a similar result is seen in which most transplanted cells die or fail to differentiate. The differential roles of PTEN defined in the present study highlight the key differences between constitutive/normal and injury-induced neurogenesis. PTEN inactivation alone is sufficient to promote a significant increase in neurogenesis, neuronal survival and improved function in the olfactory bulb but insufficient to promote long-term survival after stroke. Although both poststroke and normal neurogenesis involve growth factor signaling within glial and vascular niches (Nilsson et al., 1999; Teramoto et al., 2003; Ohab et al., 2006; Hagg, 2007; Puche and Baker, 2007) poststroke neurogenesis requires additional, likely, cellular signals that are independent of the common PI3K-AKT-mediated growth factor signaling pathway. In designing successful stem cell based therapies it will be important to determine both the molecular and cellular constituents that support survival and differentiation of stem cell progenies.

References

Arvidsson A, Collin T, Kirik D, Kokaia Z, Lindvall O (2002) Neuronal replacement from endogenous precursors in the adult brain after stroke. Nat Med 8:963–970.

Backman SA, Stambolic V, Suzuki A, Haight J, Elia A, Pretorius J, Tsao MS, Shannon P, Bolon B, Ivy GO, Mak TW (2001) Deletion of Pten in mouse brain causes seizures, ataxia and defects in soma size resembling Lhermitte-Duclos disease. Nat Genet 29:396–403.

Baker H, Cummings DM, Munger SD, Margolis JW, Franzen L, Reed RR, Margolis FL (1999) Targeted deletion of a cyclic nucleotide-gated channel subunit (OCNC1): biochemical and morphological consequences in adult mice. J Neurosci 19:9313–9321.

Bhattacharyya A, Svendsen CN (2003) Human neural stem cells: a new tool for studying cortical development in Down's syndrome. Genes Brain Behav 2:179–186.

Brunjes PC (1994) Unilateral naris closure and olfactory system development. Brain Res Brain Res Rev 19:146–160.

Bush TG, Savidge TC, Freeman TC, Cox HJ, Campbell EA, Mucke L, Johnson MH, Sofroniew MV (1998) Fulminant jejuno-ileitis following ablation of enteric glia in adult transgenic mice. Cell 93:189–201.

Carmichael ST (2005) Rodent models of focal stroke: size, mechanism, and purpose. NeuroRx 2:396–409.
Cecchi GA, Petreanu LT, Alvarez-Buylla A, Magnasco MO (2001) Unsupervised learning and adaptation in a model of adult neurogenesis. J Comput Neurosci 11:175–182.
Curtis MA, Kam M, Nannmark U, Anderson MF, Axell MZ, Wikkelso C, Holtås S, van Roon-Mom WM, Björk-Eriksson T, Nordborg C, Frisén J, Dragunow M, Faull RL, Eriksson PS (2007) Human neuroblasts migrate to the olfactory bulb via a lateral ventricular extension. Science 315:1243–1249.
Datta SR, Brunet A, Greenberg ME (1999) Cellular survival: a play in three Akts. Genes Dev 13:2905–2927.
Doetsch F (2003) The glial identity of neural stem cells. Nat Neurosci 6:1127–1134.
Doetsch F, Alvarez-Buylla A (1996) Network of tangential pathways for neuronal migration in adult mammalian brain. Proc Natl Acad Sci U S A 93:14895–14900.
Doetsch F, Caillé I, Lim DA, García-Verdugo JM, Alvarez-Buylla A (1999) Subventricular zone astrocytes are neural stem cells in the adult mammalian brain. Cell 97:703–716.
Dulac C (2005) Molecular architecture of pheromone sensing in mammals. Novartis Found Symp 268:100–107; discussion 107- 110:167–170.
Emsley JG, Mitchell BD, Kempermann G, Macklis JD (2005) Adult neurogenesis and repair of the adult CNS with neural progenitors, precursors, and stem cells. Prog Neurobiol 75:321–341.
Enwere E, Shingo T, Gregg C, Fujikawa H, Ohta S, Weiss S (2004) Aging results in reduced epidermal growth factor receptor signaling, diminished olfactory neurogenesis, and deficits in fine olfactory discrimination. J Neurosci 24:8354–8365.
Feng Y, Walsh CA (2001) Protein-protein interactions, cytoskeletal regulation and neuronal migration. Nat Rev Neurosci 2:408–416.
Fiske BK, Brunjes PC (2001) Cell death in the developing and sensory-deprived rat olfactory bulb. J Comp Neurol 431:311–319.
Fraser MM, Zhu X, Kwon CH, Uhlmann EJ, Gutmann DH, Baker SJ (2004) Pten loss causes hypertrophy and increased proliferation of astrocytes in vivo. Cancer Res 64:7773–7779.
Friedrich RW, Laurent G (2001) Dynamic optimization of odor representations by slow temporal patterning of mitral cell activity. Science 291:889–894.
Funamoto S, Meili R, Lee S, Parry L, Firtel RA (2002) Spatial and temporal regulation of 3-phosphoinositides by PI 3-kinase and PTEN mediates chemotaxis. Cell 109:611–623.
Garcia AD, Doan NB, Imura T, Bush TG, Sofroniew MV (2004) GFAP-expressing progenitors are the principal source of constitutive neurogenesis in adult mouse forebrain. Nat Neurosci 7:1233–1241.
Gheusi G, Cremer H, McLean H, Chazal G, Vincent JD, Lledo PM (2000) Importance of newly generated neurons in the adult olfactory bulb for odor discrimination. Proc Natl Acad Sci U S A 97:1823–1828.
Goldman S (2005) Stem and progenitor cell-based therapy of the human central nervous system. Nat Biotechnol 23:862–871.
Goldman SA (1998) Adult neurogenesis: from canaries to the clinic. J Neurobiol 36:267–286.
Greenberg DA, Jin K (2006) Growth factors and stroke. NeuroRx 3:458–465.
Groszer M, Erickson R, Scripture-Adams DD, Lesche R, Trumpp A, Zack JA, Kornblum HI, Liu X, Wu H (2001) Negative regulation of neural stem/progenitor cell proliferation by the Pten tumor suppressor gene in vivo. Science 294:2186–2189.
Groszer M, Erickson R, Scripture-Adams DD, Dougherty JD, Le Belle J, Zack JA, Geschwind DH, Liu X, Kornblum HI, Wu H (2006) PTEN negatively regulates neural stem cell self-renewal by modulating G0–G1 cell cycle entry. Proc Natl Acad Sci U S A 103:111–116.
Hack MA, Saghatelyan A, de Chevigny A, Pfeifer A, Ashery-Padan R, Lledo PM, Götz M (2005) Neuronal fate determinants of adult olfactory bulb neurogenesis. Nat Neurosci 8:865–872.
Hagg T (2007) Endogenous regulators of adult CNS neurogenesis. Curr Pharm Des 13:1829–1840.
Iijima M, Devreotes P (2002) Tumor suppressor PTEN mediates sensing of chemoattractant gradients. Cell 109:599–610.
Imura T, Kornblum HI, Sofroniew MV (2003) The predominant neural stem cell isolated from postnatal and adult forebrain but not early embryonic forebrain expresses GFAP. J Neurosci 23:2824–2832.
Jain M, Armstrong RJ, Elneil S, Rosser AE, Barker RA (2003) Migration and differentiation of transplanted human neural precursor cells. Neuroreport 14:1257–1262.
Jin K, Sun Y, Xie L, Peel A, Mao XO, Batteur S, Greenberg DA (2003) Directed migration of neuronal precursors into the ischemic cerebral cortex and striatum. Mol Cell Neurosci 24:171–189.
Kippin TE, Martens DJ, van der Kooy D (2005) p21 loss compromises the relative quiescence of forebrain stem cell proliferation leading to exhaustion of their proliferation capacity. Genes Dev 19:756–767.
Kwon CH, Zhu X, Zhang J, Knoop LL, Tharp R, Smeyne RJ, Eberhart CG, Burger PC, Baker SJ (2001) Pten regulates neuronal soma size: a mouse model of Lhermitte-Duclos disease. Nat Genet 29:404–411.
Lee JO, Yang H, Georgescu MM, Di Cristofano A, Maehama T, Shi Y, Dixon JE, Pandolfi P, Pavletich NP (1999) Crystal structure of the PTEN tumor suppressor: implications for its phosphoinositide phosphatase activity and membrane association. Cell 99:323–334.
Lesche R, Groszer M, Gao J, Wang Y, Messing A, Sun H, Liu X, Wu H (2002) Cre/loxP-mediated inactivation of the murine Pten tumor suppressor gene. Genesis 32:148–149.
Li J, Simpson L, Takahashi M, Miliaresis C, Myers MP, Tonks N, Parsons R (1998) The PTEN/MMAC1 tumor suppressor induces cell death that is rescued by the AKT/protein kinase B oncogene. Cancer Res 58:5667–5672.
Li L, Liu F, Salmonsen RA, Turner TK, Litofsky NS, Di Cristofano A, Pandolfi PP, Jones SN, Recht LD, Ross AH (2002) PTEN in neural precursor cells: regulation of migration, apoptosis, and proliferation. Mol Cell Neurosci 20:21–29.
Liaw D, Marsh DJ, Li J, Dahia PL, Wang SI, Zheng Z, Bose S, Call KM, Tsou HC, Peacocke M, Eng C, Parsons R (1997) Germline mutations of the PTEN gene in Cowden disease, an inherited breast and thyroid cancer syndrome. Nat Genet 16:64–67.
Liliental J, Moon SY, Lesche R, Mamillapalli R, Li D, Zheng Y, Sun H, Wu H (2000) Genetic deletion of the Pten tumor suppressor gene promotes cell motility by activation of Rac1 and Cdc42 GTPases. Curr Biol 10:401–404.
Lindvall O, Kokaia Z (2006) Stem cells for the treatment of neurological disorders. Nature 441:1094–1096.
Lledo PM, Alonso M, Grubb MS (2006) Adult neurogenesis and functional plasticity in neuronal circuits. Nat Rev Neurosci 7:179–193.
Lois C, García-Verdugo JM, Alvarez-Buylla A (1996) Chain migration of neuronal precursors. Science 271:978–981.
Luskin MB (1993) Restricted proliferation and migration of postnatally generated neurons derived from the forebrain subventricular zone. Neuron 11:173–189.
Maehama T, Taylor GS, Dixon JE (2001) PTEN and myotubularin: novel phosphoinositide phosphatases. Annu Rev Biochem 70:247–279.
Marino S, Krimpenfort P, Leung C, van der Korput HA, Trapman J, Camenisch I, Berns A, Brandner S (2002) PTEN is essential for cell migration but not for fate determination and tumourigenesis in the cerebellum. Development 129:3513–3522.
Mombaerts P, Wang F, Dulac C, Chao SK, Nemes A, Mendelsohn M, Edmondson J, Axel R (1996) Visualizing an olfactory sensory map. Cell 87:675–686.
Najbauer J, Leon M (1995) Olfactory experience modulated apoptosis in the developing olfactory bulb. Brain Res 674:245–251.
Nelen MR, van Staveren WC, Peeters EA, Hassel MB, Gorlin RJ, Hamm H, Lindboe CF, Fryns JP, Sijmons RH, Woods DG, Mariman EC, Padberg GW, Kremer H (1997) Germline mutations in the PTEN/MMAC1 gene in patients with Cowden disease. Hum Mol Genet 6:1383–1387.
Nilsson M, Perfilieva E, Johansson U, Orwar O, Eriksson PS (1999) Enriched environment increases neurogenesis in the adult rat dentate gyrus and improves spatial memory. J Neurobiol 39:569–578.
Ohab JJ, Fleming S, Blesch A, Carmichael ST (2006) A neurovascular niche for neurogenesis after stroke. J Neurosci 26:13007–13016.
Parent JM (2002) The role of seizure-induced neurogenesis in epileptogenesis and brain repair. Epilepsy Res 50:179–189.
Peterson DA (2002) Stem cells in brain plasticity and repair. Curr Opin Pharmacol 2:34–42.
Petreanu L, Alvarez-Buylla A (2002) Maturation and death of adult-born olfactory bulb granule neurons: role of olfaction. J Neurosci 22:6106–6113.
Pomeroy SL, LaMantia AS, Purves D (1990) Postnatal construction of neural circuitry in the mouse olfactory bulb. J Neurosci 10:1952–1966.

Puche AC, Baker H (2007) Olfactory cell derivation and migration. J Mol Histol 38:513–515.
Raftopoulou M, Etienne-Manneville S, Self A, Nicholls S, Hall A (2004) Regulation of cell migration by the C2 domain of the tumor suppressor PTEN. Science 303:1179–1181.
Rochefort C, Gheusi G, Vincent JD, Lledo PM (2002) Enriched odor exposure increases the number of newborn neurons in the adult olfactory bulb and improves odor memory. J Neurosci 22:2679–2689.
Rosselli-Austin L, Williams J (1990) Enriched neonatal odor exposure leads to increased numbers of olfactory bulb mitral and granule cells. Brain Res Dev Brain Res 51:135–137.
Seaberg RM, Smukler SR, van der Kooy D (2005) Intrinsic differences distinguish transiently neurogenic progenitors from neural stem cells in the early postnatal brain. Dev Biol 278:71–85.
Shors TJ, Miesegaes G, Beylin A, Zhao M, Rydel T, Gould E (2001) Neurogenesis in the adult is involved in the formation of trace memories. Nature 410:372–376.
Soriano P (1999) Generalized lacZ expression with the ROSA26 Cre reporter strain. Nat Genet 21:70–71.
Stiles B, Groszer M, Wang S, Jiao J, Wu H (2004) PTENless means more. Dev Biol 273:175–184.
Tamura M, Gu J, Matsumoto K, Aota S, Parsons R, Yamada KM (1998) Inhibition of cell migration, spreading, and focal adhesions by tumor suppressor PTEN. Science 280:1614–1617.
Teramoto T, Qiu J, Plumier JC, Moskowitz MA (2003) EGF amplifies the replacement of parvalbumin-expressing striatal interneurons after ischemia. J Clin Invest 111:1125–1132.
Trinh K, Storm DR (2004) Detection of odorants through the main olfactory epithelium and vomeronasal organ of mice. Nutr Rev 62:S189–192; discussion S224–141.
Tsai PT, Ohab JJ, Kertesz N, Groszer M, Matter C, Gao J, Liu X, Wu H, Carmichael ST (2006) A critical role of erythropoietin receptor in neurogenesis and post-stroke recovery. J Neurosci 26:1269–1274.
Vivanco I, Sawyers CL (2002) The phosphatidylinositol 3-Kinase AKT pathway in human cancer. Nat Rev Cancer 2:489–501.
Winner B, Cooper-Kuhn CM, Aigner R, Winkler J, Kuhn HG (2002) Long-term survival and cell death of newly generated neurons in the adult rat olfactory bulb. Eur J Neurosci 16:1681–1689.
Yamashita T, Ninomiya M, Hernández Acosta P, García-Verdugo JM, Sunabori T, Sakaguchi M, Adachi K, Kojima T, Hirota Y, Kawase T, Araki N, Abe K, Okano H, Sawamoto K (2006) Subventricular zone-derived neuroblasts migrate and differentiate into mature neurons in the post-stroke adult striatum. J Neurosci 26:6627–6636.
Yokoi M, Mori K, Nakanishi S (1995) Refinement of odor molecule tuning by dendrodendritic synaptic inhibition in the olfactory bulb. Proc Natl Acad Sci U S A 92:3371–3375.
Yoon H, Enquist LW, Dulac C (2005) Olfactory inputs to hypothalamic neurons controlling reproduction and fertility. Cell 123:669–682.
Yue Q, Groszer M, Gil JS, Berk AJ, Messing A, Wu H, Liu X (2005) PTEN deletion in Bergmann glia leads to premature differentiation and affects laminar organization. Development 132:3281–3291.